Multi-sector Water Allocation

The impact of nonlinear approximation network hyper-parameters for multi-objective reservoir control

M. Witvliet

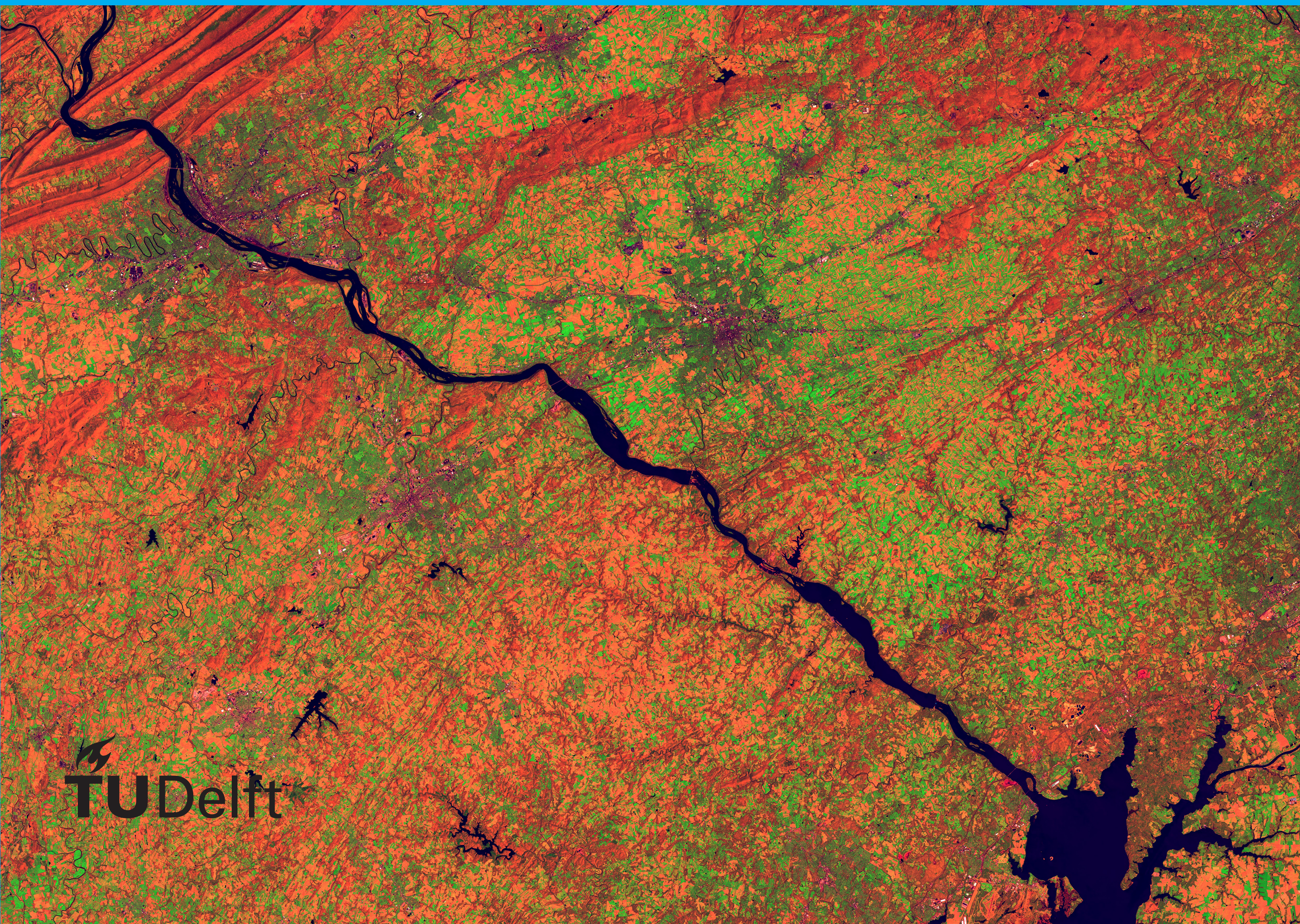

Multi-sector Water Allocation

The impact of nonlinear approximation network hyperparameters for multi-objective reservoir control

by

M. Witvliet

to obtain the degree of Master of Science
in Engineering and Policy Analysis,
Faculty of Technology, Policy and Management,
at the Delft University of Technology,
to be defended publicly on April 11, 2022 at 16:00.

Student number:	4103661	
Graduation committee:	Prof. Dr. M.E. Warnier,	TU Delft, Chairperson
	Dr. J. Zatarain Salazar,	TU Delft, first supervisor
	Prof. Dr. Ir. J. Kwakkel,	TU Delft, second supervisor

An electronic version of this thesis is available at `http://repository.tudelft.nl/`.
Associated code and figures are available at `https://github.com/jazminZatarain/MUSEH2O/`

TU Delft

Acknowledgements

It was quite a journey to write this thesis, with many late nights, cups of tea, ups and downs. It's hard to believe how quick the time has passed since I have started this thesis and it was not always easy to keep going. I would therefore like to thank everyone who kept me motivated when I needed it. I am proud to have been able to stay focused and for completing this study.

I'd like to thank my parents and my sister, for always believing in me and for their support. You were always there for me when I needed it and I'm really grateful for that.

I also like to thank the members of my graduation committee, especially Jazmin and Jan as my direct supervisors. For their guidance and support, our many bi-weekly meetings, but also for their positive attitude and enthusiasm. You kept me motivated during this thesis and made me believe in myself. You were always quick to respond whenever I had a problem or a question, and I consider myself lucky to have been supervised by you. Without their mentorship, supportive feedback and inspirational ideas this thesis would not have been what it is today.

And last but not least, I would like to thank my friends for their support and fun throughout my studies.

M. Witvliet
The Hague, March 2022

Executive Summary

Research context

Climate change and increasing populations around the world have the potential to reduce fresh water availability. Because of a 2°C global temperature increase and rising population demands, 71 percent of the world's 112 main river basins are expected to experience increased water stress by 2060. Existing river basins must be prepared to successfully manage worsening water stress problems in the future. Efficient multi-purpose reservoir management strategies are crucial in the face of increased flood and drought threats, as well as the need to fulfill shifting water allocation demands across a diverse collection of users. To properly allocate water for complicated river basins across several conflicting purposes with shared water resources, new methods such as Evolutionary Multi-Objective Direct Policy Search (EMODPS) have been designed. This method can be explored further in order to better deal with rising water stress scenarios in the future. EMODPS is a very adaptable method for determining the Pareto approximation policy strategy. Direct policy search (DPS), multi-objective evolutionary algorithms (MOEAs), and nonlinear approximation networks are the three key components of the framework. The impact of MOEAs has been studied, but the impact of nonlinear approximating networks is still unknown. Nonlinear approximating networks are used to map the system's state onto decisions in a flexible manner as time-varying, complex non-linear relationships that should approximate the unknown optimal operating policies of complex multi-objective reservoir systems. Traditionally Gaussian RBFs have been selected to be combined with EMODPS models. However, there are other types of universal approximators that could fulfill this role, hence, the performance impact of the use of other universal approximators can be explored. Universal approximators require an initial setup of hyper parameters to properly function. However, the reason behind choices of hyper-parameters are rarely documented in the literature, it is therefore unknown what the best hyper parameter setup is for EMODPS models. As a result, a more formal study is required to identify guidelines around this subject in order to avoid a lot of trial-and-error. Furthermore, the renewed interest in 'deep learning' and 'machine learning' in water resource systems is drawing a varied user base with a tendency to utilize default settings. These parameters can be case-specific as they are highly tuned and do not generalize well when used for different applications. The goal is to explore different hyper-parameter configurations in conjunction with EMODPS to help create a better understanding for non-expert users. Overcoming sensitivity to the initial parameterizations which could have a large impact on policy design and the trade-offs.

Research approach

In order to find an answer to the main research question: *How do the choices made during the experimental setup of multi-sector water allocation EMODPS models impact the model outcomes?* a modelling approach is used in conjunction the EMODPS framework and with the help of a case study. First the Lower Susquehanna river basin is selected as a case study. An experimental design is used to be able to setup the experiments that are needed to explore the research question. This thesis argues that the hyper parameters setup of nonlinear approximation networks can be explored further. Furthermore, this thesis seeks to contribute to the EMODPS framework by creating a better understanding of the performance impact of these hyper parameters.

Findings

Activation functions are hyper parameters of radial basis function networks with a lot of influence on the control policy, and these parameters do have implications for the model outcomes. An experimental design has been setup to test seven activation functions. The activation function originally used with the lower Susquehanna river basin case, together with six other popular kernels, namely, the squared exponential RBF, the inverse quadratic RBF, the inverse multiquadric RBF, the exponential RBF, the matern32 kernel and the matern52 kernel. A multi-objective multi-sector water allocation model has been built in python to test these kernels. The influence of the activation function on the search dynamics would be tested with ϵ-NSGAII as multi-objective evolutionary algorithm. The seven activation functions have been tested to explore how big their impact would be on the performance of the model, the objective space and the search behavior of the optimization algorithm. It can be concluded that the choices made during the experimental setup can have a large impact on the objective space, search behavior and eventually the final model outcomes. The exponential, matern32, matern52, inverse quadratic and inverse multiquadric kernels all under performed compared to the activation function originally used in the Susquehanna model, and the squared exponential activation function. The original RBF managed to attain the biggest objective space with the most diverse approximation set. It also demonstrated the best search behavior. A bigger objective space with a more diverse approximation set is more desirable since decision makers have more possible trade-offs to work with. This opens up room to negotiate, which is essential for the smooth progression of decision making in networks. This eventually leads to better and more informed decision making. To better understand why the original RBF performed so well, the shape characteristic of a few selected activation functions have been inspected. It has been found that the EMODPS algorithm combined with the ϵ-NSGAII MOEA prefer large negative parabolas as activation function, probably to create an as large as possible decision surface. The findings of this study have created a better understanding of the effects of the hyper-parameter setup of non-linear approximation networks in EMODPS models. A first step has been made to better understand the impact of hyperparameter configuration of nonlinear approximation networks in EMODPS models. With help of future research, more efficient multi-purpose reservoir management strategies can be created to more easily deal with the increased flood and drought threats in the future. As well as the shifting water allocation demands, which will also grow more prevalent in the oncoming decades.

Scientific Contribution

This thesis contributes to a better understanding of the initial parameterization of non-linear approximation networks within the EMODPS framework for multi-objective water reservoir models. This study is among the first to explore the effects of the use of other kernels than the conventional activation function in conjunction with radial basis function networks using EMODPS. A python model has been created to be able to test these kernels. The model, scripts and data used for this study have been made open source through GitHub, and can be expanded upon for future academic use. It's findings suggests that activation functions in non-linear approximation networks can have a large impact on the model outcomes, more specifically on the performance of the optimization algorithm, the resulting objective space, the search behavior of the optimization algorithm and eventually also on the decision-making process.

Future Research

A number of new research questions were encountered during this thesis. These topics for future research are highlighted in a list below.

- Literature suggests that different optimization algorithms or even different parameter values of optimization algorithm can influence the fitness landscape, and thus the behavior of the activation function. It therefore is worth investigating how drastic the effects of different optimization algorithms are on activation functions. Diving deeper into the the evolutionary dynamics of the MOEAs in conjunction with different activation functions. Exploring how the shape of the fitness landscape evolves during the MOEA runtime.

- Further research into the preferred characteristics of activation functions for EMODPS models would be beneficial to be able to select or even create a better activation function given a case or MOEA. Future research in this direction can also help create guidelines for non-expert users and even better understanding for expert users. It can further discover the relative merits of each activation function and in which situation it would be best to use them.

- Investigate the effects of varying activation functions on other case studies. The question is if activation functions will still perform comparably with other cases which have different input or release behavior. Currently, the chosen activation functions were only tested with the Susquehanna case. The fitness landscape can be influenced by merely using different parameters of the model, applying the same experiment on a different model can therefore yield different results for the same activation functions.

- The shape of the inverse multiquadric with the maximum radius and the shape of the original RBF with the mean radius looked very much alike (Figure 7.1f). It was expected that the optimization algorithm would shift toward an inverse multiquadric RBF with a larger radius to match the shape if the original

RBF if this would be beneficial, but this did not happen. It would therefore be interesting to explore if limiting the decision variables to a certain range, to force a bandwidth onto the optimization algorithm would yield better results.

Contents

List of Figures

List of Tables

List of Abbreviations

ANN	Artificial Neural Network
DDP	Deterministic Dynamic programming
DPS	Direct Policy Search
EMODPS	Evolutionary Multi Objective Direct Policy Search
FQI	Fitted Q-iteration
MOEA	Multi Objective Evolutionary Algorithm
NFE	number of function evaluations
ISO	Implicit Stochastic Optimization
RBF	Radial Basis Function
RBFN	Radial Basis Function Network
SDP	Stochastic Dynamic programming
SSDP	Sampling Stochastic Dynamic Programming

1
Introduction

In this introductory chapter, the research topic and scope is presented. First, a brief overview of the context is given in section 1.1, that results in a problem statement consisting of a policy problem in section 1.2 and a scientific knowledge gap in section 1.3. Section 1.4 states the research goal and main research question. Lastly, section 1.5 presents the outline of this thesis.

1.1. Context

Due to the steady increase of greenhouse gasses, the earth's temperature is rising and its climate is changing. Despite a brief reduction in carbon dioxide emissions in 2020, the world is still heading for a temperature rise of more than 3°C this century (UNEP, 2020). Far beyond the goals of of the Paris climate agreement, which aimed at limiting global warming below 2°C and pursuing 1.5°C (United Nations, 2015). Climate change and growing populations around the world are able to cause a reduction in fresh water availability according to Fung, Lopez, and New (2011), 71 percent of the 112 world's major river basins are projected to suffer greater water stress because of a 2°C global temperature increase and increasing population demands in 2060. According to recent forecasts, the United States (US) will require more than one trillion dollars in water supply infrastructure investment over the next 20 years (ASCE, 2017). On top of this, many river basins are glacier and snow fed. The glaciers which have retreated significantly over the last decade are acting as a buffer system for river basins. They store water as ice and snow when it's cold and they steadily release water when the snow melts (Pritchard, 2019). When glaciers retreat further in the future it will cause extended periods of floods and droughts, increasing the stress on river basins. Fung et al. (2011) also mentioned that the seasonality will become more extreme in a +2°C and +4°C world, which will cause wet seasons to become even wetter and dry seasons to become dryer.

Reflecting these challenges, it is important for existing river basins to be able to manage worsening water stress situations effectively in the future. Efficient multi-purpose reservoir management strategies are critical in the face of rising flood and drought risks, as well as the need to meet changing water allocation demands across a diverse set of users (Castelletti, Antenucci, Limosani, Quach Thi, & Soncini-Sessa, 2011). This advocates the need of a generalizable model for multi-purpose water allocation that can be adapted to different river basin systems. New methods such as Evolutionary Multi-Objective Direct Policy Search (Giuliani, Castelletti, et al., 2016) have been developed to be able to effectively allocate water for complex river basins across multiple competing objectives with shared water resources. This method can be explored further to be able to better handle rising water stress situations in the future.

1.2. Multi-objective optimization

With complex problems where multiple objectives must be considered, finding a set of optimal solutions, or the "Pareto front", is imperative to be able to make proper decisions. Water resource allocation where water has to be divided between different objectives is an example of this. Examples of objectives for water allocation are the drinking water supply, energy generation, agricultural activities and keeping enough water available for nature or recreation. There are several methods to allocate water between objectives, some performing better than others. Traditionally techniques such as Deterministic Dynamic programming (DDP) and Stochastic Dynamic programming (SDP) are used for water resource allocation (Giuliani, Li, et al., 2016). Aside from these widely used techniques Giuliani, Li, et al. (2016) also mentions Implicit Stochastic Optimization (ISO), Sampling Stochastic Dynamic Programming (SSDP) and Fitted Q-iteration (FQI). All these methods are however originally designed for single-objective problems, and were adapted to optimize repeatedly for every Pareto point (Giuliani, Li, et al., 2016).

The direct search approach combined with a genetic algorithm (GA) has also been used to evaluate and optimize water reservoir operating policies (Momtahen & Dariane, 2007), which performs better than the aforementioned traditional techniques and is capable of dealing with multi-objective problems. However the main weakness of GA models is the variance of the outcomes of the optimized parameters obtained from different model runs. In spite of relatively consistent results of the objective function.

A new method that can more effectively deal with multi-objective problems is Evolutionary Multi-Objective Direct Policy Search (EMODPS). EMODPS is a highly flexible technique to find the Pareto approximate policy strategy. It consists of three main elements: Direct policy search (DPS), Multi-objective evolutionary algorithms (MOEAs) and nonlinear approximating networks (Giuliani, Castelletti, et al., 2016). The direct policy search approach (Schmidhuber, 2000; Rosenstein & Barto, 2001) can be considered the foundation where EMODPS has been build upon by making it more suitable for multiple objectives. DPS is also known as parameterization-simulation-optimization in the water resources literature (Koutsoyiannis & Economou, 2003). It first parameterizes the operating policy within a group of functions (e.g. linear, piecewise linear or radial basis function) and then optimizes the parameters for the operating objectives.

The use of universal approximators such as artificial neural networks (ANNs) or radial basis functions (RBFs) are needed to partially overcome the search limitations caused by *a priori* knowledge which might restrict the decision space to a subspace that does not include the optimal solution, by providing flexibility to the shape of the operating rule (Giuliani et al., 2014). They can be used to map the system's state onto decisions in a flexible manner as time-varying, complex nonlinear relationships that should approximate the unknown optimal operating policies of complex multi-objective reservoir systems (Salazar et al., 2016). Traditionally Gaussian RBFs have been selected to be combined with EMODPS (Giuliani et al., 2014). However, there are many types of global approximators that could fulfill this role, hence, the performance impact of the use of other universal approximators can be explored. The selection of other hyperparameters, the additional factors that control the parameters in policy design, also remain highly empirical. These parameters are case-specific as they are highly tuned and do not generalize well when used for different applications.

Furthermore, when DPS problems have more than one objective, the EMODPS framework allows coupling with multi-objective optimization methods such as MOEAs. This allows approximation of the Pareto front in a single algorithm run (Giuliani, Castelletti, et al., 2016). MOEAs are stochastic search tools that use different parameters for mating, mutation, selection and archiving (Salazar et al., 2016). There are many different MOEAs, some more advanced or optimized for a specific situation than others. The performance of several popular MOEAs within the EMODPS framework has already been explored extensively by (Salazar et al., 2016; Gupta, Hamilton, Reed, & Characklis, 2020). According to Salazar et al. (2016) the MOEAs; Borg (Hadka & Reed, 2013), ϵ-NSGAII (Kollat & Reed, 2005) and ϵ-MOEA (Deb, Mohan, & Mishra, 2003) were most effective to be utilized with EMODPS.

The key benefits of the EMODPS according to Salazar et al. (2016) are (1) the ability to optimize multiple objectives at the same time in a single model run, (2) the objective functions and model constraints do not have to be time separable, (3) the framework can be paired with any simulation model, (4) additional uncertainties can be easily evaluated by using nonlinear approximators to incorporate exogenous information such as weather observations or forecasts.

1.3. Scientific knowledge gap

In order to test policy outcomes, an abstraction of the real system in which outcomes produced by different policy alternatives and/or states of a given system are evaluated is often needed. When performing mapping of states to actions via direct policy search in multiple objectives, a highly flexible structure that is capable of capturing nonlinear relationships is needed. So far, universal nonlinear approximators such as RBFs have been a suitable choice with examples of success in multi-purpose reservoir control (Giuliani et al., 2014; Giuliani, Castelletti, et al., 2016; Salazar et al., 2016; Gupta et al., 2020; Doering, Quinn, Reed, & Steinschneider, 2021). Nonetheless, the reason behind choices of hyperparameters are rarely documented in the literature, it is therefore unknown what the best hyperparameter setup is for EMODPS models. It requires a more formal study to find guidelines around this subject prevent to a lot of trial-and-error. Additionally, the new found interest around 'deep learning' and 'machine learning' in water resources systems is attracting a diverse user-base, with tendency to use default parameters. These parameters can be case-specific as they are highly tuned and do not generalize well when used for different applications. The goal is to explore different hyperparameter configurations in conjunction with EMODPS to help create a better understanding for non-expert users. Overcoming sensitivity to the initial parameterizations which could have a large impact on policy design and the trade-offs.

While Python has become one of the biggest and most popular programming languages for scientific computing, there is still a lack of water resource allocation models in Python. Python has been a popular programming language for a while, resulting in robust decision making libraries such as project platypus and EMAworkbench. If multi-sector water allocation using EMODPS were to be modelled in python it could make use of these libraries and help obtain insights for complex relationships across factors affecting policy design.

This motivates the search for flexible open-source tools to support the design of operating policies for multiple-competing objectives which allow flexibility in policy design. Other expected added benefits of this research is to allow users to design Pareto approximate operating policies by providing easy connection to existing frameworks such as project platypus to access a suite of state-of-the-art optimization algorithms, as well as the EMAworkbench which expands this library with additional analysis tools.

1.4. Research goal and main research question

The objective of this thesis is to explore to what extent the hyperparameter configuration of nonlinear approximation networks of EMODPS models can affect the recommendations that will influence efficient reservoir management strategies. To do this a case study will be used to develop a multi-sector water allocation python model. This model will be adapted to support multiple hyperparameter configurations that can be tested. The python model will be constructed in such a way that it can later be expanded upon by further research and academic use.
This leads to the following research question:
How do the choices made during the hyperparameter setup of nonlinear approximation networks in multi-sector water allocation EMODPS models impact the model outcomes?

1.5. Outline

The rest of the thesis is structured as follows.

- Chapter 2 the research approach, this chapter gives further insight into the methodologies that are used to answer the research question. The main research question is divided into sub-questions and the methods required to conduct the research are discussed.
- Chapter 3 presents a case study, it specifies the characteristics and boundaries of the case study.
- Chapter 4 defines the experimental design.
- Chapter 5 establishes the model setup and implementation.
- Chapter 6 presents the results of the experiments that were defined earlier in chapter 3.
- Chapter 7 has a detailed discussion of the implications of the results to the research question.
- Chapter 8 concludes the research by answering all the research questions, the limitations of the research are addressed and possible future lines of research will be identified.

2
Research Approach

This chapter describes the methodology used chosen to answer the research question. The main research question is divided into five parts, with corresponding sub-questions, together with the methods that are required to answer these sub-question.

As previously stated the choices of hyperparameters are rarely documented in the literature, it is therefore unknown what the best hyperparameter setup is for multi-objective optimization models. A better understanding of the influence of hyperparameters is required to find guidelines to prevent trial-and-error for the experimental setup. To be able to better understand the influence of hyperparameters an experimental design will be setup, this will guarantee a well organised research experiment. Additionally, a modelling approach is used in conjunction with the EMODPS framework as proposed by (Giuliani, Castelletti, et al., 2016). There is a lack of theory around hyperparameter setup for EMODPS models, the objective of this research is to explore the effect of changes to the initial experimental model setup and to explain the implications for the optimized model outcomes. These findings will display the impacts of new theories could be discovered to generate new scientific insights of the initial parameterizations which could have a large impact on policy design and decision making. Gerring (2006) argues that case studies enjoy a natural advantage in research of an exploratory nature. To conduct this research a single case study will be selected.

2.1. Research questions

To select the different hyperparameters configurations, which are chosen in the initial model setup during the experimental configuration, an experimental design will be used. This will give an overview of the experiments that will be conducted during this thesis. To facilitate this a python decision model for multi-sector water resource allocation using EMODPS will be built. A modelling approach is required to provide insight in possible futures with regard to the system behavior and the effectiveness of policies. Moreover, the modelling approach is suitable when interactions between different components of a system are to be captured, which is an important part of this thesis. The Susquehanna river basin case will be used to construct and test this model. The core of the Susquehanna river basin model will remain the same but it will be adapted to be able to use different hyperparameter configurations.

In the first phase the research consists of the definition of the research topic. This was done by studying background information in conjunction with a brief literature review, determining an objective and problem definition. This highlighted the scientific research gap which enabled the formulation of the main research question. This will all lead to a research definition which forms the basis of the thesis. In the previous chapter a main research question was formulated. The main research question that is currently defined as:

How do the choices made during the hyperparameter setup of nonlinear approximation networks in multi-sector water allocation EMODPS models impact the model outcomes?

In order to answer the main research question, the following sub-questions have been formulated:

1. *What case study can be selected to study the impact of experimental setup choices in EMODPS models?*
   Method : Case study
   Thesis Chapter : Chapter 3, The Susquehanna River Basin Case

   In the second phase, the case study will be chosen and described. The model boundaries of the case are defined and the case characteristics are identified. Also the objectives which are to be optimized are defined.

2. *What is/are the most important independent variable(s) to study the impact of experimental setup choices for EMODPS?*
   Method : Experimental design
   Thesis Chapter : Chapter 4, Experimental design

   The third phase consists of the formulation of the experimental design. To be able to create a better understanding of the existing Susquehanna river model, more relevant literature about universal approximators and it's hyperparameters will be studied. It's also required to make a more educated decision what is needed for a good experimental design configuration. Some additional literature research will be performed by studying scientific papers on the subject. However, as mentioned earlier, the choices of hyperparameters are rarely documented in the literature, and it might be difficult to establish proper test ranges of hyperparameters such as learning rates, number of layers, number of nodes per layers and the type of activation function. Therefore it might be necessary to fall back on nonlinear approximation network theory to try and find best practices. Sub-question two, will be answered by constructing an experimental design. Qualitative data such as scientific journals is used, together with tools such as Google scholar, Scopus and the TU Delft Library to find the initial bulk of information. When a good initial understanding is achieved, the experimental design will be formalized into a table with the experiment setup.

3. *Is the EMODPS model implemented as intended?*
   Method : EMODPS Framework
   Data : Water flow and demand data
   Thesis Chapter : Chapter 5, Model implementation

   The fourth phase will formalize the case into the model that has been chosen in the second phase. The Python language together with EMODPS framework is used to implement the model. The experimental design choices that were selected earlier in phase three is used as model inputs. After the model implementation, the model is verified by performing a visual inspection of the water releases to each of the model objectives. It will also be determined whether the output of the model is useful and suitable for its purpose. If needed the model can be adapted to get the sought-after results. When these outcomes are satisfactory, the different configurations specified in the experimental design can be tested with the model, which will then be analyzed and evaluated in the next phase.

4. *What differences in performance in the objective space can be observed when varying the hyperparameters of the control policy?*
   Method : Performance metrics
   Thesis Chapter : Chapter 6, Results

5. *What differences in the search behavior of the algorithm can be observed when varying the hyperparameters of the control policy?*
   Method : Performance metrics
   Thesis Chapter : Chapter 6: Results

   Finally, the model outcomes of the fourth phase can be put to use in the fifth phase. Both question 4 and 5 will be answered in this chapter. Here all the outcomes of different configurations of hyperparameters will be evaluated with the visual analytics and general multi-dimensional performance metrics that are further elaborated in section 2.2.4. hyperparameters will be varied to be able to observe performance differences in the model outcomes. And the observed output differences of the separate nonlinear approximators of the EMODPS model will be assessed. The metrics will be evaluated by visually inspecting the trade-off space and comparing the different performance metrics. The performance metrics and trade-offs will be visualized using a combination of matplotlib and seaborn.

2.2. Research Methods

In an effort to properly answer the research questions proposed in section 2.1, research methods are used. These are the particular strategies for the collection and the analysis of data (Hammarberg, Kirkman, & de Lacey, 2016).

2.2.1. Case study

Gerring (2006) defines a case study as: *"An intensive study of a single unit or a small number of units (the cases), for the purpose of understanding a larger class of similar units (a population of cases)"*. This definition makes the distinction between a single case and a number of cases. There are strengths and weaknesses of case study research versus cross-case research. Gerring (2006) argues that a single case can be studied more intensively than a cross case study. To be able to reach the sufficient depth that is required for this research, a single case will be studied.

2.2.2. Experimental design

Experimental design is a method for carefully examining many types of problems that arise within research. It is a method to help plan and setup experiments. It is clear that if tests are carried out at random, the results will similarly be at random. As a result, it is essential to arrange the experiments in such a way that interesting information is obtained. Several experimental variables or factors can impact the outcome of any experimental procedure. A screening experiment is carried out to identify the experimental variables and interactions that have a significant influence on the outcome, as evaluated by one or more responses. When the experimental variables are defined, the experiments can be designed and carried out in such a way that the most information is obtained from the minimum number of experiments. (Lundstedt et al., 1998)

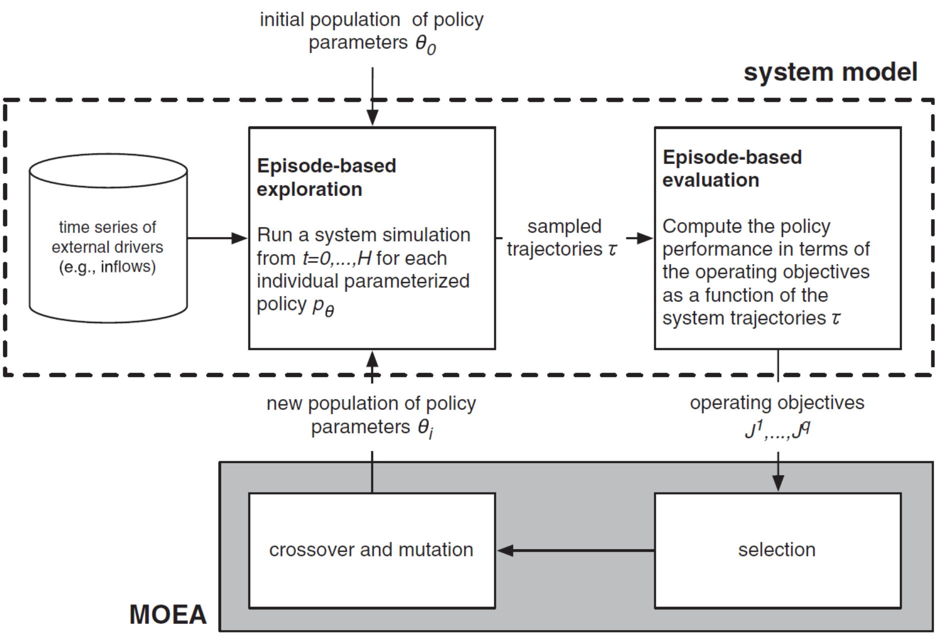

Figure 2.1: EMODPS framework (Giuliani, Castelletti, et al., 2016)

2.2.3. Evolutionary Multi-Objective Direct Policy Search (EMODPS)

Optimization-based techniques explore the space in a more focused manner for locations with certain qualities. Search delivers in-depth insights into specific locations in the uncertainty or policy levers domain. And can be used to answer questions such as "What is the worst or best that might happen?" "How significant is the gap in performance between competing policies?" "What would a suitable strategy be, given one or more scenarios?" (Kwakkel & Haasnoot, 2019). The formerly mentioned framework that will be used to construct the model is the EMODPS framework (Figure 2.1) as described by (Giuliani, Castelletti, et al., 2016). It is a simulation-based framework which has three main elements: direct policy search (DPS), nonlinear approximating networks (e.g. ANN or RBFs) and multi-objective evolutionary algorithms (MOEAs). The framework can be used to discover Pareto approximate control policies for multi-function reservoir systems. DPS first parameterizes the operating policy within a group of functions (e.g. linear, piecewise linear, radial basis function) and then optimizes the parameters for the operating objectives. The most important aspects of this framework are (1) using nonlinear approximators for the setup of the candidate operating policies, and (2) the identification of parameterizations that yield Pareto approximate reservoir control policies using multi-objective evolutionary search, forming the trade-offs between conflicting objectives (Salazar et al., 2016).

2.2.4. Assessment Metrics

Two different techniques are utilized be able to assess the performance of different hyperparameters. The first technique is the visualisation of trade-offs space by using python visualization techniques. Visual analytics will be utilized, which can be defined as *"the science of analytical reasoning facilitated by interactive visual interfaces."* (Thomas, 2005). For example by visually inspecting the trade-off space. Secondly the performance of the RBFs in this study will have to be assessed on both convergence and a diversity as is proposed by (Zitzler, Thiele, Laumanns, Fonseca, & Da Fonseca, 2003). These two categories cannot be appropriately quantified using a single performance metric (Deb, Pratap, Agarwal, & Meyarivan, 2002). Therefore five multi-objective performance metrics will be used to assess the performance of the model outcomes. These metrics are: generational distance, additive ϵ-indicator and the hypervolume indicator of the decision space, epsilon progress and archive size. These metrics are commonly used to assess multi-objective optimization problem performance, where the hypervolume indicator is the most popular indicator of the five (Guerreiro, Fonseca, & Paquete, 2020). Despite the hypervolume indicator's popularity it has one downside, and that is that it's very computationally expensive. Python modules such as matplotlib and seaborn will be valuable to be able to visualize these trade-offs and performance metrics.

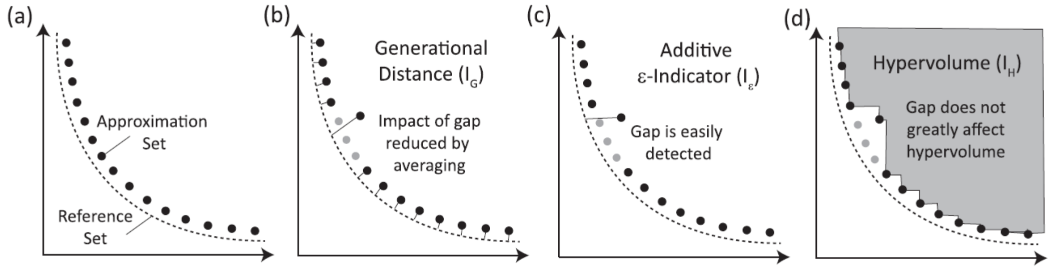

Figure 2.2: Examples of how generational distance, additive ϵ-indicator and hypervolume capture convergence, diversity and consistency (absence of gaps). (a) The dashed line indicates a good approximation to the reference set. (b) The generational distance averages the distance between the approximation set and the reference set, necessitating just one point near the reference set to be able to perform well. (c) Because the ϵ-indicator concentrates on the worst-case distance necessary to translate a point to dominate its nearest neighbor in the reference set, the metric quickly reveals a gap. (d) The hypervolume is defined by the volume of the objective space dominated by the approximation set. Because it covers both convergence and variety, it is the most challenging statistic to meet. Figure from Reed et al. (2013).

Generational distance Generational Distance (Figure 2.2b) gives a good first approximation of the performance of the approximation set. It measures the average Euclidean distance between the points in an approximation set and the nearest corresponding points in the reference set (Giuliani, Castelletti, et al., 2016). The metric is then the average of these distances. Since the true Pareto front needs to be approximated as much as possible, this metric is to be minimized. The generational distance is considered to be an easy metric to meet, because it requires only one solution set close to the reference set to be able to achieve a good performance score.

Additive Epsilon-Indicator The additive ϵ indicator (Zitzler et al., 2003) assesses consistency, where consistency refers to Pareto approximate sets that capture all aspects of trade-offs (Figure 2.2c). The metric is calculated as the longest distance that an approximation set must move in order to dominate the reference set, making it extremely sensitive to gaps in trade-offs. If there are gaps between the current set of solutions and the true (optimal) solutions in a Pareto approximate set, then solutions must be translated a much greater distance, dramatically increasing the value of the epsilon indicator (Salazar et al., 2016). Since a low value is desired, the metric is to be minimized. The Epsilon indicator can be thought of as a measure of an approximation set's consistency with the reference set, indicating that all aspects of the trade-off are present

(Hadka & Reed, 2012). It is a harder metric to meet because it focuses on the worst case distance needed in the approximation set in order to dominate its nearest neighbor in the reference set (Reed et al., 2013).

Hypervolume The hypervolume indicator (Zitzler et al., 2003) takes into account both convergence and diversity. It accomplishes this by examining the multidimensional "volume" formed by each set in relation to a reference point. Where each objective adds another dimension to the multidimensional volume. The hypervolume is calculated as the difference in hypervolume between the reference set, and the Pareto approximation set (Figure 2.2). Since it represents the volume of the objective space dominated by an approximation set, the metric is to be maximized. requires high performance for both convergence and diversity to be able to produce a high hypervolume value. This means it necessitates the full set of trade-offs to be of high quality. Therefore it is considered the hardest metric to meet (Reed et al., 2013).

Epsilon Progress ϵ-progress is a computationally efficient indication of search progression and stagnation (Salazar et al., 2016). When the current solution sits in a different ϵ-box that dominates the previous solution, ϵ-progress occurs. It establishes a minimal threshold (ϵ) that a MOEAs solution must reach in order to avoid search stagnation. The ϵ-box divides up the objective space into several boxes with the size ϵ. The boxes prevent the archive from retaining too many solutions by filtering the amount of solutions that are kept. The smaller the size of the ϵ-box, the more solutions kept by the archive. Each ϵ-box can only hold one solution at a time. If two solutions are found that reside in the same ϵ-box, the solution closest to true (optimal) solution will be kept, while the other will be eliminated (Lau, 2021).

Archive Size The Archive size is the amount of non-dominated solutions that the archive holds. ϵ MOEAs utilize ϵ-values to limit the size of the archive. All solutions that are ϵ-dominated are eliminated. This helps to avoid deterioration, which indicates that the ability of the MOEA to find new solutions is diminishing (Lau, 2021). The final amount of non-dominated solutions at the end of all model iterations are used to compute the performance metrics. A bigger archive size can give a more complete image of the trade-off space. But this can only be argued when both convergence and diversity are also high. The archive size can also tell something about the search behavior of the algorithm, when there is a drop in archive size, this means that the algorithm is diversifying somewhere. Then the algorithm is able to collapse again, because it made epsilon progress. It therefore tells something about micro evolution on different parts of the Pareto front.

2.3. Research Flow Diagram

In section 2.1, the five research phases have been discussed. These phases have been summarized in a research flow diagram below (Figure 2.3). The goal of the research flow diagram is to give an overview of the structure of this study, it visualizes how the research phases and methods are linked. The phases will more or less be executed sequentially. However, modelling is an iterative process, which means that it will probably be required to improve on work that has been done, this is indicated by the feedback loop in phase four. It is also possible that an adaption has to be made to work in earlier phases, even though that work does not necessarily corresponds with the current phase.

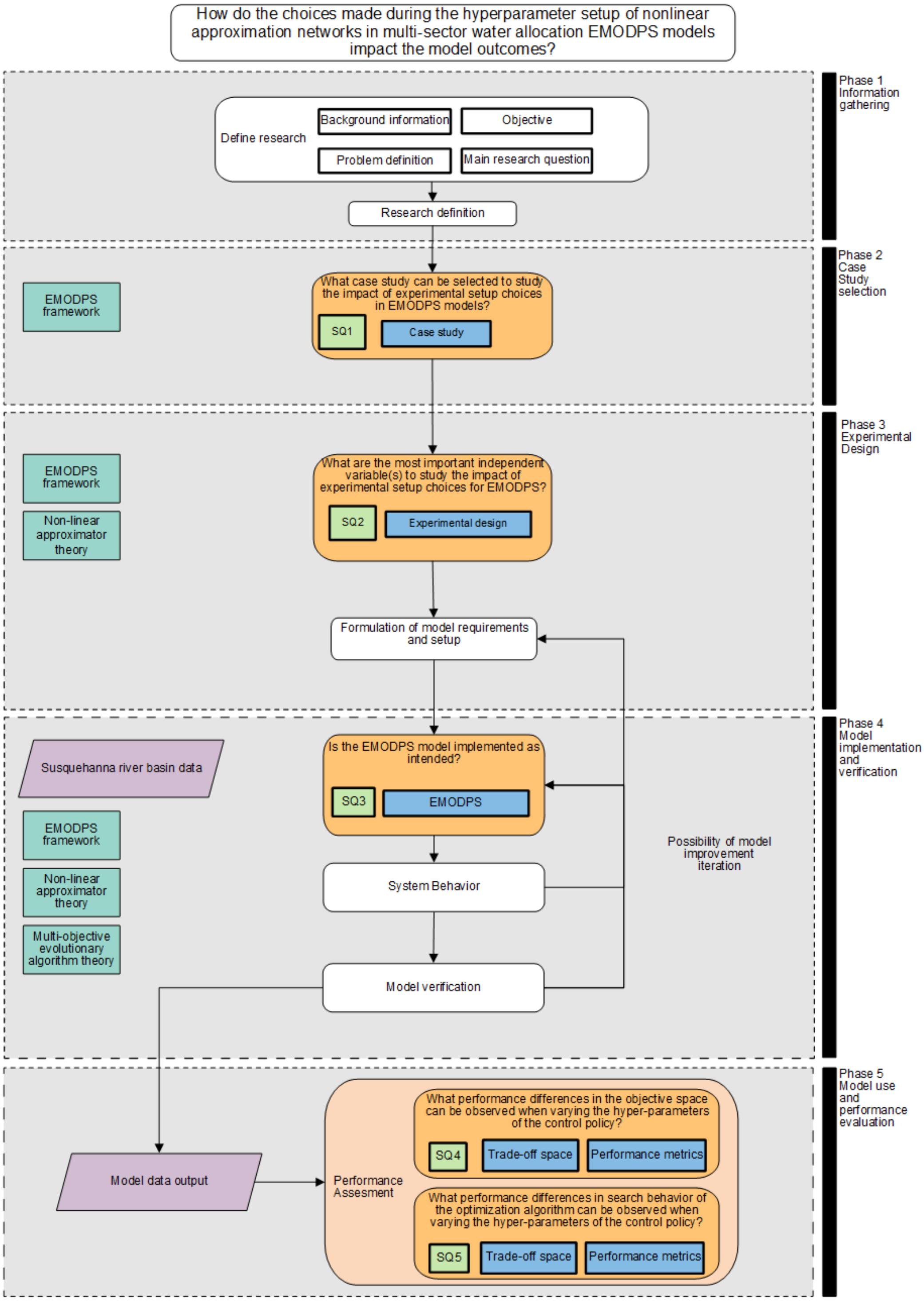

Figure 2.3: Research flow diagram

3

The Lower Susquehanna River Basin Case

3.1. Introduction

In this chapter, the case study that is used for the research is presented. The focus of this chapter is to answer the second sub-research question: *What case study can be selected to study the impact of experimental setup choices in EMODPS models?*. The Susquehanna case contains two basins and six objectives which makes this case highly suitable to be used in conjunction with the EMODPS framework as multi-objective problem. The lower Susquehanna river basin case will be described in section 3.2, followed by the model formulation in section 3.3 where the case characteristics will be explained and all the objectives will be listed.

3.2. Case Description

The exploratory analysis will be based on a case concerning the lower Susquehanna river basin, this case was also used by (Giuliani et al., 2014). The lower Susquehanna river basin encompasses the Conowingo reservoir, an interstate water body shared by the states Pennsylvania and Maryland (Figure 3.1).

The Susquehanna river is the longest river in the eastern part of the United States, providing drainage to an area of almost 71.000 km2 and supplying 50% of the fresh water that flows into Chesapeake Bay. Due to the large amount of water passing this river basin, the largest non-federal hydroelectric dam was constructed in 1928 for power generation purposes. The Susquehanna river basin is known for the presence of numerous stakeholders, which are all dependant on a continuous water supply from the basin. The hydroelectric dam regulates a large part of the water flow of the river basin, impacting all other stakeholders. Currently, the Conowingo dam supplies water to Chester (PA) and Baltimore (MD), as well as cooling water for the Peach Bottom nuclear power station. The downstream releases of the dam are subject to minimum flow requirements which were set by the Federal Energy Regulatory Commission (FERC) to conserve fishing resources. In 1968, the Muddy Run Pumped Storage Hydroelectric Facility was built and connected to the reservoir. The Muddy Run storage facility acts as a battery and can cycle water back and forth from the Conowingo reservoir for additional power generation when required. When the reservoir has a low water level, FERC regulations tend to cause a depletion of storage levels, increasing conflict between the objectives of stakeholders and lowering the recreational value of the system. Water availability is often sufficient

Figure 3.1: Map of the Susquehanna River Basin, highlighted in yellow is the lower Susquehanna River Basin section (Salazar et al., 2016)

in average flow circumstances to supply the hydroelectric operations, water supply, meet environmental flow requirements, and sustain recreational activities. However, in low flow conditions, Conowingo operations face difficult trade-offs in order to supply water to Baltimore, Chester, and the Peach Bottom atomic power station while minimizing negative affects on recreational and touristic interests. (Giuliani et al., 2014)

3.3. Model Formulation

The model is based on the identification and refinement of the Conowingo dam's operating policy. It focuses on defining and optimizing the operating policy for the Conowingo dam, whereas Muddy Run operates according to a predetermined weekly rule. This rule specifies a hydropeaking strategy in which turbines operate during peak energy hours and pumps operate at night and on weekends when energy prices are low.

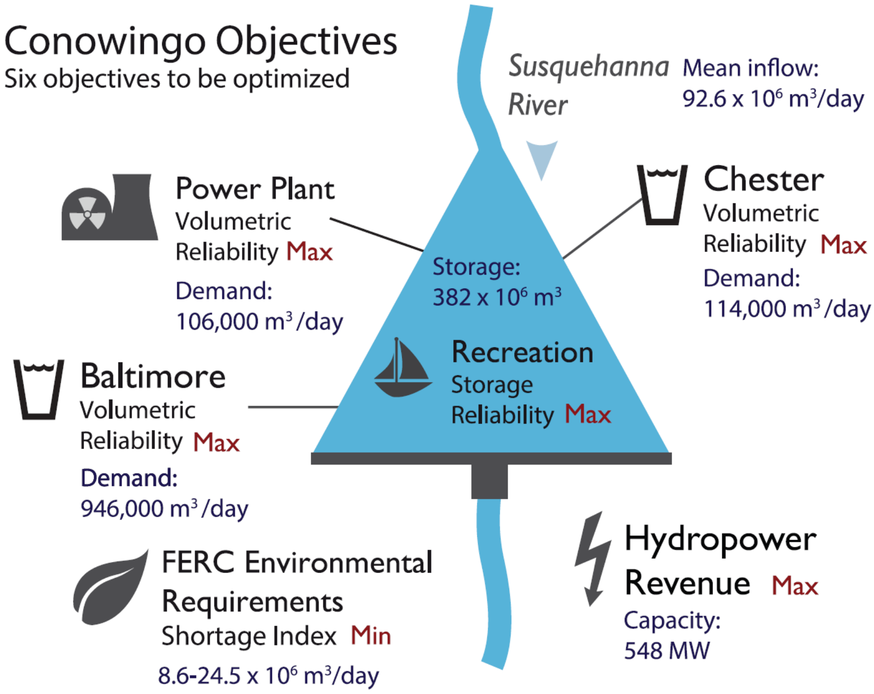

Figure 3.2: Conceptual representation of Susquehanna basin model (Salazar et al., 2016)

The model (Figure 3.2) is primarily based on a depiction of the dynamics of the two water reservoirs as defined by the mass balance equations of the water volume contained in the reservoirs of Conowingo and Muddy Run. The release functions are defined below in equation 3.1:

$$\begin{aligned} s_{t+1}^{CO} &= s_t^{CO} + q_{t+1}^{CO} + q_{t+1}^{CO,L} - r_{t+1}^{CO} - E_{t+1}^{CO} - q_{t+1}^{p} + r_{t+1}^{MR} \\ s_{t+1}^{MR} &= s_t^{MR} + q_{t+1}^{MR} - r_{t+1}^{MR} - E_{t+1}^{MR} + q_{t+1}^{p} \end{aligned} \tag{3.1}$$

Where q_{t+1}^{CO} and $q_{t+1}^{CO,L}$ are the main and lateral inflow to the Conowingo reservoir and q_{t+1}^{MR} is the inflow to Muddy Run. s^i represents the volume of the water stored at each reservoir, where i = Conowingo reservoir or Muddy Run reservoir. The volume r_{t+1}^i which is released between t and t+1 is determined for each reservoir by the release function $r_{t+1}^i = f(s_t^i, u_t^i, q_{t+1}^i, E_{t+1}^i)$. Which depends on the storage s_t^i, the decision u_t^i, the inflow q_{t+1}^i and the evaporation E_{t+1}^i. The water pumped from Conowingo to Muddy Run is represented by q_{t+1}^p. Additional characteristics of the Lower Susquehanna River which are used in the model are described in table 3.1.

Model Objectives

The six objectives described below, are used to simulate the multi-stakeholder interests affected by the Conowingo dam operation. These objectives are modeled over the simulation time horizon of one year. A yearly simulation horizon has been chosen, because of the system's limited regulatory capacity and low dependence on

Conowingo reservoir capacity	310,000 acre-feet (0.38 km3)
Muddy Run capacity	56,731 acre-feet (0.07 km3)
Conowingo dam turbines capacity (13 turbines)	86,000 cfs
Conowingo dam installed capacity	573 MW
Muddy Run turbines capacity (eight turbines)	32,000 cfs
Muddy Run pumping capacity (eight pumps)	28,000 cfs
Muddy Run installed capacity	800 MW

Table 3.1: Lower Susquehanna River Characteristics (Giuliani et al., 2014)

the reservoir levels at the start of the simulation (Salazar et al., 2016).

Hydropower revenue (to be maximized) is defined as the economic revenue gained from hydropower production at the Conowingo hydropower dam in US$/MWh defined in Eq. 3.2. The energy prices are defined by the seven hour moving average of the energy price trajectory in the Pennsylvania, New Jersey–Maryland (PJM) energy market (Exelon, 2010). The hourly energy production (MWh) is defined by Eq.3.3 , where η is the turbine efficiency, g is the gravitational acceleration ($9.81 m/s^2$), γ_w is the water density ($1000 kg/m^3$), $\bar{h_t}$ is the net hydraulic water level difference (head) in meters and q_t^{Turb} is the turbine flow in m^3/s.

$$J^{hyd} = \sum_{t=1}^{H} (HP_t \cdot \rho_t) \tag{3.2}$$

$$HP_t = \eta g \gamma_w \bar{h_t} q_t^{Turb} \cdot 10^{-6} \tag{3.3}$$

Water supply reliability to the Atomic Power Plant, Chester and Baltimore (to be maximized) The daily average volumetric reliability defined as:

$$J^{VR,i} = \frac{1}{H} \sum_{t=1}^{H} (Y_t^i / D_t^i) \tag{3.4}$$

where $Y_t^i (m^3)$ is the daily delivery, $D_t^i (m^3)$ is the corresponding demand, and i represents the water supply to Baltimore, Chester or the Atomic Power Plant. Figure 3.3 illustrates the demand in cubic feet per second for each objective.

Environmental Shortage (to be minimized) specified as the daily average shortage index in regard to the FERC minimum flow requirements, defined as follows:

$$J^{SI} = \frac{1}{H} \sum_{t=1}^{H} \left(\frac{max(Z_t - Y_t, 0)}{Z_t} \right)^2 \tag{3.5}$$

where Y_t (m3) is the daily release and Z_t (m3) is the corresponding FERC flow requirement. The quadratic formulation (Eq. 3.5) is intended to penalize substantial deficits in a single time step while allowing for more frequent, minor shortages (Hashimoto, Stedinger, & Loucks, 1982). Figure 3.3 depicts the monthly water supply demands as well as the FERC minimum flow criteria.

Recreation (to be maximized) defined in Eq. 3.6 as the storage reliability throughout the tourist season's weekends. Given by the relationship between the number of weekend days in the peak season that are less than the intended level (n_F) and the total number of weekends in the tourist season (N_{we}). To ensure recreational activities, the target level is 32.5 m (106.5 ft).

$$J^{SR} = 1 - \frac{n_F}{2N_{we}} \tag{3.6}$$

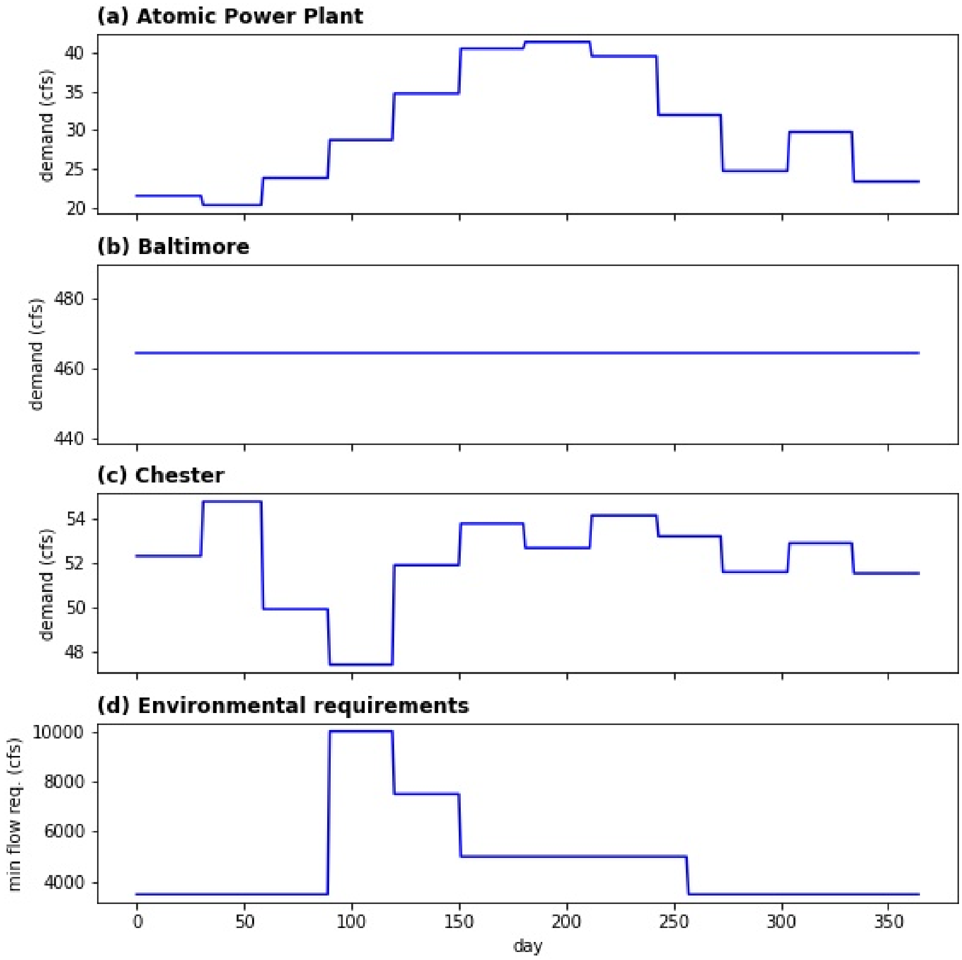

Figure 3.3: Release requirements of objectives

3.4. Conclusion

In this third chapter, the first sub-question is answered:
What case study can be selected to study the impact of experimental setup choices in EMODPS models?
The lower Susquehanna river basin model has been selected as case study. This case is particularly suitable for the usage of the EMODPS framework, since it has multiple reservoirs and multiple objectives. Additionally, the Susquehanna river basin case has been chosen since it is a stylized case study that has been frequently used for other multi-objective optimization studies using EMODPS (Giuliani et al., 2014; Salazar et al., 2016; Doering et al., 2021).

4

Experimental Design

4.1. Introduction

In this chapter, nonlinear approximation networks, and in particular radial basis function networks will be discussed. The focus of this chapter is to answer the second sub-research question: *What is/are the most important independent variable(s) to study the impact of experimental setup choices for EMODPS?*

To be able to answer this sub-research question some additional theory about nonlinear component in EMODPS models is required, which is discussed in section 4.2. Then in section 4.3, it will be elaborated further how radial basis function networks work. In section 4.4 the hyperparameters of radial basis function networks are identified, and it is discussed how they can influence the radial basis function network.

Several hyperparameters of nonlinear approximating networks will be discussed. In the end an experimental design will be established, which will be used in future chapters. The experimental design method gives a better understanding of the factors that influence a particular system. It creates a set of procedures to systematically test a hypothesis and gives a structured overview which factors are to be considered.

4.2. nonlinear approximation networks

EMODPS relies on the nonlinear approximating networks to parameterize candidate operating policies. These nonlinear approximating networks are machine learning techniques where data is combined with a model, to make a prediction. However there are several ways to achieve this. Giuliani, Castelletti, et al. (2016) compared two popular nonlinear approximating networks and found that artificial neural network (ANN) were less effective than Radial basis functions (RBFs) for this application. Therefore, for this research, only RBF networks will be explored as a nonlinear component of EMODPS. RBF networks place an emphasis on retaining as much as possible the linear character of the RBF network, despite the fact that for good generalisation there has to be some kind of nonlinear optimisation. The two main advantages of this approach are that the mathematics are kept relatively simple with linear algebra and the computations are inexpensive because there is no need for optimization by gradient descent algorithms (Orr, 1996). Some technical terms from the field of statistics also apply to machine learning. However, the machine learning field has given new names to already existing concepts in the field of statistics (Sarle, 1994). These terms are summarized in table 4.1 to get more familiar with the concepts used in machine learning.

Machine learning algorithms can be used for several applications, often divided in the categories classification and regression. A task is considered regression if the desired output consists of one or more continuous variables. It's considered a classification if the goal is to assign the input vector to one of several discrete categories (Svensén & Bishop, 2007). The EMODPS framework using the nonlinear approximating network can be considered a regression problem.

A distinction can also be made between supervised and unsupervised learning. Applications in which the training data comprises examples of the input vectors along with their corresponding target vectors are known as supervised learning problems. When the training data consists of a set of input vectors x without any corresponding target values, it is considered unsupervised learning. The goal of unsupervised learning problems might be to discover groups of similar examples within the data (clustering) or determine the distribution of data (density estimation). Finally there is reinforcement learning, where the algorithm wants to perform actions in order to maximize a reward. This will be discovered by a process of trial and error (Svensén

Statistics	Neural networks
model	network
estimation	learning
regression	supervised learning
interpolation	generalisation
observations	training set
parameters	(synaptic) weights
independent variables	inputs
dependent variables	outputs

Table 4.1: Equivalent terms in statistics and neural networks (Orr, 1996)

& Bishop, 2007). The EMODPS method has a reinforcement learning component (within the Multi objective evolutionary Algorithm) and a (un)supervised learning component (within the nonlinear approximating network).

4.3. The Radial Basis Function Network

RBF networks have been demonstrated to be universal approximators. Any continuous function specified on a compact set can theoretically be estimated to a given accuracy by increasing the number of hidden nodes (Hartman, Keeler, & Kowalski, 1990; Park & Sandberg, 1991). Radial basis function Networks (RBFNs) work in a fundamentally different way than other neural network architectures. One of the main differences is that a RBF network always consists of three layers with neurons; an input layer, a hidden layer with a nonlinear activation function and a linear output layer as seen in figure 4.1.

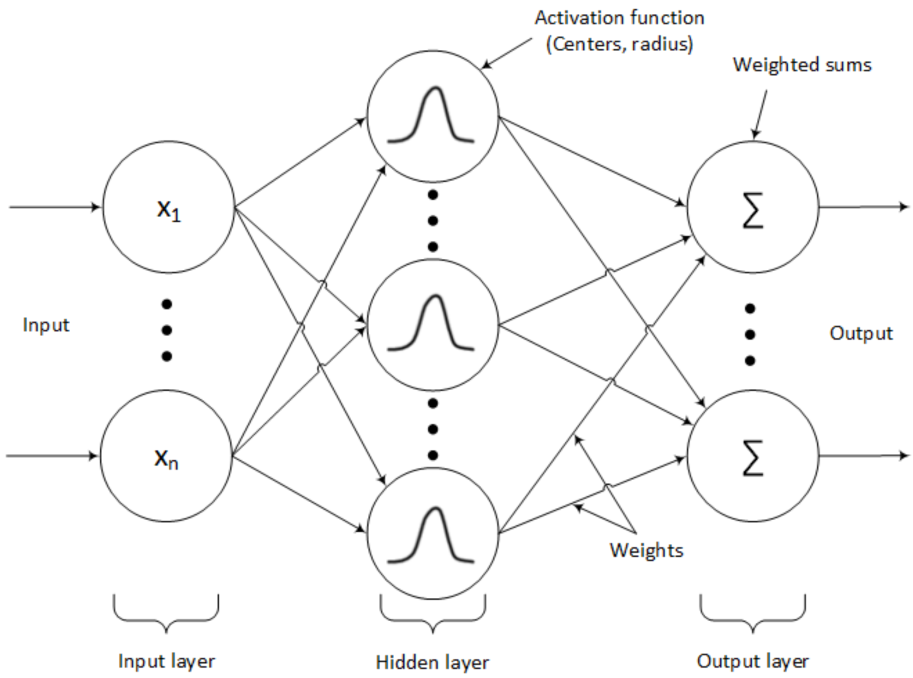

Figure 4.1: Radial Basis Function structure, adapted from (Aggarwal, 2018)

However, unlike feed-forward networks such as Multi-layer Perceptrons, the hidden layer and output layer are trained in another way. The hidden layer is trained unsupervised, whereas the output layer is trained supervised (Aggarwal, 2018). And the hidden layer generally contains more nodes than the input layer. The input layer just pass on the input variables to to the hidden layer. Each neuron in the hidden layer has a kernel function, also known as an activation function, distinguished by a center x_i and radius σ. The essence is to apply locality-sensitive transformations to transform the data points into high-dimensional space, allowing the altered points to be linearly separable (Aggarwal, 2018), as visualized in figure 4.2. This gives a function of the distance between two points, where correlation is high when the points are close together and is low when they are far apart. The output layer consists of a neuron for each output, giving the predicted value by multiplying the sum of the weights with the (euclidean) distance for each RBF. This gives RFBN the ability to handle nonlinear problems.

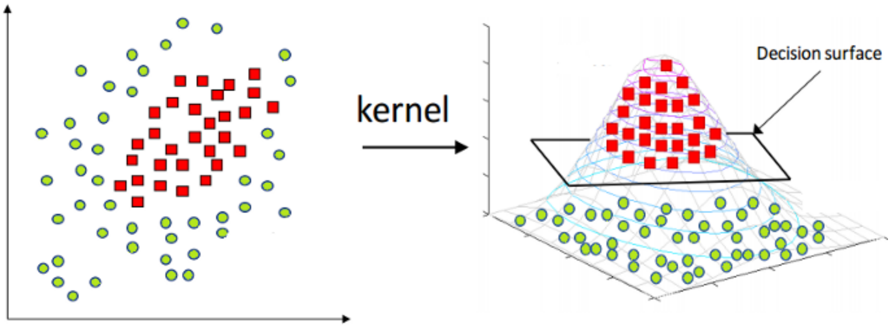

Figure 4.2: Transforming data points to a higher dimensional space (G. Zhang, 2018)

The transformation from the input layer to the hidden layer is nonlinear, whereas the transformation from the hidden layer to the output layer is linear. The vector u_t, given an input vector x, the output of the kth node in the output layer (with $k = 1, ..., N_u$), that implements a sum of basis functions defined on its inputs, can be expressed as:

$$u^k = \sum_{i=1}^{n} w_i^k \phi_i(x_t) \tag{4.1}$$

This computes the variance for every linear combination where **n** is the number of RBFs and $\mathbf{w_i}$ is the weight of the ith RBF ϕ_i. The weights are formulated in such a way that they sum to one (i.e., $\sum_{i=1}^{n} w_i = 1$) and are non-negative (i.e., $w_i \geq 0 \forall i$). The function is only a valid covariance function when its variance is non-negative for every possible choice of **n**. The function models the joint variability of the functions random decision variables. It returns the modelled covariance between each pair in x_a and x_b. $\phi_i(x_t)$ is an activation function. This function is characterized by its center, which is a vector with an equal number of inputs to the node. (Golbabai, Mammadov, & Seifollahi, 2009). The activation function that was used in the Susquehanna case was:

$$\phi_i(x) = \exp\left[-\sum_{j=1}^{m} \frac{(x_j - c_{j,i})^2}{b_{j,i}^2}\right] \tag{4.2}$$

where **m** is the number of input variables **x**, and $\mathbf{c}_i$, $\mathbf{b}_i$ are the m-dimensional center and radius vectors of the ith RBF, respectively. The centers of the RBF must lie within the bounded input space and the radii must strictly be positive (i.e., using normalized variables, $\mathbf{c_i} \in [-1, 1]$ and $\mathbf{b}_i \geq (0, 1]$). The parameter vector θ is therefore defined as $\theta = [c_{i,j}, b_{i-,j}, w_i^k]$, with $i = 1, ..., n$, $j = 1, ..., m$, and $k = 1, ..., N_u$ (Giuliani, Castelletti, et al., 2016).

For a more elaborate explanation of RBF networks I can recommend (Orr, 1996) or (Haykin, 2010).

4.4. hyperparameters

There are several parameters that are able to influence the behavior of the RBF network, but when combining a RBF network with a MOEA such as in EMODPS, not all hyperparameters can be adjusted since they are controlled by the MOEA. The hyper paremeters controlled by the MOEA are Sigma and the Learning rate.

4.4.1. Hidden layer

While RBF networks typically have three layers, the amount of hidden units, or the amount of RBF functions used in the hidden layer can be varied. The number of hidden units is typically larger than the amount of input nodes, but it is never larger than the number of training points. A small radius (sigma) combined with a large number of hidden units increases the model complexity, which is a good configuration when the amount of data is large. To prevent overfitting, smaller data sets require fewer hidden units and a larger radius

(Aggarwal, 2018). The number of RBFs typically depend on the number of input variables that you want to use to inform the control policy.

4.4.2. Sigma

The size of the radius, also known as sigma, is the variance and controls the width of the activation function. The width is important since this determines the significance of the euclidean distance, which is the distance between the center and the input value. In figure 4.3 it can be noted that as sigma increases, the numeric correlation between x and x_i will also be larger (N. Lawrence, 2015). The two points will have a higher chance of correlating with each other when sigma is large, which produces a wider curve than when sigma is small. The radius's size is also determined by the RBF's centers. The radius should ideally be selected so that each point is (primarily) influenced by only a few number of centers, which correspond to its closest clusters. Under-fitting and over-fitting will occur if the radius is set too large or too narrow in comparison to the distance between centers (Aggarwal, 2018).

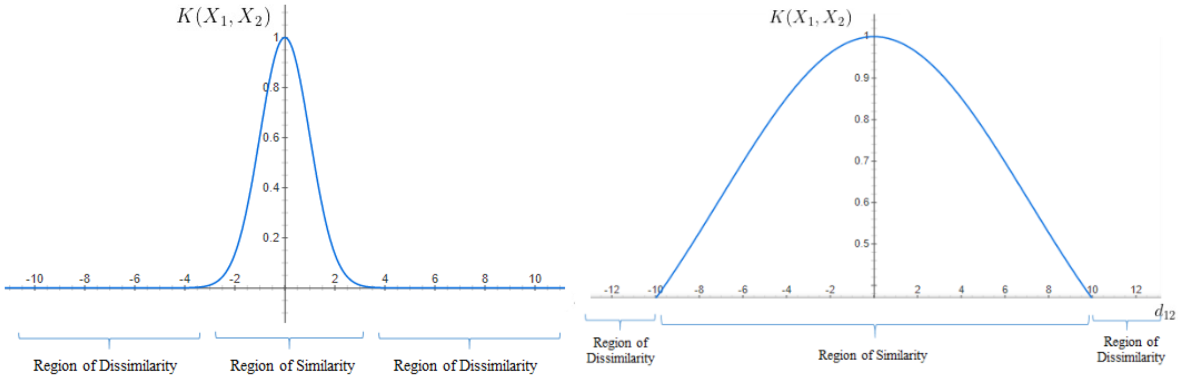

Figure 4.3: Influence of sigma (Sreenivas, 2020)

4.4.3. Learning rate

The learning rate is a hyperparameter that controls how much to change the model in response to the estimated error each time the model weights are updated. The amount by which the weights are changed. Choosing the learning rate is challenging as a value too small may result in a long training process that could get stuck, whereas a value too large may result in learning a sub-optimal set of weights too fast or an unstable training process. In the case of EMODPS, the generation of new weight values by the MOEA. Therefore the learning rate is controlled by the chosen MOEA and cannot be influenced when using EMODPS.

4.4.4. Popular Activation functions (Kernels)

In radial basis functions, the activation functions which are used are radial. Hardy (1990) originally discovered the multiquadric method in 1971 and since then several other activation functions have been developed. Activation functions, also known as covariance functions or kernel functions, come in different forms. Before an activation function qualifies as a radial basis function it has to (1) be classified as at least semi-positive definite and (2) be isotropic which is also described as stationary (Williams & Rasmussen, 2006). Positive definite functions have the property that the function of x is greater or equal to zero for all x, or the function of x is equal to zero if x is equal to zero. The most used activation functions are positive definite since you don't need to define extra parameters to be able to use the function. Activation functions that are stationary or isotropic only depend on the difference between $x - x'$, also known as the euclidean distance. This is different for non-stationary activation functions such as the linear kernel. Which means that if the data is shifted while the kernel parameters remain constant, the corresponding model will yield different predictions (Duvenaud, 2014). Isotropic functions have identical function values in all directions, meaning that they are spherical.

Because of the unknown effect of the use of other activation functions, the type of activation function used will for this research be limited to popular isotropic activation functions. That way the effects of these activation functions have on EMODPS models can be explored. Most books don't mention activation functions other than the Squared Exponential kernel, and sometimes the Gaussian kernel (Aggarwal, 2018; Haykin, 2010; Orr, 1996). However, Fasshauer (2007) created a comprehensive collection of all kinds of basis functions that are frequently used. Additionally, Williams and Rasmussen (2006) also mentioned the Matern activation functions which are also considered to be isotropic and positive definite. As a result, all the popular activation functions which are isotropic and positive definite plus the multiquadric function are shown in table 4.2. By the exploring a selected amount of literature regarding radial basis functions and radial basis function networks, it has been found that the selected functions are most frequently used (Fasshauer, 2007; Schaback, 2007; Askari & Adibi, 2015; H. Zhang, Chen, Guo, & Fu, 2014).

Activation Function	$\phi(r)$	Positive Definite	Source
Susquehanna Model Original	$exp(-\frac{(x-x')^2}{\sigma^2})$	yes	(Giuliani et al., 2014)
Squared Exponential	$exp(-\frac{\|\|x-x'\|\|^2}{2\sigma^2})$	yes	(Williams & Rasmussen, 2006)
Gaussian	$exp-(\sigma * \|\|x-x_i\|\|)^2$	yes	(Fasshauer, 2007)
Inverse quadratic	$\frac{1}{1+(\sigma*\|\|x-x_i\|\|)^2}$	yes	(Fasshauer, 2007)
Multiquadric	$\sqrt{\|\|x-x_i\|\|^2+\sigma^2}$	Conditional (order 1)	(H. Zhang et al., 2014)
Inverse multiquadric	$\frac{1}{\sqrt{1+(\sigma*\|\|x-x_i\|\|)^2}}$	yes	(Fasshauer, 2007)
Exponential	$exp(\frac{-\|\|x-x'\|\|}{\sigma})$	yes	(Fasshauer, 2007)
Matern(3/2)	$(1+\frac{\sqrt{3}*\|\|x-x_i\|\|}{\sigma})exp(-\frac{\sqrt{3}*\|\|x-x_i\|\|}{\sigma})$	yes	(Williams & Rasmussen, 2006)
Matern(5/2)	$(1+\frac{\sqrt{5}*\|\|x-x_i\|\|}{\sigma}+\frac{5*\|\|x-x_i\|\|^2}{3\sigma^2})exp(-\frac{\sqrt{5}*\|\|x-x_i\|\|}{\sigma})$	yes	(Williams & Rasmussen, 2006)

Table 4.2: Commonly used activation functions

Other types of activation functions As mentioned, a function can only be considered a radial basis function if they are isotropic. However, there are also other types of activation functions that can be used as covariance function. For example functions that need a condition before the positive definite properties are valid. Those functions are called conditionally definite positive functions (Fasshauer, 2007). An example of a conditionally definite positive function are polynomial functions. Then there are also compactly supported radial functions cannot be strictly positive definite on Rs for all s, there are no truly conditionally positive definite functions with compact support. They are also non stationary. A popular compactly supported activation function is the Wendland Kernel. These function however, go beyond the scope of this research.

Combining kernels Aside from using activation from literature, it is also possible to combine functions, which gives the ability to create functions that are more fit for purpose for a model. By addition and multiplication of kernels is possible to build a new kernel with more desirable properties (Duvenaud, 2014). For instance, combining kernels makes it possible to add noise to an activation function which could be desirable for some applications. Multiplying is the standard way to combine two kernels. Due to the nature of positive-definite kernels, you will always end up with a positive-definite kernel when two positive-definite kernels are multiplied together. The multiplication of kernels can be thought of as an 'AND' operation. The resulting kernel will have a high value only if both of the two base kernels have a high value. The addition of two kernels can be thought of as an 'OR' operation. The resulting kernel will have a high value if either of the two base kernels would have had a high value (Duvenaud, 2014). However, if one would apply these techniques, a very good understanding is required about the characteristics of activation functions. Without this knowledge, it is very hard to predict how a combined kernel would behave when used as an activation function. Therefore it is not an option within the scope of this research.

4.5. Testing activation functions

Of the RBF kernels described in table 4.2, all are positive-definite except Hardy's Multiquadric kernel. Despite this the multiquadric kernel is guaranteed to produce well-posed systems because it is conditionally negative-definite. However, all activation functions have a negative parabolic shape. Except for the multiquadric kernel, which has a positive parabolic shape. Because of this, it is impractical to be considered as an activation function in a EMODPS model.

The other eight RBFs that were mentioned in table 4.2 were implemented in Python to test if they would behave properly with an EMODPS model. All functions have been plotted with three centers in three different configurations. The inputs of the EMODPS model are normalized and the activation functions used need to be able to cope with this. To check the functions, they were plotted in a 3d space and visually inspected. To do this, the radius σ was varied between 0.05 and 0.15 to showcase the behavior of each function. However, the radius parameter (σ) sometimes posed a problem since the working range of the activation function required to exceed 1 to be able to function as expected. The values of the radius σ had to be normalized between 0 and 1 to function properly with the EMODPS model. Therefore, fore some activation functions, a workaround was required and some activation functions had to be adapted. Additionally, all RBF kernels are implemented with the Euclidean distance as distance measure, except for the Original RBF Kernel since it was implemented differently and it's setup will not be altered so it could also be used as a reference. It was opted to implementation of the Euclidean distance for all other RBF kernels because the working range of the RBFs improved when the Euclidean distance was implemented, another reason was that the Matern3/2 and Matern5/2 kernel did not function properly without the Euclidean distance implementation.

4.5.1. Original Susquehanna Model RBF

The first RBF that was tested was the original RBF $exp(-\frac{(x-x')^2}{\sigma^2})$ as used in the Susquehanna case. This RBF is a modified version of a Gaussian RBF (Giuliani et al., 2014). For ease of reference this activation function will be referred to as the original RBF. This RBF is an adapted version of the Squared Exponential RBF $exp(-\frac{||x-x'||^2}{2\sigma^2})$, the first adaptation is that the original RBF is divided by σ^2 instead of $2\sigma^2$. As mentioned earlier, the second adaptation is that this activation function does not use the euclidean distance to calculate the difference between x and x', but instead just subtracts x and x' to determine the distance. Since this was the way the Susquehanna model was originally configured it's setup will be respected. Figure 4.4 below illustrates the shape of the Original RBF with three different values of the radius σ. The values σ 0,05, 0,1 and 0,15 have been chosen to showcase the range of the radius in which the RBF can operate as expected.

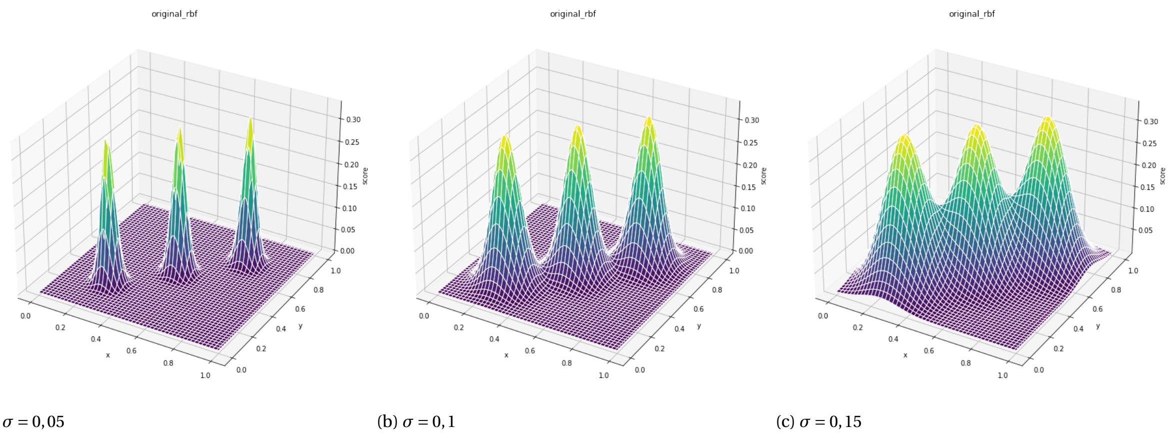

(a) $\sigma = 0,05$

(b) $\sigma = 0,1$

(c) $\sigma = 0,15$

Figure 4.4: Original RBF $exp(-\frac{||x-x'||^2}{\sigma^2})$ with three different radii (σ)

4.5.2. Squared Exponential RBF

The squared exponential kernel has been plotted in Figure 4.5 and is using the Euclidean distance to determine the distance between the input and center values. The figure illustrates that the squared exponential kernel functions properly between the range of 0,05 and 0,15. This means that the squared exponential function is working as expected and can be tested in conjunction with the EMODPS model. It can be noted that the squared exponential kernel looks very similar to the original kernel used in Figure 4.4.

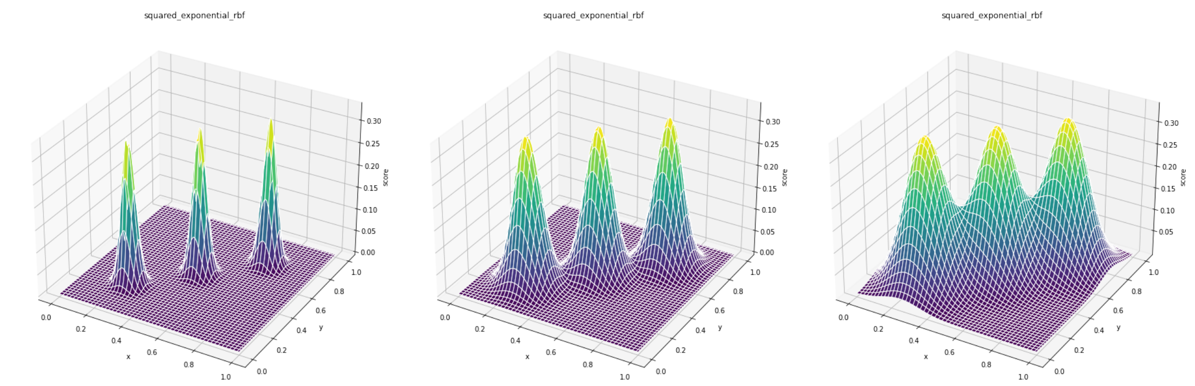

(a) $\sigma = 0,05$ (b) $\sigma = 0,1$ (c) $\sigma = 0,15$

Figure 4.5: Squared Exponential RBF $exp(-\frac{||x-x'||^2}{2\sigma^2})$ with three different radii (σ)

4.5.3. Gaussian RBF

The Gaussian activation function which can be seen in (Figure 4.6, requires the radius σ to be between 5 and 30 to be able to perform well. When the radius is normalized between 0 and 1 it cannot produce a satisfactory outcome, as visualized in figure 4.6a. If the Guassian RBF would have to be adapted to be able to make it work with a radius between 0 and 1. This can only be accomplished easily by dividing by σ instead of multiplying by $sigma$. However if this were to be done, one would get the same equation as the Squared Exponential Kernel. Therefore the Gaussian activation function cannot be used with the EMODPS model for this research.

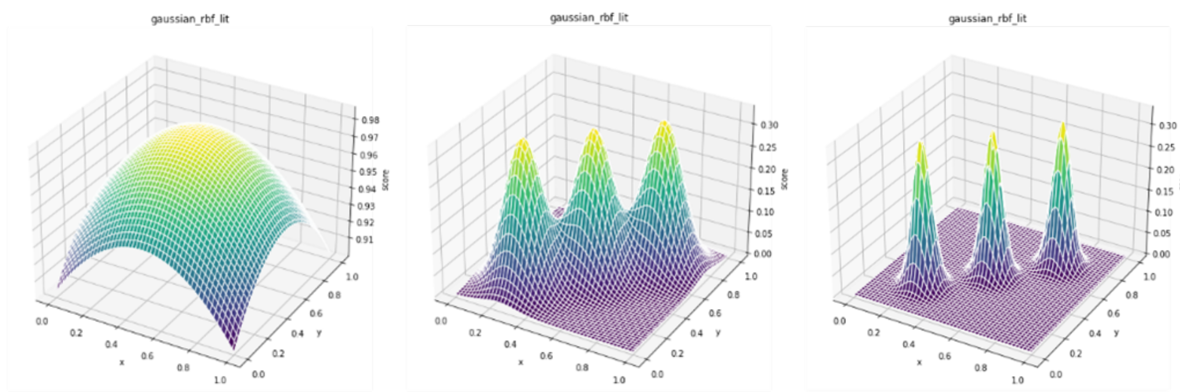

(a) $\sigma = 1$ (b) $\sigma = 5$ (c) $\sigma = 15$

Figure 4.6: Gaussian RBF $exp - (\sigma * ||x - x_i||)^2$ with three different radii (σ)

4.5.4. Inverse Quadratic RBF

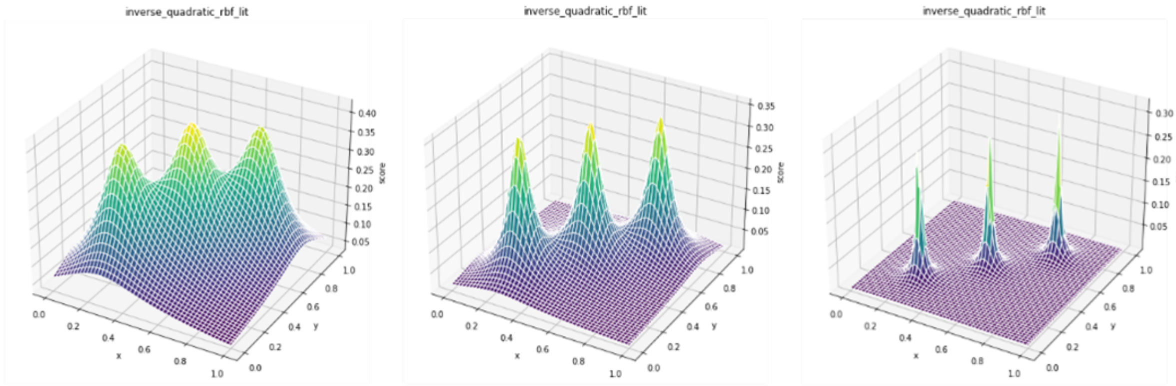

(a) Inverse Quadratic with $\sigma = 5$ (b) Inverse Quadratic with $\sigma = 10$ (c) Inverse Quadratic with $\sigma = 40$

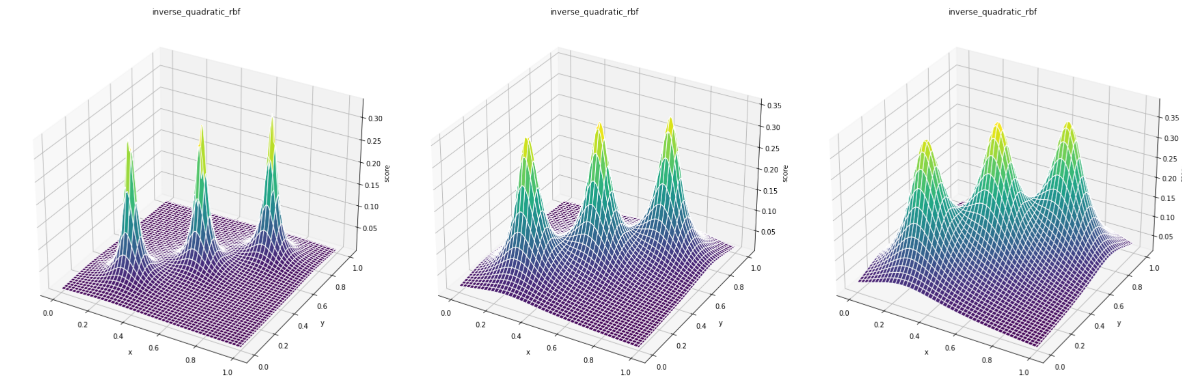

(d) Adapted Inverse Quadratic with $\sigma = 0.05$ (e) Adapted Inverse Quadratic with $\sigma = 0.1$ (f) Adapted Inverse Quadratic with $\sigma = 0.15$

Figure 4.7: Inverse Quadratic RBF $\frac{1}{1+(\sigma * ||x-x_i||)^2}$ and Adapted Inverse Quadratic $\frac{1}{1+(\frac{||x-x_i||}{\sigma})^2}$ with three different radii (σ)

The inverse quadratic activation function has similar problems as the gaussian kernel, as can be seen in Figure 4.7a-c, the function works well with a sigma between 5 and 40, but does not work with a radius between 0 and 1. To be able to use the function in conjunction with EMODPS it has been adapted from $\frac{1}{1+(\sigma * ||x-x_i||)^2}$ to $\frac{1}{1+(\frac{||x-x_i||}{\sigma})^2}$. As illustrated in Figure 4.7d-f the shape of the adapted function looks to be similar to the normal inverse quadratic kernel, the plot in figure 4.7b and e is almost identical. The other figures would also look similar if they were plotted at exactly the right radius value. It can be observed that the adapted version has more distinct peaks when the radius σ decreases, while the base of the peak gets more elevated when σ increases, this is the opposite of the normal inverse quadratic function. Since the MOEA will determine the ideal radius for the RBF, this will probably have no effects on the performance of the activation function. The plot also illustrates that this kernel has a sharper peak and a wider base compared to the original and squared exponential kernel.

4.5.5. Inverse Multiquadric RBF

The inverse multiquadric activation function has a similar problem as the gaussian and inverse quadratic kernel. This activation function also functions properly with a sigma between 5 and 40 as can be seen in Figure 4.8a-c. Just like the inverse multiquadric kernel his function could also be adapted to accept a normalized sigma value between 0 and 1. The inverse multiquadric function was adapted from $\frac{1}{\sqrt{1+(\sigma * ||x-x_i||)^2}}$ to $\frac{1}{\sqrt{1+(\frac{||x-x_i||}{\sigma})^2}}$. The adapted kernel is illustrated in figure 4.8d-f. It can be observed that the adapted version has more distinct peaks when the radius σ decreases, while the base of the peak gets more elevated when σ increases, this is the opposite of the normal inverse multiquadric function, just like the adapted inverse quadratic function. Since the MOEA will determine the ideal radius for the RBF, this will probably have no effects on the performance of the activation function.

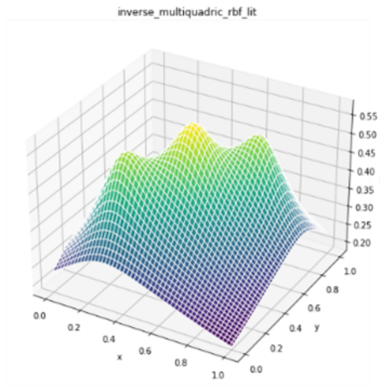

(a) Inverse Multiquadric with $\sigma = 5$

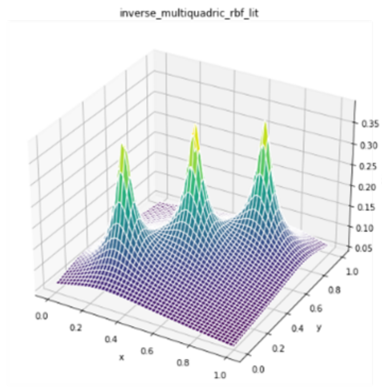

(b) Inverse Multiquadric with $\sigma = 20$

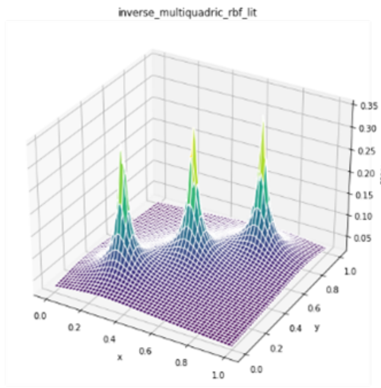

(c) Inverse Multiquadric with $\sigma = 40$

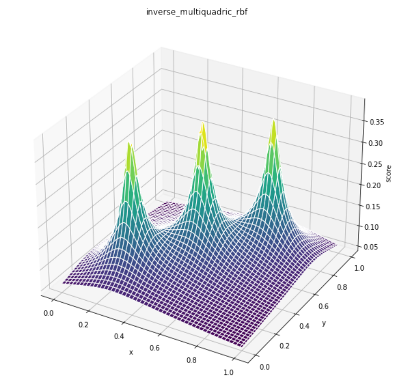

(d) Adapted Inverse Multiquadric with $\sigma = 0.05$

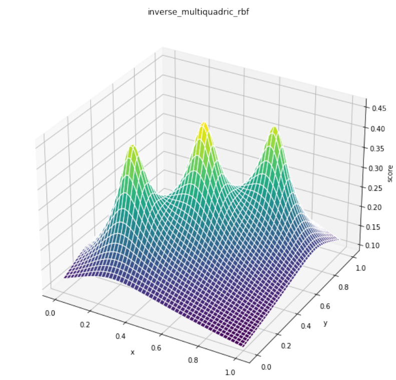

(e) Adapted Inverse Multiquadric with $\sigma = 0.1$

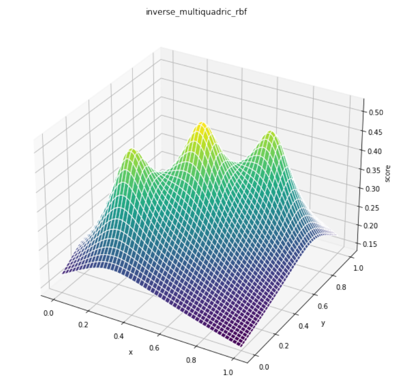

(f) Adapted Inverse Multiquadric with $\sigma = 0.15$

Figure 4.8: Inverse Multiquadric RBF $\frac{1}{\sqrt{1+(\sigma*||x-x_i||)^2}}$ and Adapted Inverse Multiquadric $\frac{1}{\sqrt{1+(\frac{||x-x_i||}{\sigma})^2}}$ with three different radii (σ)

4.5.6. Exponential RBF

The exponential activation function has been plotted in Figure 4.9 and is using the Euclidean distance to determine the distance between the input and center values. The figure illustrates that the exponential kernel functions properly between the range of 0,05 and 0,15. This means that the exponential function is working as expected and can be tested in conjunction with the EMODPS model.

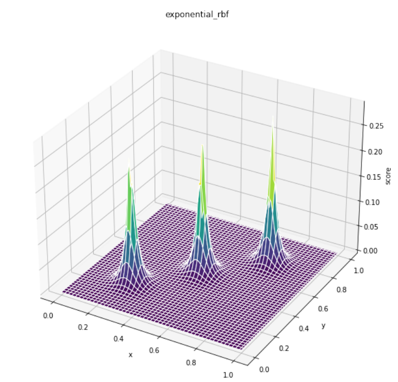

(a) $\sigma = 0,05$

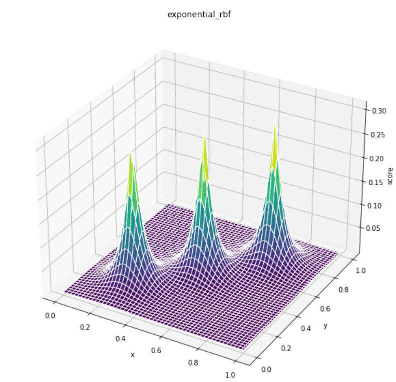

(b) $\sigma = 0,1$

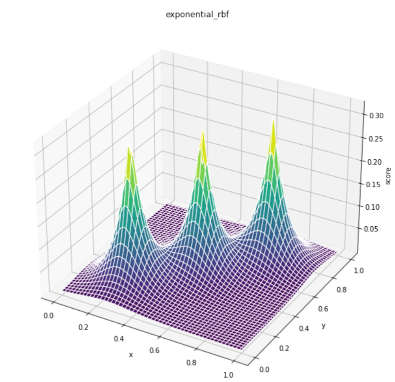

(c) $\sigma = 0,15$

Figure 4.9: Exponential RBF $exp(\frac{-||x-x'||}{\sigma})$ with three different radii (σ)

4.5.7. Matern(3/2) RBF

The matern(3/2) activation function has been plotted in Figure 4.10 and is using the Euclidean distance to determine the distance between the input and center values. The figure illustrates that the matern(3/2) kernel functions properly between the range of 0,05 and 0,15. This means that the exponential function is working as expected and can be tested in conjunction with the EMODPS model. It has to be noted that the matern(3/2) kernel is only isotropic (spherical) when the Euclidean distance is used.

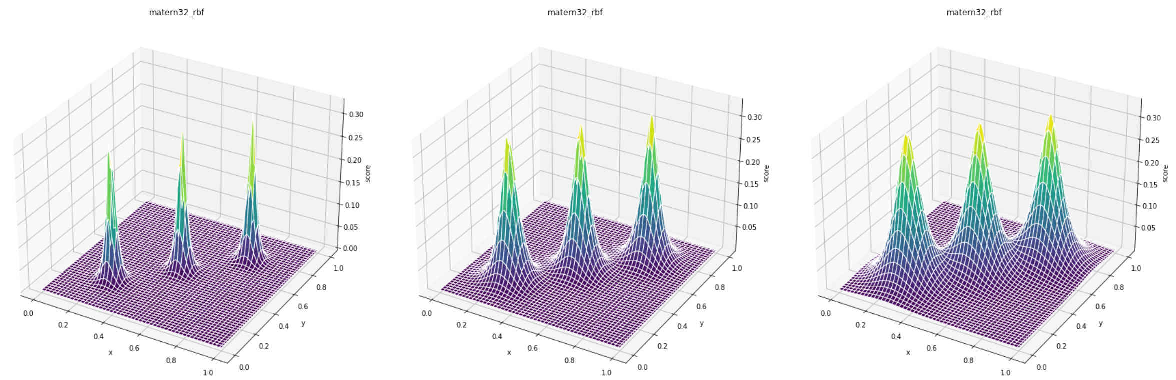

(a) $\sigma = 0,05$ (b) $\sigma = 0,1$ (c) $\sigma = 0,15$

Figure 4.10: Matern(3/2) RBF $(1+\frac{\sqrt{3}*||x-x_i||}{\sigma})exp(-\frac{\sqrt{3}*||x-x_i||}{\sigma})$ with three different radii (σ)

4.5.8. Matern(5/2) RBF

The matern(5/2) activation function has been plotted in Figure 4.11 and is using the Euclidean distance to determine the distance between the input and center values. The figure illustrates that the matern(5/2) kernel functions properly between the range of 0,05 and 0,15. This means that the exponential function is working as expected and can be tested in conjunction with the EMODPS model. It has to be noted that the matern(5/2) kernel is only isotropic (spherical) when the Euclidean distance is used.

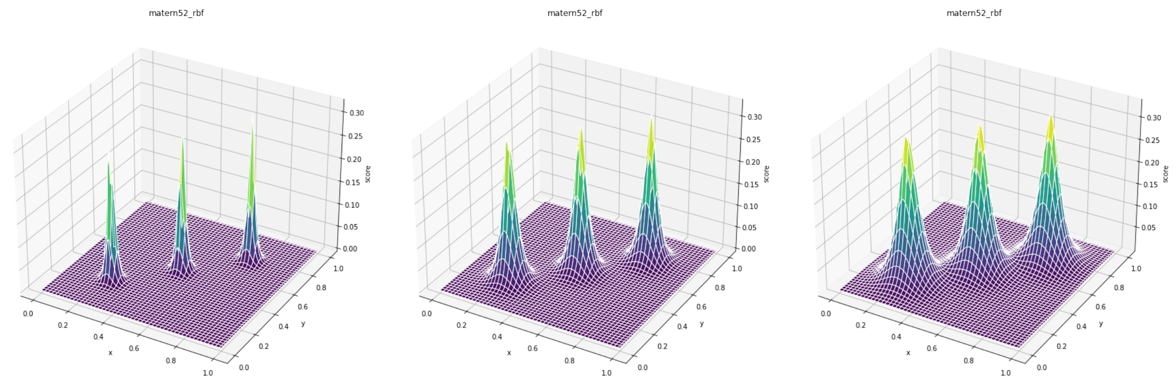

(a) $\sigma = 0,05$ (b) $\sigma = 0,1$ (c) $\sigma = 0,15$

Figure 4.11: Matern52 RBF $(1+\frac{\sqrt{5}*||x-x_i||}{\sigma}+\frac{5*||x-x_i||^2}{3\sigma^2})exp(-\frac{\sqrt{5}*||x-x_i||}{\sigma})$ with three different radii (σ)

4.6. Experimental design

To create the experimental design all activation functions that passed the visual inspection of paragraph 4.4 were selected. Both the gaussian and multiquadric activation functions have been dropped from the selection because they were unable to work in conjunction with an EMODPS model. The kernels that were feasible are popular according to the literature and are all considered well posed and positive definite. The choice has been made to focus on the behavior of positive definite activation functions, and leave compactly supported activation functions and combined activation functions for future research. Aside from the activation functions, the number RBFs used in the hidden layer is also a hyperparameter that could be varied. However, there the number of RBFs typically depend on the amount of input variables. If this hyperparameter would also be varied in conjunction with the activation functions, it would cause the experiment to exponentially grow. To focus the research, the decision has been made to focus the entire experimental design on understanding how the shape of a RBF affects the performance of an EMODPS model, and set the number of RBFs used in the hidden layer as a constant. The hypothesis to be tested by this experimental design is linked to the main research question, and can be formulated as: *The shape of an activation function affects the performance of EMODPS models.*

As established earlier, the outcome of the radial basis function is dependant on the setup of it's hyperparameters. While testing different activation functions the other hyperparameters need to be controlled for each activation function. The amount of RBF functions used in the hidden layer will be kept at a constant amount of 4. The range of the centers, radii (sigma) and weights will be controlled by the MOEA of the EMODPS model, but is operated in a normalized range between -1 - 1, 0 - 1 and 0 - 1 respectively. Because these variables operate in a range, they can be considered to be continuous variables. This configuration is shown in table 4.3.

Activation Function	Number of RBFs	Center (range)	Radius (range)	Weights (range)
Original function	4	-1 - 1	0 - 1	0 - 1
Squared Exponential	4	-1 - 1	0 - 1	0 - 1
Adapted Inverse Quadratic	4	-1 - 1	0 - 1	0 - 1
Adapted Inverse Multiquadric	4	-1 - 1	0 - 1	0 - 1
Exponential	4	-1 - 1	0 - 1	0 - 1
Matern3/2	4	-1 - 1	0 - 1	0 - 1
Matern5/2	4	-1 - 1	0 - 1	0 - 1

Table 4.3: Experimental Design

Because the center, radius and weights are all continuous variables and are varied automatically by the MOEA, the activation function is the only independent variable present in this design. This means that the experimental design is essentially a factorial design with just one level. Since such a factorial design would look exactly the same as table 4.3, it won't add any additional value. To guarantee reproducible results, a seed will be chosen, which will be used for each activation function. A seed guarantees the same starting point for each model run. It's also important to test the functions across different seeds, since changing a starting point can have great impact on the model outcome. Therefore 10 different seeds are used for each function to prevent an accidental bad results. Each experiment will be run until they have reached 100.000 function evaluations (the maximum amount of generations the MOEA will run the many-objective algorithm).

4.7. Conclusion

In this fourth chapter, the second sub-question was answered:
What is/are the most important independent variable(s) to study the impact of experimental setup choices for EMODPS?
It has been concluded radial basis function networks can be influenced by it's hyperparameters. The hyperparameter with the most influence on the control policy that can be varied in an EMODPS setting is the activation function of the radial basis function network. Several popular activation functions have been considered and of those functions seven have been selected to be used for the research on understanding how the shape of an activation function affects the performance of EMODPS. The seven activation functions that have been selected are:
The Original kernel used in the Susquehanna case, the squared exponential kernel, the adapted Inverse Quadratic kernel, the adapted inverse multiquadric kernel, the exponential kernel, the matern(3/2) kernel and the matern(5/2) kernel.

5

Model implementation

5.1. Introduction

This chapter will discuss the implementation of the python EMODPS model. This model will implement the lower Susquehanna river basin case which was previously mentioned in chapter 3. The aim of this chapter is to answer the third sub question of this study: *Is the EMODPS model implemented as intended?*

5.2. Python model

A python multi-objective water allocation model has been implemented of the lower Susquehanna river basin case. The model includes a dynamic mass balance across a historical time series of inflow and evaporation rates, as well as the releases from the Conowingo and Muddy Run reservoirs. Muddy Run is a reservoir located on higher ground, which can be used as storage tank. The hydro power plant takes advantage of intra-daily cycles in energy prices. When energy prices are low, water is pumped uphill from the Conowingo Reservoir into the Muddy Run Reservoir. This water is released during peak hours to maximize the combined system's hydropower profit. (Salazar et al., 2016). The model aims to find good solutions to all objectives by finding the Pareto-approximate operating policies for multipurpose water reservoirs by utilizing EMODPS. EMODPS combines Direct policy search (DPS), a nonlinear approximating network, and a Multi-Objective Evolutionary Algorithm to achieve this. It uses Direct Policy Search (DPS) to first parameterize the operating policy using a given family of functions and then optimize the decision variables with according to the objectives of the model. Since the model is involving multiple objectives, DPS can be coupled with a Multi Objective Evolutionary Algorithm (MOEA). It uses the nonlinear approximating network to calculate the water release for each of objective for every time step of the model, as illustrated in Figure 5.1. The model is implemented as such that each time step represents 6 hours of a day. At the end of each model year the release information is send back to the MOEA to improve evaluate and adjust the decision variables. Because of the reservoir system's limited regulation capacity and low dependence on its initial state (the reservoir levels at the beginning of the simulation), a yearly simulation horizon is used (Salazar et al., 2016). Then the MOEA will start a new model run with updated decision variables in an attempt to optimize the solution further.

5.3. Model parameters

The lower Susquehanna river basin model has several parameters which are used to initialize the model. These parameters can be divided into three categories, model initialization parameters, RBF initialization parameters and MOEA initialization parameters. These parameters are displayed in table 5.1 below.

The model is ran with the default epsilon values, which are mentioned in table 5.1 for each objective. The model also uses the historical data of the worst year recorded. This data has been chosen to clearly expose trade-offs between the objectives in the system. This 365 day period is repeated for each run to be able to optimize the best policy for this period.

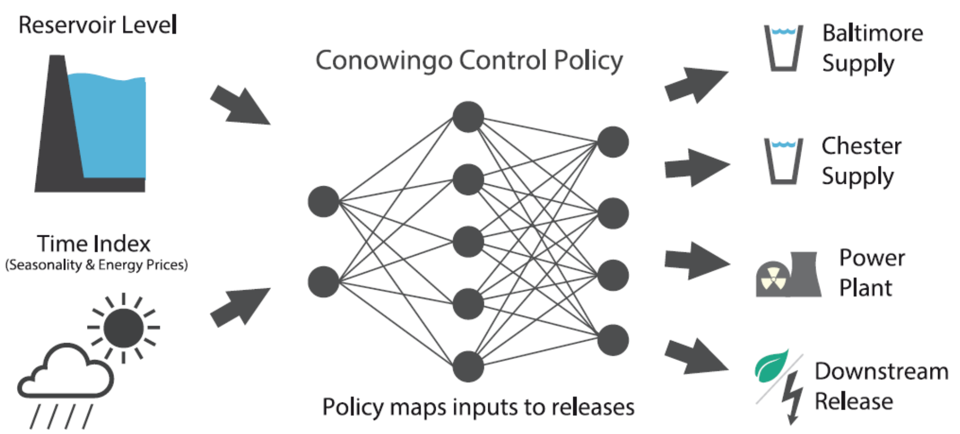

Figure 5.1: Illustration of the control policy represented using the radial basis function. (Salazar et al., 2016)

5.3.1. Nonlinear approximating network

The model is set up to use several different activation functions in the nonlinear approximating network to calculate the water release for each of objective for every cycle of the model, using the reservoir level and time index as inputs. The state of the system (the reservoir level) is coupled to the time index as an input to take the time-dependency and cyclostationarity of the system into account and, consequently, of the operating policy (Bertsekas & Birge, 1976; Giuliani, Castelletti, et al., 2016). The control policy then maps the inputs to releases of each objective, conceptualized in Figure 5.1. The model is configured with 4 outputs, the water supply for Baltimore and Chester, the release for the atomic power plant and the downstream release, which determines the objectives: hydropower revenue, environmental shortage index and the storage reliability index for recreation.

Normalization

When using RBF networks, it's important to normalize numeric input values so that larger values, for example a reservoir level of 300 feet, don't overwhelm small values, such as a time index with a value of 2. Therefore the inputs to the radial basis function of the model have been normalized by dividing the current input by the maximum possible input.

5.3.2. Multi-Objective Evolutionary Algorithm

The Python library Project-platypus is used to operate the DPS and MOEA portion of the EMODPS method. MOEAs are iterative search algorithms that evolve a Pareto-approximate set of solutions. The MOEA generates decision variables for the model to experiment with and incrementally improves these values to search for the Pareto front. Salazar et al. (2016) tested several popular MOEAs using EMODPS (Figure 5.2). Overall the ϵ-MOEA, ϵ-NSGAII and the Borg MOEA demonstrated high levels of performance due to their epsilon dominance-archiving capability. Ultimately the ϵ-NSGAII was chosen to be used with this model, since it has a good trade-off between convergence speed and maximum attained hypervolume.

Epsilon dominance NSGAII (ϵ-NSGAII, (Kollat & Reed, 2005)) is an extension of the original Non-dominated Sorted Genetic Algorithm II (NSGAII, (Deb et al., 2002)). NSGAII is a widely used algorithm in itself and features fast non-dominated sorting technique that can search for the entire Pareto front in a single run. It also uses a crowding distance operator to preserve diversity. Furthermore, the algorithm selects the best performing entities in the algorithm based on a ranking system and crowding distance, this ensures that the best performing entities are most likely to survive. ϵ-NSGAII builds further on this algorithm by including adaptive population sizing, epsilon dominance archiving, and time continuation as part of a limited degree of self-adaptive search. The ϵ-NSGAII algorithm employs a series of linked runs in which small populations are used to prepare search with incrementally doubled population sizes. Preconditioning happens when current solutions from the epsilon-dominance archive are injected into the first generations of larger population simulations. This causes at first small populations to evolve until it seizes to make substantial progress. This will trigger a size increase of the population, where 25% of the new large smaller population consists of archived solutions found by the initial small population, and the remaining 75% are randomly generated to continue

Model initialization parameters	
Initial condition Conowingo basin	108.5 feet
Initial condition Muddy Run	505 feet
Initial start date	5 (friday)
Number of years ran	1 year (historical)
RBF initialization parameters	
number of inputs	2 (time, storage of Conowingo)
number of outputs	4 (Baltimore supply, Chester supply, Power plant supply, downstream release)
number of rbfs	4
MOEA initialization parameters	
Number of objectives	6
Number of function evaluations	100.000
Epsilon hydropower	0.5
Epsilon atomic power plant	0.05
Epsilon Baltimore	0.05
Epsilon Chester	0.05
Epsilon Environment	0.001
Epsilon Recreation	0.05

Table 5.1: Parameters which are used to initialize the model

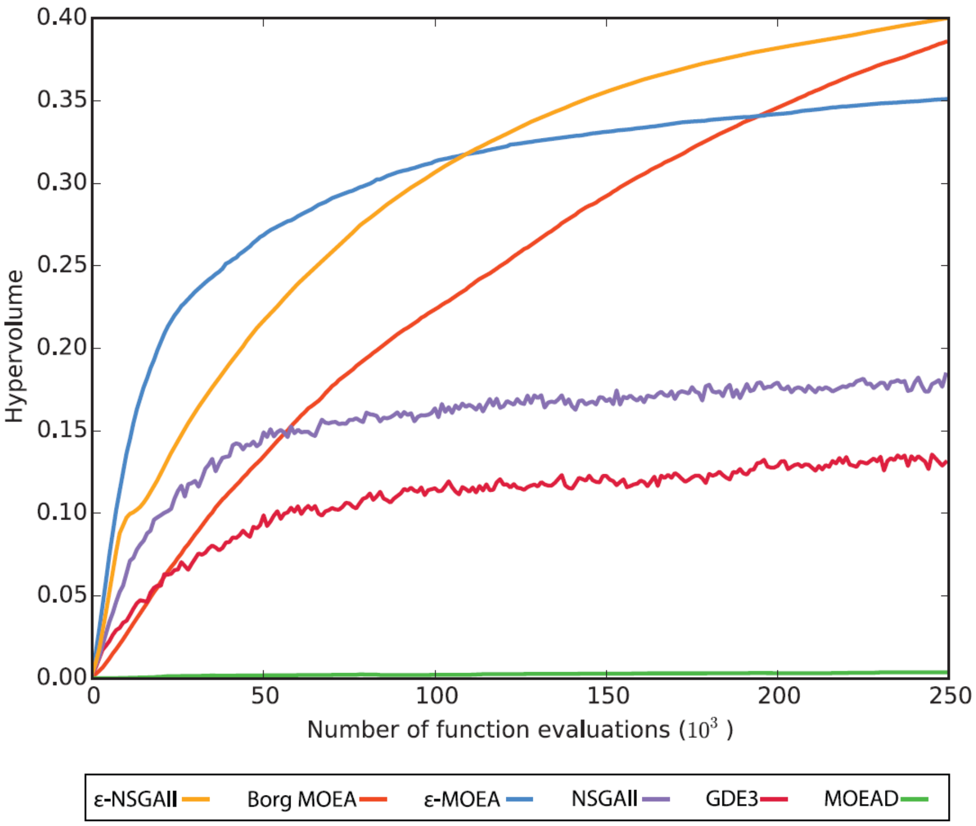

Figure 5.2: MOEAs tested by Salazar et al. (2016)

the search (Salazar et al., 2016).

5.4. Model verification

To verify if the model is functioning correctly the demand together with the release of four objectives have been plotted (Figure 5.3) with the demand on the y-axis and the amount of days on the x-axis. This visually shows the releases of water in cubic feet per second (cfs) as produced by individual solutions over time. When the model starts its optimization process it is still adjusting it's decision variables, this results in sub-optimal releases which can be seen in the lower half of graph 5.3a, b and c. Over time the model adjusts and the releases will start to meet the requested demand which is represented by the black line in each graph. This behavior was expected and suggest that the model properly performs the optimization process and finds better solutions to meet the demand of the objectives. Since it's simulating the worst year where there is a water shortage it is unable to fully meet the demand of all objectives. This figure has been generated for every activation function, this can be seen in appendix A. Additionally the model outcomes (non-dominated solution sets) have been inspected to check if the values appear to be in a range which would be expected. The trade-off space created by the model outcomes has also been inspected to make sure the model does not produce any unexpected results.

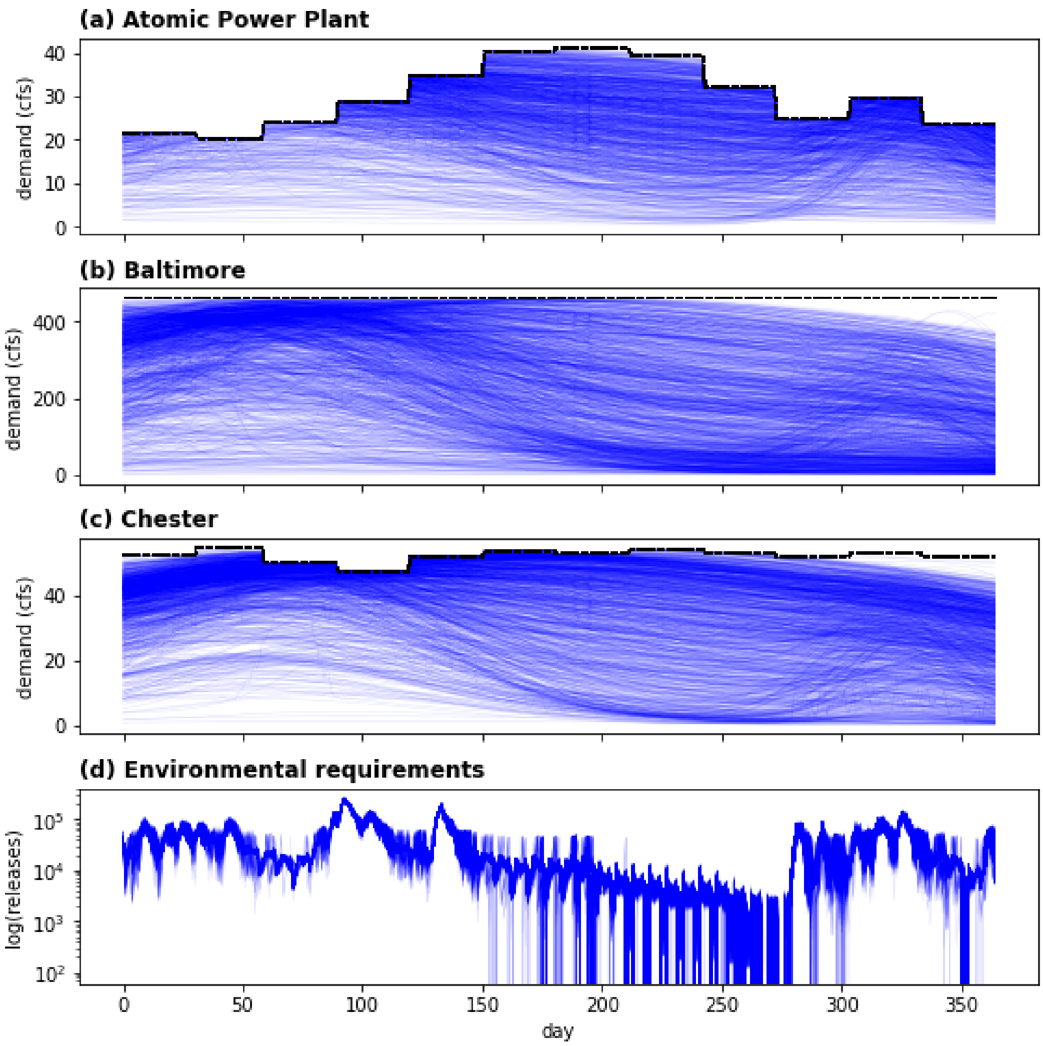

Figure 5.3: Water releases to objectives Original RBF

5.5. Conclusion

In this fifth chapter, the third sub-question was answered:
Is the EMODPS model implemented as intended?
The Susquehanna river basin EMODPS model has been implemented in python and has been expanded to work with several activation functions. The initial model state has been setup according to the experimental design created in Chapter 4. Additionally, ϵ-NSGAII has been chosen to be used as MOEA, since this MOEA had a good compromise between convergence speed and maximum attained hypervolume. To verify the model the outcomes have been checked by order of magnitude. Lastly, the release of water over time to the objectives have also been plotted for all activation functions and have been verified to be proper model behavior (appendix A). The intention was to implement a working multi objective water allocation python model with help of the EMODPS framework which could test the effects of different activation functions to be able to study the model outcomes. It can be concluded that the model has been implemented as intended.

6
Results

6.1. Introduction

This chapter will discuss the results of the experiments that have been performed with several popular activation functions in the EMODPS model performed on the lower Susquehanna river basin case. The aim of this chapter is to answer the fourth sub question: *What differences in performance in the objective space can be observed when varying the hyperparameters of the control policy?* And the fifth sub question of this study: *What differences in the search behavior of the algorithm can be observed when varying the hyperparameters of the control policy?* The results presented in this chapter are derived from variation in the hyperparameter setup of the EMODPS model as described in the experimental design in chapter four. To be able to answer these questions, the EMODPS model results of each activation function specified in the experimental design will have to be interpreted in section 6.2. Visual analytics and common performance metrics (e.g. generational distance, epsilon indicator and hypervolume) are methods that will be used to accomplish this. Then, the earlier interpreted results from 6.2 section will be compared in section 6.3 to be able to determine the performance difference between RBFs. Finally, sub question four and five will be answered in section 6.4. Each tested activation function has been given it's own color that will be used for that function throughout this chapter. The only exception is the parallel coordinate plot where each activation function is greyed out to show the objective space.

6.2. Feature scoring analysis

To check the impact of the different decision variables used, a short feature scoring is performed. Feature scoring is a family of machine learning techniques for identifying the relative importance of various features for a certain outcome or class of outcomes (Kwakkel, 2017). The feature scoring analysis has been performed considering all used decision variables and all model outcomes of interest, with the extra trees algorithm. The analysis is performed for each activation functions to be able to see differences. The results are presented as heatmaps to be able to quickly inspect the highest scoring parameters in Appendix B. It was expected that the radii would be variables with the most impact on the outcomes of interest. While the radii are scoring the highest overall across most functions relative to all other variables, the score is influencing the objectives only slightly more than the other decision variables. The objectives that were most influenced were hydropower and environmental shortage for most activation functions, except for the Matern32 kernel. The outcomes are therefore not as clear cut as initially expected.

6.3. Assessment of the Original RBF performance

In this section, the trade-off space and performance of the original rbf is evaluated. The trade-off space and performance metrics of the remaining six activation functions can be found in Appendix C. All the solutions of the 10 seeds that were generated for each activation function have been combined into a Pareto optimal front (reference set) for each RBF. This has been done using the Pareto.py library, which implements an epsilon non-dominated sorting algorithm to create a Pareto-efficient set. The performance metrics of each RBF are initially generated with their own reference set, containing only the solution sets found by the 10 seeds of said RBF. Therefore the figures in this section of generational distance, additive epsilon indicator and hypervolume can not yet be compared to similar figures of other RBFs. To be able to compare RBFs the metrics would have to be calculated with the same reference set, which will happen in section 6.2. First, the trade-off space is visually inspected in in section 6.2.1. Then, in the following sections, five commonly used performance metrics for multi-objective optimization (generational distance, additive epsilon-indicator, hypervolume indicator, epsilon progress and archive size) are discussed with respect to the overall best known approximation of the true Pareto front. This true Pareto front has been obtained as the set of non-dominated solutions from the results of the 10 optimization runs of the 10 seeds. Multiple metrics are required, since multi-objective optimization requires convergence to the Pareto-optimal set and preservation of variety in the Pareto-optimal set solutions. These two tasks cannot be appropriately quantified using a single performance metric (Deb et al., 2002).

6.3.1. Visualization of trade-offs

First, the trade-offs are visualized with a parallel coordinates plot (Figure 6.1, which highlight the trade-off space between objectives. This figure is accompanied by a box plot (Figure 6.2) which has been generated with the same data.

The trade-off space of the reference set of the Original RBF can be seen in Figure 6.1. Each line represents a potential policy choice (a solution set of 6 objectives) that was found by the model, with lines closer to the top of the y-axis scoring more favorable. The objectives are hydropower ($/MWh), water supply reliability to the atomic power plant, Baltimore and Chester, the daily average shortage index for the environmental shortage and the storage reliability of the water level for recreation. The environmental shortage objective is to be minimized but has been inverted in these figures to make them easier to interpret. This particular parallel coordinates plot is scaled between the maximum and minimum value found for this RBF. The maximum extreme solutions for each objective are represented by a colored line, to be able to better visualize trade-offs. All other solutions are greyed out to illustrate the full objective space.

When inspecting the plot closely it can be noted that two solutions have been found that score high on the objectives: hydropower revenue, atomic power plant demand, Baltimore demand, Chester demand and recreation. While scoring relatively low on the environmental shortage index. These two policies were found by selecting the maximum solution for the objectives atomic power plant and Baltimore. The only objective where this policy is scoring low, is on the environmental shortage index. When inspecting the maximum solution of the environmental objective almost the exact opposite is true, scoring high on both environment and recreation while scoring low on all other objectives. This indicates a clear trade-off is between the environmental shortage index and the other objectives.

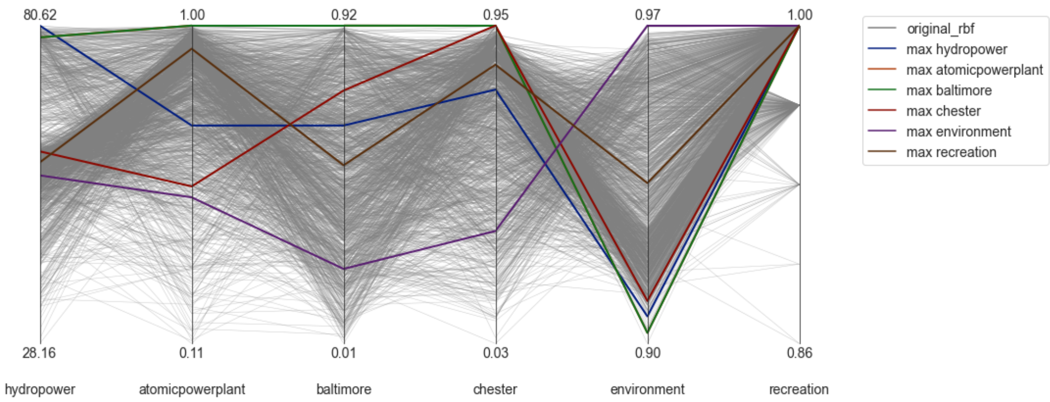

Figure 6.1: Parallel Coordinates plot Original RBF

The purpose of Figure 6.2 is to better understand the distribution of the trade-off space of the Original RBF's pareto set. The hydropower objective has been normalized in this figure to be able to compare it more easily to the other objectives. The Atomic power plant, Chester and Baltimore are all demand reliability objectives. When comparing these objectives it can be noted that the water supply reliability for Baltimore, and to a lesser extent, Chester, are unable to achieve a reliability of 100% for the majority of policies. These objective are therefore harder to meet. The environmental shortage index scores between 90 and 97% reliability for this RBF, however, this is a bit misleading since this objective has to process a lot more water flow compared to the other objectives, this means that a deficit of 5% in reliability is still a lot of missing water which would be able to cause a shortage. When looking at the spread of the objectives, it can be noted that the original RBF has found a large trade-off space containing a wide range of solution sets. This is especially visible for the objectives atomic power plant, baltimore and chester, where solutions were found ranging from close to 0% reliability to almost 100% reliability.

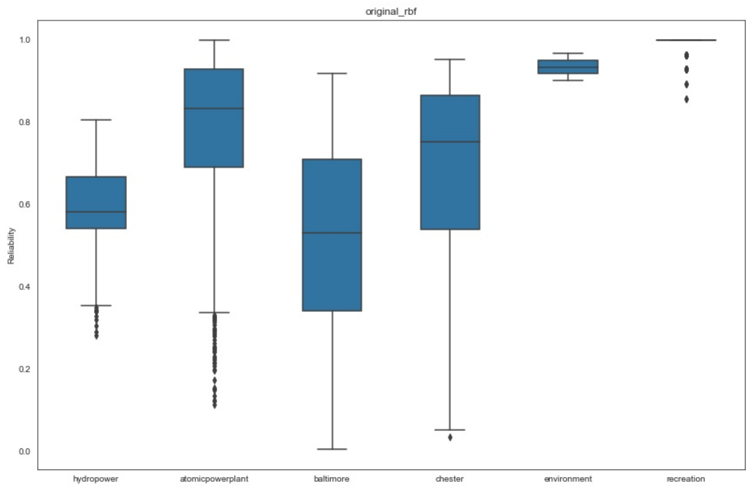

Figure 6.2: Boxplot Original RBF

6.3.2. Generational distance

Generational distance measures the average Euclidean distance between the points in an approximation set and the nearest corresponding points in the reference set. The metric measures the average of these distances. It is considered an easy metric to meet, but is useful to include to make sure that none of the activation functions are failing to optimize for the Pareto set. In a situation where only one solution set is close to the reference set, the Generational Distance metric would indicate a good performance. Since this metric directly measures the distance between the approximation set and the reference set a lower score is considered better. Figure 6.3 below shows the generational distance on the y-axis across the number of function evaluations (nfe) on the x-axis for 10 different seeds. All seeds start with a generational distance value of approximately 0,20 at the beginning of the optimization. This then drops rapidly to very low values at the end of the run. Figure 6.3 illustrates that all 10 seeds of the model were able to fairly quickly attain one or more points near the reference set. Resulting in a low generational distance score for all seeds.

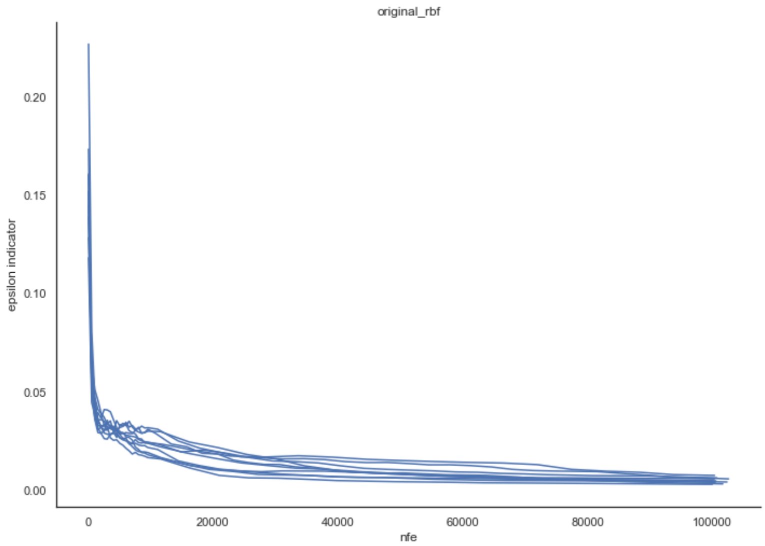

Figure 6.3: Generational Distance Original RBF per generation across 10 seeds

6.3.3. Additive Epsilon Indicator

The additive epsilon indicator (Zitzler et al., 2003) assesses consistency, where consistency refers to Pareto approximate sets that capture all aspects of trade-offs. This is also referred to as diversity. This metric is extremely sensitive to gaps in the Pareto approximate sets. Because of this sensitivity it is considered a harder metric to meet than for instance generational distance. If any gaps are found the value of the additive epsilon indicator will increase. Low values are therefore desirable for this metric. Figure 6.4 illustrates the epsilon indicator plotted across the amount of function evaluations for the original RBF across 10 seeds. All seeds start at the beginning of the optimization run with a value between 0.6 and 1. The additive epsilon indicator slowly improves until the optimization stops at 100.000 function evaluations. It can be noted that the epsilon indicator is fluctuating between high and low values, sometimes pretty drastically. This can be explained by new found solution sets that dominate previously found Pareto sets, but are less diverse. The lack of diversity creates gaps in the Pareto front which causes a larger additive epsilon value.

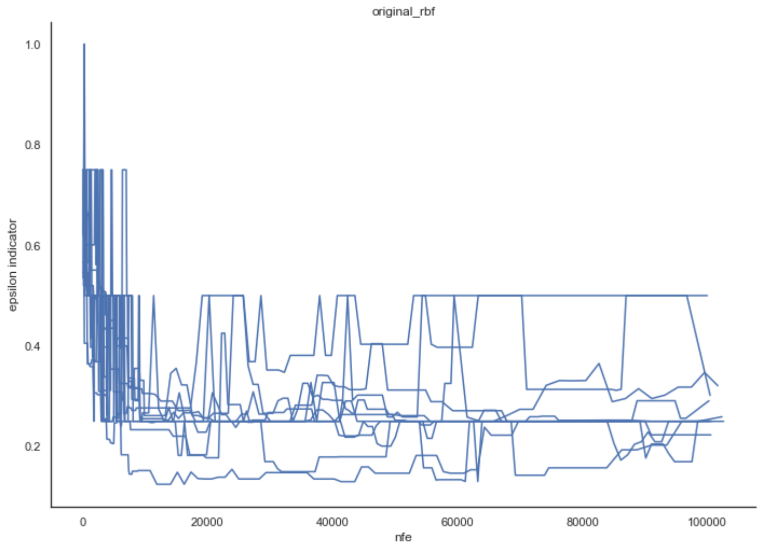

Figure 6.4: Additive epsilon indicator Original RBF per generation across 10 seeds

6.3.4. Hypervolume indicator

Hypervolume is the volume of objective space dominated by a given set of solutions. By computing the archive's hypervolume for each iteration, progress can be tracked (Kwakkel, 2019). The hypervolume indicator takes into account both proximity and diversity (Zitzler et al., 2003). Because both proximity and diversity are needed for this metric to perform well, it is considered the hardest metric to meet. It accomplishes this by examining the multidimensional "volume" formed by each set in relation to a reference point. The volume created by the objective space that is dominated by the approximation set. The more volume dominated the better, therefore this metric is to be maximized. Convergence can also be determined by looking at the trend of the hypervolume indicator plotted across the number of function evaluations. When the subsequent solutions are no better than the preceding set of solutions, a MOEA is said to have "converged" at a solution. That is, you have arrived at the best set of solutions that are achievable (Lau, 2021). Figure 6.5 illustrates the hypervolume performance per generation across 10 seeds. The Original RBF kernel is successful in converging since the hypervolume is able to stabilize for almost all seeds. There is still a trend upwards noticeable for some of the seeds, so the hypervolume will probably not be fully converged yet. However, it did gain a lot of hypervolume relative to the starting point of the optimization process. It can be noted that some seeds had a bad starting point, were unable to catch up, and could therefore not reach a higher hypervolume in 100.000 function evaluations compared to the other seeds.

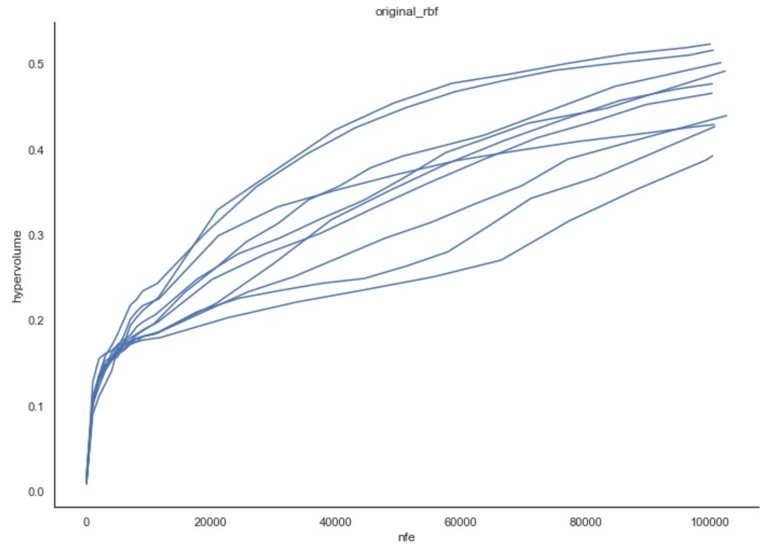

Figure 6.5: Hypervolume Original RBF per generation across 10 seeds

6.3.5. Epsilon Progress

ϵ-progress is a indication of search progression and stagnation (Salazar et al., 2016). When the current solution sits in a different ϵ-box that dominates the previous solution, ϵ-progress occurs. It establishes a minimal threshold (ϵ) in order to avoid search stagnation. If two solutions are found that reside in the same ϵ-box, the solution closest to true Pareto front will be kept, while the other will be discarded (Lau, 2021). The fewer new solutions are added, the closer to convergence. When interpreting Figure 6.6 it can be observed that all seeds are fairly close together, and that there is a steep trend without much indication that the model would stop making progress. This indicates that the model with the Original RBF is still attaining epsilon progress even though the hypervolume was in the process of converging. This could be explained by gaps in the Pareto set that are being filled in, creating a more diverse Pareto set. This would not add much hypervolume but would improve the coverage, which will show an increase in the size of the archive, which can be verified in Figure 6.7. If these gaps were filled in. A lower epsilon indicator value (Figure 6.4) is also expected to indicate a decrease in gaps in the Pareto set. However this is harder to verify, while some seeds do indeed get a lower additive epsilon indicator value around 90.0000 - 100.000 nfe, there are also other seeds which increase in additive epsilon indicator value.

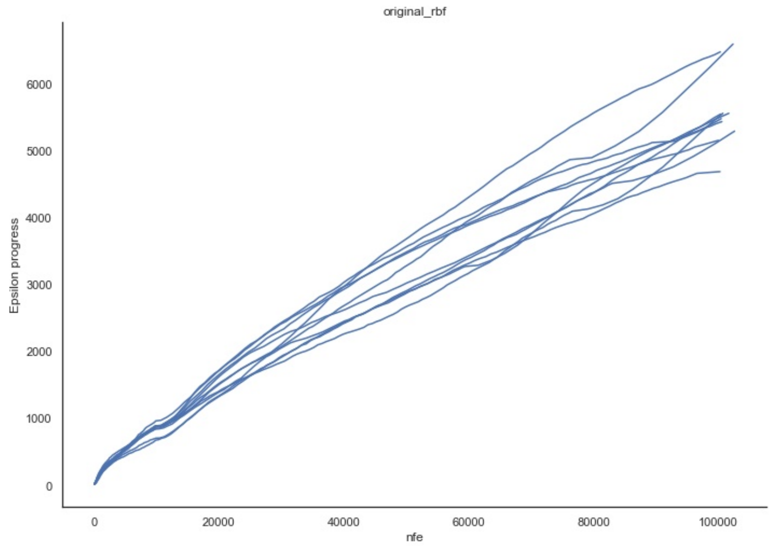

Figure 6.6: Epsilon Progress Original RBF per generation across 10 seeds

6.3.6. Archive Size

The Archive size is the amount of non-dominated solutions that the archive holds. Tracking archive size can give a more complete image of the objective space. A bigger archive size can be beneficial, but this can only be argued when both convergence and diversity are also high. The archive size can also tell something about the search behavior of the algorithm, when there is a drop in archive size, this means that the algorithm is diversifying somewhere. Then the algorithm is able to collapse again, because it made epsilon progress. It therefore tells something about micro evolution on different parts of the Pareto front. Figure 6.7 shows the archive size progress for the original RBF, it slowly increases per generation for all seeds. The largest archive size of 1200 is twice as big as the smallest archive is of 600. Less non-dominated solutions in the archive isn't necessarily bad, since quality of the Pareto sets is also important.

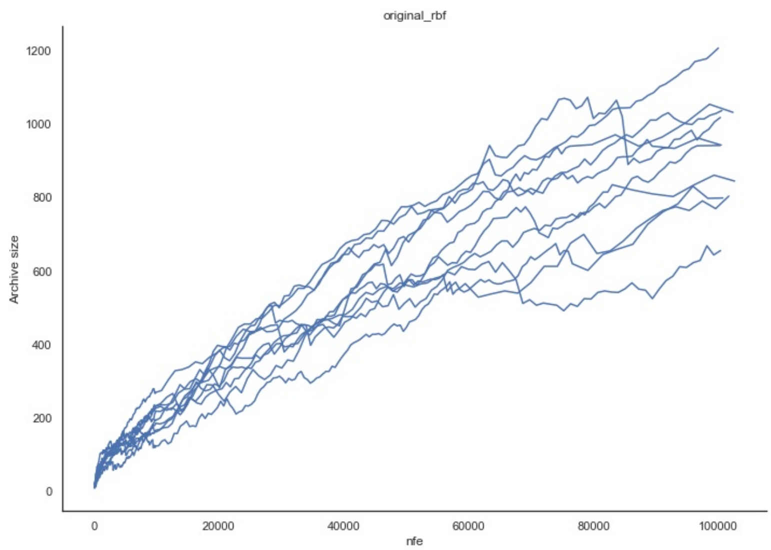

Figure 6.7: Archive size Original RBF per generation across 10 seeds

6.4. Comparison of trade-offs and performance metrics

In this section, the trade-offs and performance metrics of the earlier discussed activation functions are compared. The first figures in section 6.3.1 are highlighting the trade-off space for each activation function. These parallel coordinates plot and associated boxplot in section 6.3.2 can be compared directly since the figures can be plotted directly without being calculated relative to the reference set. In section 6.3.3 a full overview is illustrated of all performance metrics. However, the performance metrics of each activation function were all calculated relative to their own a reference set in section 6.2. To be able to compare these metrics, an all encompassing reference set across all 70 seeds and activation functions has been created. The Figure 6.10 in section 6.3.3 has been generated with this reference set. The set contribution of each activation function to the global reference set can be found in table 6.1.

6.4.1. Parallel Coordinates compared

In this section the all parallel coordinates plots of the seven tested activation functions have been plotted side by side (Figure 6.8). Each plot has been given a color corresponding with their RBF.

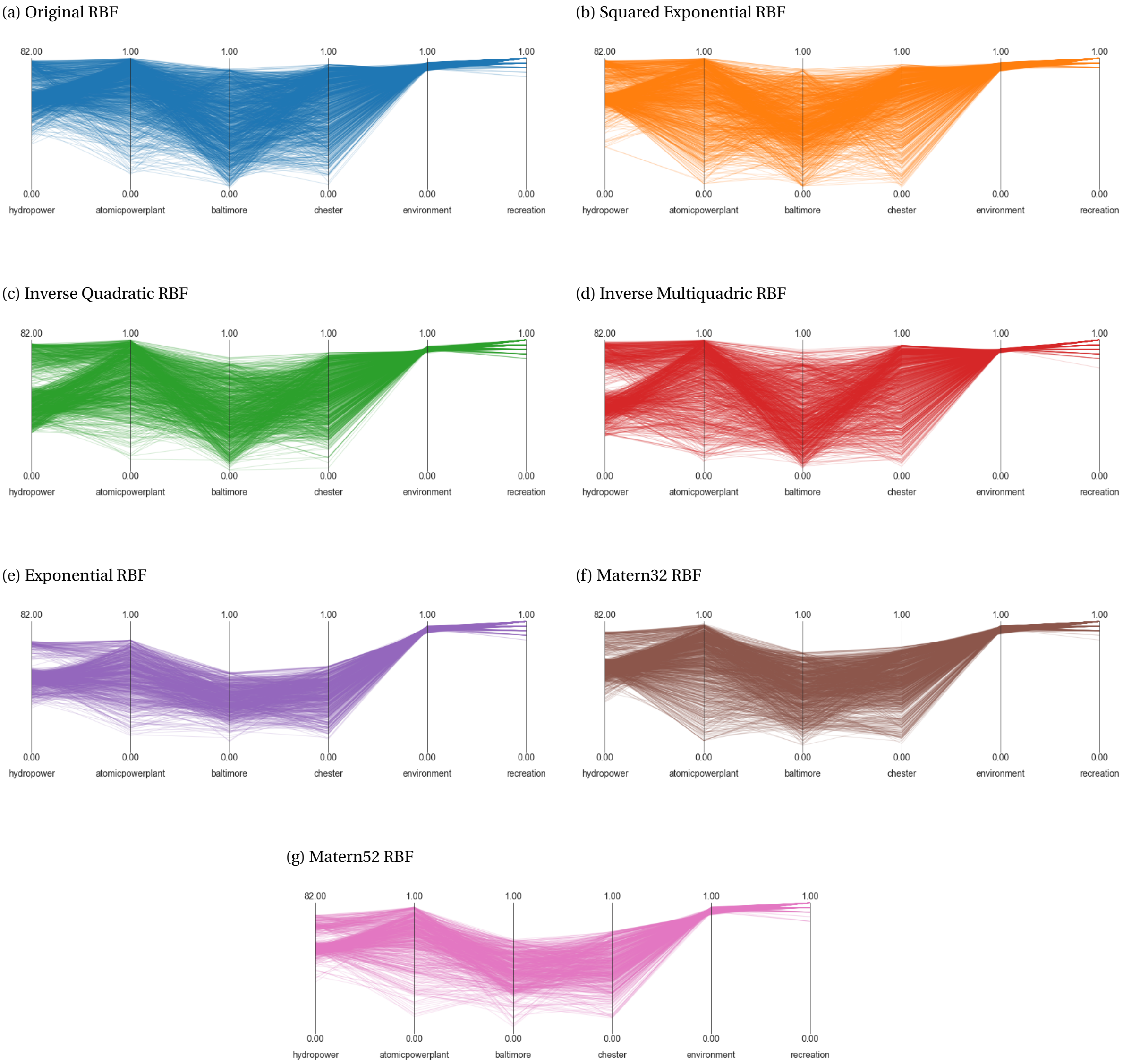

Figure 6.8: Parallel coordinates compared

The y-axis of the parallel coordinate plots have also been adjusted to be equal for every plot, this way it is easier to see the differences in the trade-off space between activation functions. When comparing the trade-off space it can be noted that the original RBF, the squared exponential RBF and the inverse multiquadric RBF in Figure 6.8a,b,d are performing quite well creating a diverse solution space. This is most desirable since decision makers have more possible trade-offs to work with. The inverse quadratic RBF in Figure 6.8c is performing slightly worse but is still finding quite a diverse set of solutions. However, the Exponential RBF, Matern32 kernel and Matern52 kernel in Figure 6.8e,f,g are performing a lot worse relative to the other activation functions, finding a very narrow set of solutions. This is an indication that the exponential RBF, Matern32 kernel and Matern52 kernel have more difficulty traversing the fitness landscape, causing the approximation set to be less diverse.

6.4.2. Boxplots compared

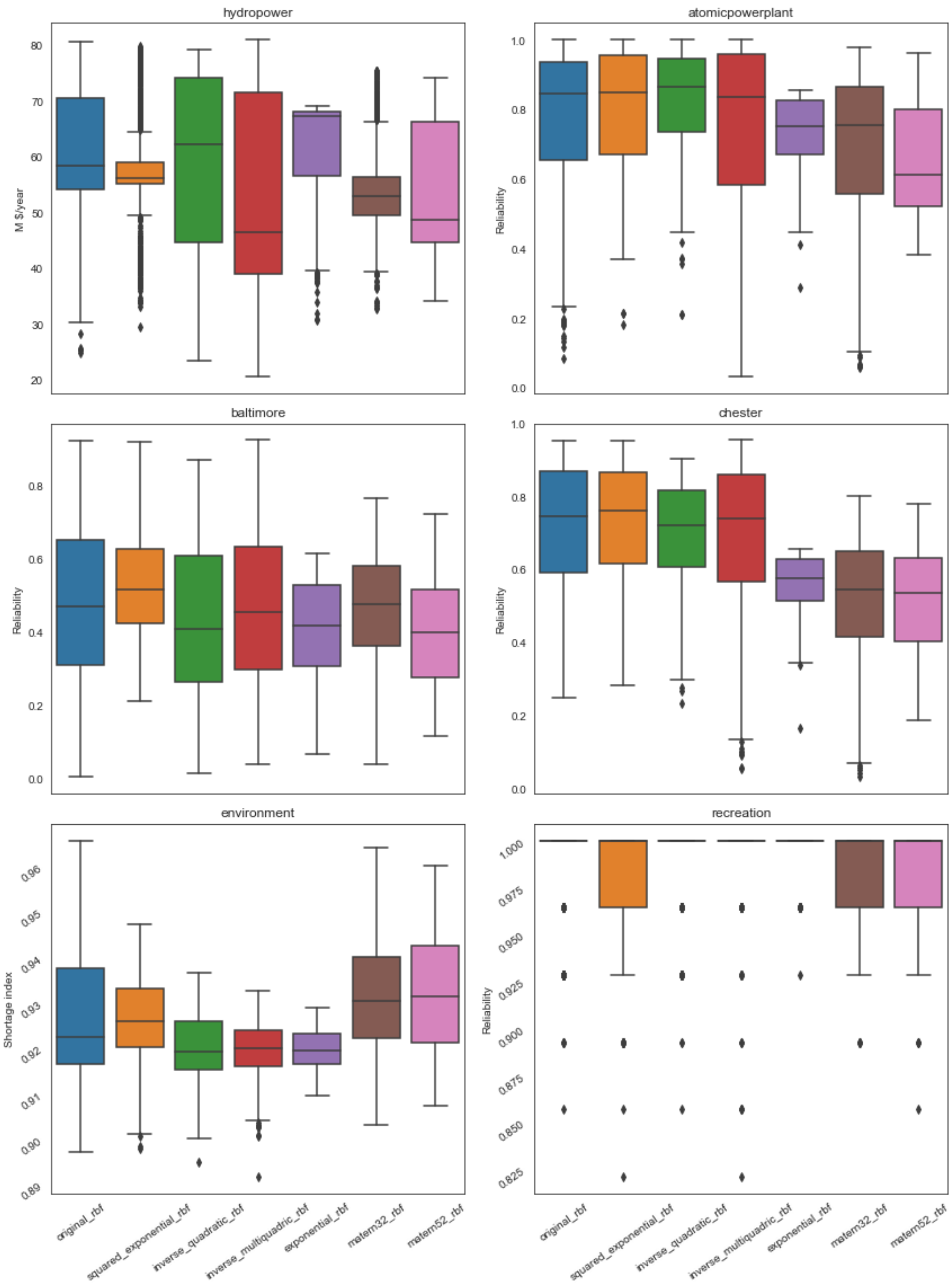

Figure 6.9: Comparing RBFs per objective

Just like the parallel coordinate plots, the boxplots of the trade-off space can also be compared. This time each objective is plotted separately, with each pane containing the same objective and the distribution of every activation function for that objective (Figure 6.9). The figure displays a similar story as the parallel coordinate plot in the previous section. However, in this plot the difference between the seemingly similar performing original RBF, squared exponential RBF and inverse multiquadric RBF can be seen more clearly. This is especially noticeable for the hydropower, baltimore, environment and recreation objectives. The performance differences for each objective will briefly be discussed.

Hydropower revenue
What immediately stands out is the comparatively short boxplot of the squared exponential rbf. Most of the scores of this rbf are located between 65 and 50 M $/year. It does achieve more solutions with higher and lower performance, but these scores are outliers. The inverse multiquadric rbf finds the biggest range of solutions for hydropower, followed by inverse quadratic and the original RBF.

Atomic power plant demand reliability
Most activation functions are able to achieve a good score on this objective, only the exponential rbf is clearly lacking. The inverse multiquadric has the biggest boxplot for the objective, followed by the original RBF and the matern32 kernel.

Baltimore demand reliability
For this objective, the boxplot of the squared exponential is again relatively short compared to the others, but it does manage to find good scoring solutions, unlike the exponential, matern32 and matern52 kernel which are clearly lacking.

Chester demand reliability
The exponential, matern32 and matern52 perform poorly for the Chester objective, not finding the best possible solutions. While the others find decent scores for this objective. The inverse multiquadric finds the biggest range again, while the inverse quadric does not manage to find the high score the other three did manage to find.

Environmental Shortage index
The original RBF finds the biggest range for the environmental objective. Curiously the inverse multiquadric rbf finds just a small range compared to the other objectives, and is unable to identify the better scoring options for this objective. It's also interesting that the Matern32 and matern52 kernels do find a good range of solutions for this objective. This could be explained by the trade-off that was found between the environmental objective and the other objectives in section 6.2.1.

Recreation storage reliability
For this objective there it can be noted that there are some activation functions that do not find lower scoring solutions. Especially the exponential RBF is missing outliers hat the other functions did find.

There are big differences between the Pareto sets that were found. Some activation functions such as the squared exponential, generally find high scoring solutions for the objectives, but do not find lower scoring alternatives for the objectives. Others such as the exponential, matern32 and matern52 kernel generally do not find the best possible solutions for most objectives. This does mean that certain kind of trade-offs are apparently not identified by all activation functions, and are therefore influencing the decision making process. The activation function that finds diverse amount of Pareto sets according to this figure is the original RBF.

6.4.3. Performance metrics compared

Figure 6.10 is a summary overview of all performance metrics that were plotted for each activation function. As mentioned before, the metrics in Figure 6.10 have been calculated relative to a "global" overarching reference set that was generated from the non-dominated solutions from all 7 tested activation functions across 10 seeds. Which makes it possible to compare them. The performance metrics across activation functions generated with the global reference set are discussed below:

Generational distance compared

The generational distance is the easiest metric to meet so there is not much difference to be discovered between the activation functions. It can be noted that overall the original RBF attained the lowest generational distance. And there seems to be one seed of the matern32 kernel that does not come as close as the other seeds to the true Pareto front.

Additive epsilon indicator compared

As mentioned earlier, the additive epsilon indicator measures gaps in the Pareto front. The graphs are a bit more outspoken than the generational distance since it is a harder metric to meet, nonetheless, most activation functions average around 0.35. There are some interesting differences to be noted when looking at the this metric. First off, the graphs look different compared to when the activation functions were plotted individually. This is because the epsilon indicator is calculated in reference to the global reference set. The global reference set is a better True Pareto front since it contains all the non-dominating solutions of all activation functions. Therefore gaps are likely to increase for activation functions that contributed less to the global reference set. A good example of this is the inverse multiquadric RBF where the epsilon indicator values increase by almost 0,2. Both the original and squared exponential activation function seem to perform good in terms of epsilon indicator, which means they found likely found the most diverse approximation sets that contain the least gaps in reference to the true Pareto front. The inverse quadratic, exponential and matern32 kernels have a very large spread, with both higher and lower values, indicating that some seeds have managed to find diverse approximation sets, and other haven't. This suggests that there is a local optimum present where some of the seeds of these activation functions can't escape. It might also be something weird in the fitness landscape. There is also one seed of the matern52 kernel which has an epsilon indicator score close to 1. This is hard to explain since the other seeds seem to perform normally.

Hypervolume progress compared

When comparing the maximum attained hypervolume it is clear that the original and squared exponential activation function made much more progress than the other five functions. While the exponential RBF attained the absolute lowest hypervolume. The seeds from the original and squared exponential RBF are also a more spread out than the other functions. This is especially true for the inverse quadratic, inverse multiquadric and exponential RBF, Which can suggest that the fitness landscape as produced by these functions is less sensitive to search through the random seeds that were used. What is curious is that the hypervolume from the inverse quadratic and inverse multiquadric are both relatively low compared to the original and squared exponential RBF, given that they did find a seemingly large and diverse objective space. This could be explained by the lower score on the environment objective for both these activation functions, creating a big gap in the objective space. This can also explain the higher epsilon indicator scores for both these functions.

When the trends of the hypervolume progression are compared, it can be noted that the inverse quadratic, inverse multiquadric and exponential rbf have almost fully converged in terms of hypervolume. The matern32 and matern52 kernels are also starting to flatten out. However in terms of epsilon progress they are not quite there yet. While there is still a clear upward trend visible for the original and squared exponential RBF. When given enough function evaluations these two functions might find even better approximation sets.

Zooming in on the hypervolume panel of the squared exponential RBF. This plot shows two seed where the line stabilizes and then picks up again around 25.000 and 50.000 nfe respectively, this could be explained as a second evolutionary drive. This suggests that the search space as produced by the squared exponential might be a bit tougher to search through compared to the original RBF. This also confirmed by the additive epsilon indicator, which is a bit messier and has a higher overall score, averaging the seeds, compared to the original RBF. However, a second explanation could be that those seeds were temporarily stuck in the local optimum, and were able to recover after some time.

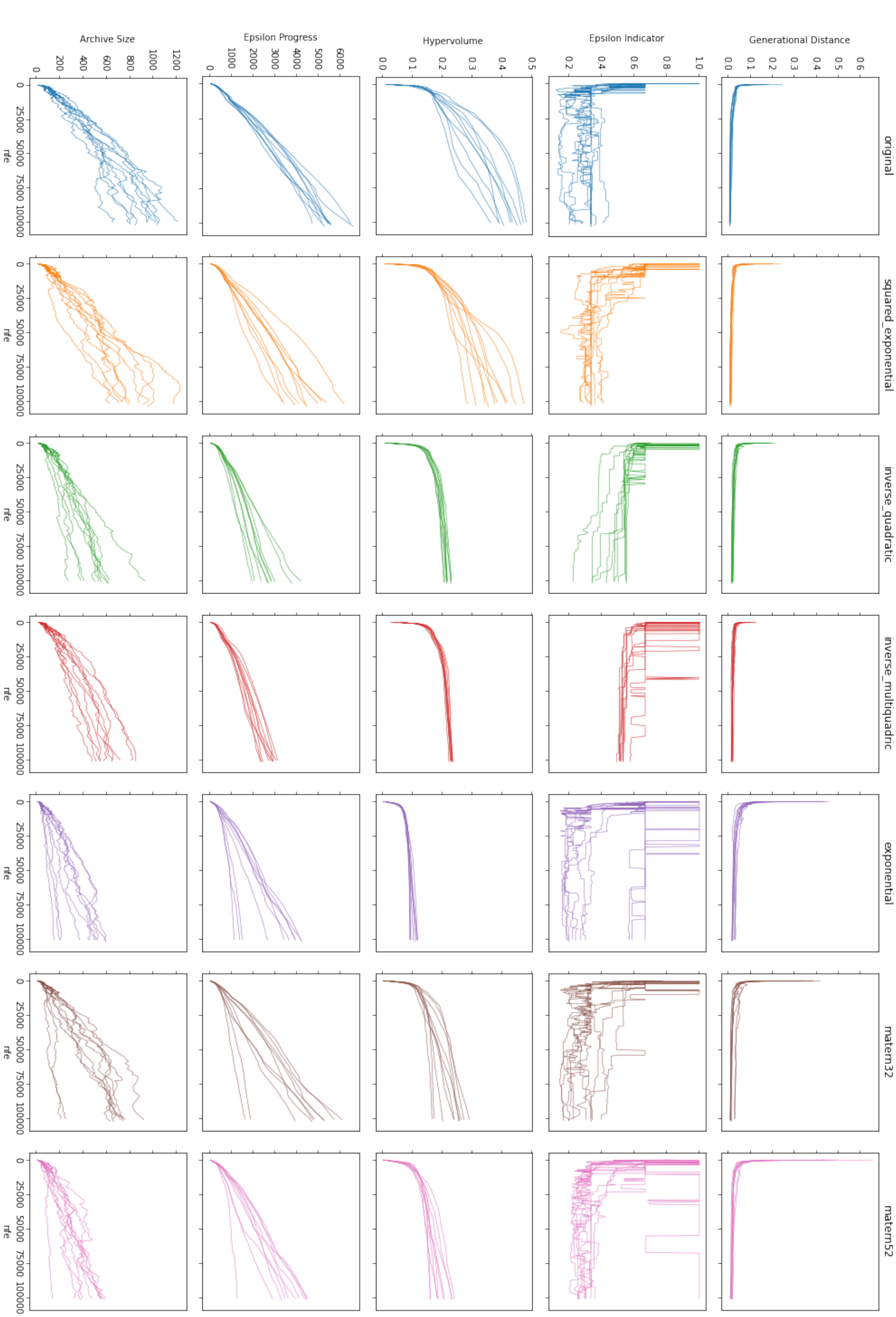

Figure 6.10: Comparison of hypervolume, Additive epsilon indicator and generational distance of different RBFs

Epsilon Progress
Epsilon progress is still being made by all activation functions, indicating that neither of the functions are fully converged yet. However there are some activation functions that are very close, especially the inverse quadric and inverse multiquadric. This indicates that given more function evaluations most activation functions would have found a more complete approximation set. However, given the time it took to run 100.000 nfe, it the activation functions have converged enough to draw compare their performance.

Archive size
When comparing the archive size it can be noted that the archive size of the original and squared exponential are significantly bigger than the others. It's also visible that in the inverse quadratic, inverse multiquadric, exponential, matern32 and matern52 kernels all have a very similar archive size. Only the original and squared expontial have a larger archive size, and thus have found more solutions. Given the epsilon indicator and hypervolume progress it can be concluded that these two activation functions have managed to find a bigger and more diverse approximation set.
On a final note, in most plots there seem to be 2 stable regions that present themselves, in some plots more visible than others. This also hints towards a earlier mentioned local optimum, the original and squared exponential seem to be able to handle this better while the inverse quadratic, inverse multiquadric and exponential could be stuck in it. Other MOEA's might handle local optima differently. This is interesting to test with future research.

Activation Function	Non-dominating solutions	Generational distance average	Epsilon indicator average	Hypervolume average	Set Contribution
Original	1514	0.005	0.308	0.426	56%
Squared Exponential	1357	0.007	0.337	0.378	28%
Adapted Inverse Quadratic	1266	0.016	0.425	0.216	4%
Adapted Inverse Multiquadric	1157	0.014	0.522	0.229	10%
Exponential	946	0.019	0.343	0.102	0.1%
Matern3/2	1294	0.012	0.269	0.234	1%
Matern5/2	857	0.011	0.362	0.196	2%

Table 6.1: Average best attained performance metrics per activation function

Table 6.1 has been made to summarize the results of Figure 6.10. It features the average of of the ten seeds of the maximum (or minimum) attained value of the generational distance, epsilon indicator and hypervolume for each activation function. This way the performance can be more easily compared in a table for quick reference. The contribution of each activation function to the global reference set is also presented in Table 6.1. This represents the amount of non-dominated solutions which are present in the global reference set which were generated from the model with that activation function. As can be seen in the table, the Original RBF contributed by far the most (56%) to the global reference set, followed by the squared exponential RBF (28%).

6.5. Kruskal-Wallis and Mann-Whitney tests

A Kruskal-Wallis and Mann-Whitney test have been performed in Appendix D. The maximum attained hypervolume results for every activation function were compared to check if they were statistically similar. Additionally, the all results for each objective for all activation function have been compared, to see if any of the activation functions produced similar data samples for an objective. Some test were considered similar based on the H value of the Kruskal-Wallis test, however, none of these tests were considered to be statistically significant.

6.6. Conclusion

In this sixth chapter, the fourth sub-question was answered:
What differences in performance in the objective space can be observed when varying the hyperparameters of the control policy?
And the fifth sub-question, was answered:
What differences in the search behavior of the algorithm can be observed when varying the hyperparameters of the control policy?

6.6.1. Performance in the objective space

When comparing the trade-off space it could be noted that the original RBF, the squared exponential RBF were performing well, finding a large and diverse objective space. The inverse quadratic RBF and inverse multiquadric RBF are performing slightly worse but is still finding quite a diverse set of solutions. However, both the hypervolume and epsilon indicator from the inverse quadratic and inverse multiquadric were both relatively low compared to the original and squared exponential RBF, given that they did find a seemingly large and diverse objective space. This could be explained by the lower score on the environment objective for both these activation functions, creating a gap in the objective space. Which could be resulting in less potentially important trade-offs. The exponential, Matern32 and Matern52 kernel are really struggling to find good policies, performing a lot worse relative to the other activation functions and finding a very narrow set of solutions. Especially the exponential RBF has a low hypervolume and a large spread of the epsilon indicator, which indicates large gaps in the approximation set. This is an indication that the exponential RBF has a lot more difficulty traversing the fitness landscape, causing the approximation set to be less diverse.

6.6.2. Influence on the search behavior of the algorithm.

The inverse quadratic, the inverse multiquadric and exponential RBF display very little spread in hypervolume for all ten seeds compared to the other activation functions. While they also perform worse than the other functions, this indicates some resistance to the effects of random seeds. It also indicate that they have more difficulty traversing the fitness landscape.

Additionally, there appeared to be two stable regions that presented themselves in the objective space, in some performance metrics plots more visible than others. This hints towards a local optimum, the original and squared exponential seem to be able to handle this better while the inverse quadratic, inverse multiquadric and exponential seem to be stuck in it. There was also a moment where some seeds of the squared exponential appeared to be stuck, but recovered itself with a second evolutionary drive. This indicates that the squared exponential has more difficulty in searching, but it could also be that it had encountered the local optimum and was able to steer clear of it. It can be concluded that the algorithm is able to create a smoother fitness landscape with the original and squared exponential RBF compared to the other activation functions. Resulting in faster search behavior and a overall higher hypervolume, more epsilon progress and a bigger archive.

7 Discussion

This chapter discusses the implications of the results presented in the previous chapter. The aim of this study (main research question) is to explore how the choices made during hyperparameter setup of nonlinear approximation networks in multi-sector water allocation EMODPS models impact the outcomes of the model.

7.1. Would other MOEAs such as Borg or epsilon-MOEA influence the fitness landscape differently than epsilon-NSGAII, causing RBFs to perform differently with other MOEAs?

Activation functions were found that displayed characteristics that indicate that there might be two stable regions in the objective space. This could be explained by local optima in the fitness landscape for those activation functions in this model. However, not all activation functions fully displayed these characteristics. The ability to clear local optima is also a characteristic of MOEAs (Maier et al., 2014). This begs the question if activation functions will perform differently with other optimization algorithms. The fitness can be described as a landscape which portrays the search space of an optimisation problem as a multidimensional landscape defined by the possible solutions, through which the optimisation algorithm moves, mapped to the corresponding fitness value (Smith, Husbands, & O'Shea, 2002). Therefore, the fitness landscape does not only depend on the problem which it has to solve, but is also affected by the choice of algorithm, and the parameter values (Maier et al., 2014). The fitness landscape's qualities dictate how easy or difficult it is to solve a certain optimisation challenge. For example, the overall shape of the landscape, such as a "large bowl" shape, can direct the algorithm to the global optimum, whereas a rough surface with multiple local optima may provide challenges. However, it is possible to obtain fitness landscapes with significantly different attributes for the same types of problems depending on how problems are formulated, how constraints are handled, and the simulation model and optimisation algorithm used (Maier et al., 2014). This suggests that different optimization algorithms or even different parameter values could influence the fitness landscape, and thus the behavior of the activation function. This can explain why certain activation functions are able to deal with presumed local optima better than others for this particular MOEA and model. Since MOEAs also have a significant effect on the fitness landscape, it is worth investigating what the effects of different MOEAs are on several different activation functions. Will the performance be similar to what was found during this research, or will different activation functions perform better with another MOEA. This might be done by diving deeper into the the evolutionary dynamics of the MOEAs in conjunction with different activation functions. Exploring how the shape of the fitness landscape evolving during the MOEA runtime.

7.2. Why do the Original and Squared Exponential RBF perform so much better than the other kernels in terms of performance metrics?

Both the original and the squared exponential RBF outperformed the other activation functions as showcased in Chapter 6. Now it is determined that activation functions do significantly influence the performance of EMODPS models, the question arises why these two kernels perform better than the others. The only differences between the model runs were was the activation function, therefore the shape of the activation function, that in turn influences the fitness landscape, is responsible for the difference in performance. The question that arises is: What characteristics of shape of the activation function are causing them to behave more desirably in conjunction with EMODPS models? Firstly, the original RBF used in the model is a modified version of a Gaussian RBF (Giuliani et al., 2014). However, the Squared Exponential RBF is very similar to the original RBF, both in terms of equation as terms of shape, as displayed in Chapter 4. Therefore it was to be expected that these two activation functions would perform similarly. The shape of an activation function changes the fitness landscape that the optimizer has to traverse. Some activation functions provide shapes that gives a fitness landscape that an optimizer can traverse more quickly than other shapes. To explore the different properties, the decision variables of the non-dominated solutions that are in the reference set have been inspected. The original, inverse multiquadric and the exponential RBF have been chosen because they have distinctly different shapes as can be seen in Chapter 4, and also showed different performance metric characteristics. The center, radius and weights of the decision variables have been summed together and divided by eight, eight and sixteen respectively. Then the descriptive statistics of these tables were inspected, resulting in Table 7.1, 7.2 and 7.3 below.

	center	radius	weight
count	1514	1514	1514
mean	0.57	0.62	0.37
std	0.11	0.11	0.09
min	0.06	0.36	0.13
25%	0.51	0.54	0.30
50%	0.60	0.60	0.36
75%	0.64	0.68	0.43
max	0.74	0.97	0.68

Table 7.1: Original RBF decision variables summarized

	center	radius	weight
count	1157	1157	1157
mean	0.34	0.53	0.34
std	0.20	0.15	0.10
min	-0.32	0.11	0.13
25%	0.21	0.42	0.27
50%	0.37	0.52	0.32
75%	0.51	0.63	0.39
max	0.74	0.98	0.75

Table 7.2: Inverse multiquadric RBF decision variables summarized

	center	radius	weight
count	946	946	946
mean	0.62	0.65	0.43
std	0.08	0.12	0.09
min	0.28	0.45	0.19
25%	0.62	0.56	0.36
50%	0.64	0.61	0.43
75%	0.66	0.69	0.49
max	0.73	0.99	0.74

Table 7.3: Exponential RBF decision variables summarized

While the center and the weight decision variable could also be of influence, it would be very difficult to test, since they do not directly influence the shape of the function. Therefore the focus will be on the radius. To get an idea of the shape of the RBF during optimisation, the minimum, mean and maximum radius value is plotted for each activation function. This results in figure 7.1 on the next page. The figure showcases that the EMODPS algorithm combined with the ϵ-NSGAII MOEA prefer large negative parabolas as an activation function. This also explains why the exponential RBF (Figure 7.1g, 7.1h, 7.1i) performs so poorly. The decision surface of the exponential RBF is so small that it is really difficult for this function to determine what good solutions are, and create a smooth fitness landscape. However, it is noteworthy that the shape of the inverse multiquadric with the maximum radius and the shape of the original RBF with the mean radius look very much alike. One would expect that the optimization algorithm would shift toward an inverse multiquadric RBF with a larger radius if this would be beneficial. Interestingly this did not happen, since the mean of the radius of the inverse multiquadric RBF is lower than the mean of the original RBF. It would therefore be interesting to explore if limiting the decision variables to a certain range, to force a bandwidth onto the optimization algorithm would yield better results. This could be beneficial for RBFs such as the inverse multiquadric or the inverse quadratic, even though the MOEA does not seem to prefer this radii range. When the characteristics of good performing activation functions and decision variable ranges are more well known, limiting the range of the decision variables might also be beneficial for the efficiency of an RBF, resulting in less training and faster convergence in the beginning of the optimization.

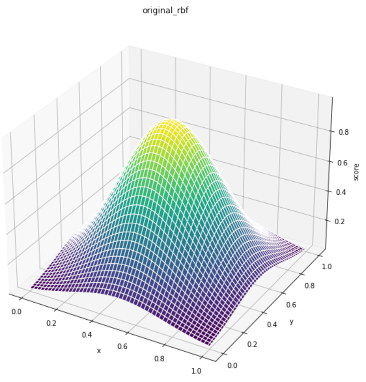

(a) Original RBF minimum radius

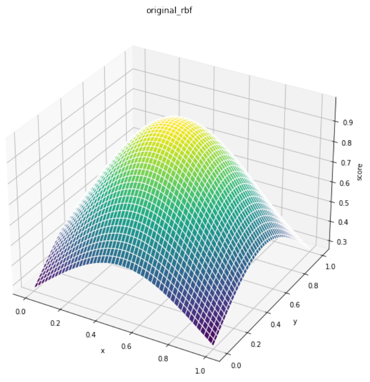

(b) Original RBF mean radius

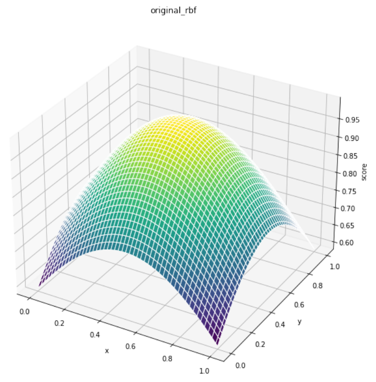

(c) Original RBF maximum radius

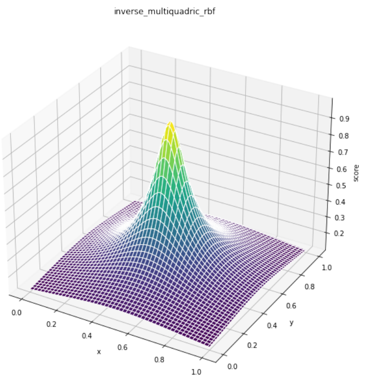

(d) Inverse multiquadric RBF minimum radius

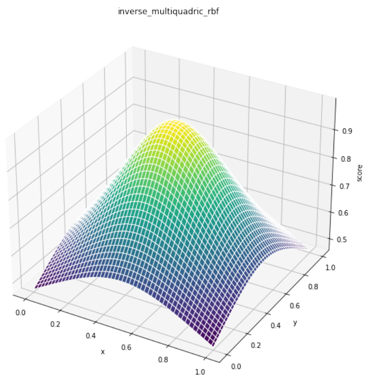

(e) Inverse multiquadric RBF mean radius

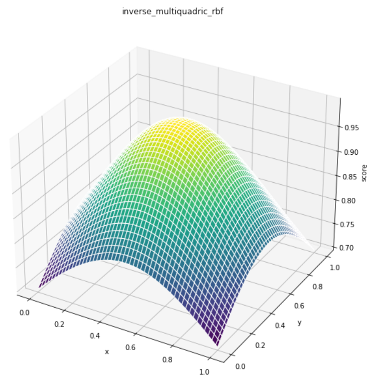

(f) Inverse multiquadric RBF maximum radius

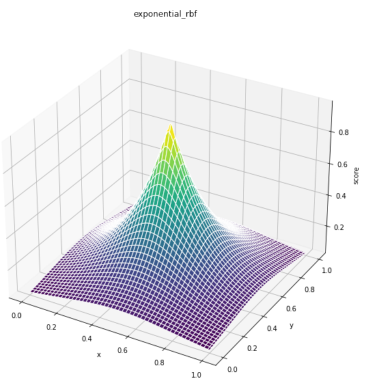

(g) Exponential RBF minimum radius

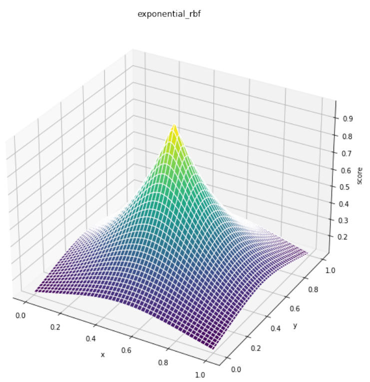

(h) Exponential RBF mean radius

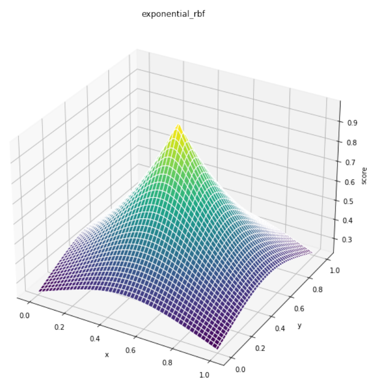

(i) Exponential RBF maximum radius

Figure 7.1: Activation functions plotted with preferred decision variable values

7.3. Given the results, what are the implications for decision-making

The decision-making process in a multi-actor environment have found to be complex. Research should enhance the quality of decision-making. And increasing the involvement of experts in the decision-making process should lead to better decisions. However, empirical research demonstrates that the relationship between research and decision-making quality is not as straightforward as this, particularly in complex decision-making processes involving many actors, numerous interests, and unstructured situations. For example, it is not possible to simply focus on effectiveness (the ability to solve a problem) and efficiency (with minimum cost and effort) of the decision-making. Since these criteria assume there is only one problem owner. These metrics are no longer unequivocally applicable when there are many problems or problem owners (De Bruijn & Ten Heuvelhof, 1999).

If actors are unable to implement policies or strategies unilaterally, and are in need of the support of others, the actors find themselves in a network (De Bruijn & Ten Heuvelhof, 2008). A network can be defined as a group of actors with different goals and interests, as well as different resources, who rely on one another to achieve their objectives. Several actors participate in decision making within the network structure. They have alternate views and depend on one another. Interdependence means that the actors are unable to solve the problem on their own. They must work together to achieve their own objectives. The decision-making process will only be effective if it is collective decision-making (De Bruijn & Ten Heuvelhof, 2008).

A key concern of network decision making is that it remains limited to one subject: one-issue decision making. There is a potential of a deadlock if various actors hold opposing viewpoints on this issue. There is minimal possibility for compromise when a number of performers favor option A and a number of other actors support option B. A multi-issue problem opens up the possibility of exchanges. Actors have room to give and take, which is essential for the smooth progression of decision making in networks. A second advantage of a multi-issue problem is that it results in shifting coalitions and hence provides incentives for cooperative behavior (De Bruijn & Ten Heuvelhof, 2008). However, the actors can have a wide range of mutual differences (variety), which makes cooperation and collaborative decision-making difficult. In other cases, specific actors may be completely uninterested in cooperating in decision-making (closedness). Finally, the number of actors engaging in the decision-making process might change over time (dynamic), causing actors join or leave the network (De Bruijn & Ten Heuvelhof, 2008).

The purpose of doing optimization with an EMODPS model is to reveal trade-offs for decision makers. If certain kinds of trade-offs are not identified by the model due to for example sub-optimal hyperparameter selection, it can influence the decision making process by being unable to convey all possibilities to all actors. Decision makers can apply or prefer different decision-making strategies to find an optimal policy for all actors involved. Strategies such as, utilitarianism, egalitarianism, prioritarianism, sufficientarianism and the Pareto principle could be identified and used to quantify options to facilitate negotiation between actors (Yalew, Kwakkel, & Doorn, 2021). When a less diverse trade-off space is found, the options highlighted with such strategies can be less appealing, or not exist at all for some actors. Hampering the ability to compromise or cooperate and therefore also hampering the decision-making process. This highlights the possible implications of selecting worse performing activation functions in a multi-objective setting. Decision makers prefer room for giving and taking, a wide range of different options which facilitates the ability to negotiate or cooperate with other actors. This way actors are able to explore different trade-offs, with the possibility of finding a collaborative solution that would be acceptable for each actor.

8
Conclusion

In this last chapter of the thesis, a conclusion follows. First the research questions and corresponding answers are repeated in section 8.1. Then, the main conclusion follows in section 8.2. Then, in section 8.3 the research limitations are briefly discussed. This chapter concludes with a list of suggestions for further research in section 8.4.

8.1. Sub-research Questions and conclusions

1. **What case study can be selected to study the impact of experimental setup choices in EMODPS models?**
   As a case study, the lower Susquehanna river basin model was used. Since it includes multiple reservoirs and several objectives, this case lends itself particularly well to the use of the EMODPS framework. Furthermore, the Susquehanna River Basin case was chosen because it is a stylized case study which has been widely used in earlier multi-objective optimization studies utilizing EMODPS.

2. **What is/are the most important independent variable(s) to study the impact of experimental setup choices for EMODPS?**
   A small dive in radial basis function networks determined that The activation function of the radial basis function network is the hyperparameter with the biggest influence on the control policy that could be modified when using an EMODPS model. Several popular activation functions were investigated, and seven of them were chosen to be used for research into how the shape of an activation function influences the performance of an EMODPS model. The seven activation functions that were selected to be tested were:
   The Original kernel used in the Susquehanna case, the squared exponential kernel, the adapted Inverse Quadratic kernel, the adapted inverse multiquadric kernel, the exponential kernel, the matern(3/2) kernel and the matern(5/2) kernel.

3. **Is the EMODPS model implemented as intended?**
   The Susquehanna River Basin EMODPS model has been built in Python and enhanced to work with a variety of activation functions which were specified in the experimental design. Furthermore, $epsilon$-NSGAII was chosen as the MOEA because it provided a good balance of convergence speed and maximum attainable hypervolume. The model has been verified by checking the order of magnitude of the the outcomes and by examining the behavior of the model by plotting the release of water over time to the objectives. The model behaved as expected, which resulted in a working multi-objective water allocation python model with which was built according to the EMODPS framework. The model allows different hyperparameter setups and focused on implementing different activation functions for the nonlinear approximation network.

4. **What differences in performance in the objective space can be observed when varying the hyperparameters of the control policy?**
   When comparing the trade-off space, the original RBF and the squared exponential RBF performed well, identifying a wide and diverse objective space. The inverse quadratic RBF and inverse multiquadric RBF performed slightly worse, but still found a wide range of solutions. However, both the

hypervolume and epsilon indicator from the inverse quadratic and inverse multiquadric were both low compared to the other well performing activation functions, given that they did find a seemingly large and diverse objective space. This was explained by the lower score on the environment objective for both the inverse quadratic and inverse multiquadric RBF, resulting in a gap in the objective space. Such a gap may result in less possible trade-offs, which could be vital for the decision making process. The exponential, Matern32 and Matern52 kernel were really struggling to find good policies, performing a lot worse relative to the other activation functions and finding a very narrow set of solutions. Especially the exponential RBF had a large spread of the epsilon indicator and a relatively low hypervolume, which indicates large gaps in the approximation set. This is an indication that the exponential RBF has a lot more difficulty traversing the fitness landscape, resulting in a less diversified approximation set.

5. **What differences in the search behavior of the algorithm can be observed when varying the hyperparameters of the control policy?**
   The inverse quadratic, the inverse multiquadric and exponential RBF display very little spread in hypervolume for all ten seeds compared to the other activation functions. While they also perform worse than the other functions, it might indicate some resistance to the effects of random seeds, it might also indicate that they have more difficulty traversing the fitness landscape.

   Furthermore, there appeared to be two stable sections in the objective space, which were more visible in some performance metrics plots than others. This suggests a local optimum; the original and squared exponential appear to be able to manage it better, whilst the inverse quadratic, inverse multiquadric, and exponential may be caught in it. It can be concluded that the algorithm is able to create a smoother fitness landscape with the original and squared exponential RBF compared to the other activation functions. This resulted in faster search behavior and a higher total hypervolume, more epsilon progress, and a larger archive.

8.2. Main conclusion

The findings of the previous analyses enable a formulation of an answer to the main research question. The main research question was formulated as follows:
How do the choices made during the hyperparameter setup of nonlinear approximation networks in multi-sector water allocation EMODPS models impact the model outcomes?
To test policy outcomes, an abstraction of a real system in which outcomes are analyzed that are created by various policy alternatives and/or states of a given system is frequently required. EMODPS is an effective water allocation framework that uses universal nonlinear approximators to parameterize candidate operating policies. These nonlinear approximating networks are machine learning techniques where data is combined with a model, to make a prediction. nonlinear approximation networks such as radial basis function networks, have hyperparameters which are parameters whose value is used to control the learning process. Subsequently, this can directly influence the behavior within the model. Activation functions are hyperparameters of radial basis function networks with a lot of influence on the control policy, which have been found to have implications for the model outcomes and subsequently on the objective space. The influence of the activation function on the search dynamics was tested with ϵ-NSGAII as the multi-objective evolutionary algorithm. Seven different activation have been tested to explore how big their impact would be on the performance of the EMODPS model, the objective space and the search behavior of the MOEA. It can be concluded that the choices made during the experimental setup have a large impact on the objective space, search behavior and eventually the final model outcomes. The exponential, matern32, matern52, inverse quadratic and inverse multiquadric kernels all under performed compared to the squared exponential RBF and the RBF originally used in the Susquehanna case. In what ways did this impact the model outcomes?

- Impact on the objective space: Varying the activation functions had a large impact on the objective space. The original and squared exponential RBF managed to attain a big objective space with a diverse approximation set. The inverse quadratic RBF and inverse multiquadric RBF performed slightly worse, but still found a wide range of solutions. However, the quality of these solutions was lower than the aforementioned RBFs, which was indicated by the performance metrics which were much lower compared to the RBFs with a bigger objective space. The exponential, Matern32 and Matern52 kernel performed a lot worse compared to the other four RBFs, finding a narrow set of solutions.

- Impact on search behavior: The ability to clear local optima is a characteristic of MOEA, which is found to be influenced by the activation function. Together they create the quality of the fitness landscape that dictates how easy or difficult it is to solve a certain optimisation challenge. The overall shape of the landscape can guide the algorithm to the global optimum, whereas it can also get stuck on local optima. For this case there appeared to be two stable sections in the objective space, which were more visible in some performance metrics plots than others. The original and squared exponential RBF were able to steer clear of this local optimum most of the time, whilst the inverse quadratic, inverse multiquadric, and exponential RBF were hindered by it. The optimization algorithm was able to create a smoother fitness landscape with the original and squared exponential RBF compared to the other activation functions. This resulted in faster search behavior and a higher total hypervolume, more epsilon progress and a larger archive. Different activation functions can influence the fitness landscape, and thus the search behavior. This explains why certain activation functions are able to deal better with local optima than others for this particular case and MOEA.
- Impact on decision-making: If certain trade-offs are not identified by the optimization algorithm due to sub-optimal hyperparameter selection, it will influence the decision making process by being unable to convey all the full objective space to all actors. A bigger objective space with a more diverse approximation set is more desirable since decision makers have more possible strategies or trade-offs to work with. This opens up the possibility of exchanges. Actors have room to negotiate, which is essential for the smooth progression of decision making in networks. This highlights the importance of finding the biggest and most diverse approximation set. Actors are able to explore more strategies and trade-offs, giving them the best chance of finding a collaborative solution that would be acceptable for each actor. Facilitating a better and more informed decision-making process.

The ideal shape characteristic of the activation function that would be most desirable to work in conjunction with EMODPS has also been briefly explored. It has been found that the EMODPS algorithm combined with the ϵ-NSGAII MOEA prefer large negative parabolas as activation function, to create an as large as possible decision surface. However, based on these results, it is hard to recommended more guidelines for non-expert users. It is for example still unknown why a similarly shaped inverse multiquadric RBF performs so differently compared to the original RBF, as seen in chapter 7. Besides, these results could be case specific, but a first step has been made to explore the characteristics activation functions which will help to set more proper guidelines in the future.

8.3. Limitations and reflection

Every research has its limiting factors, it can be beneficial to name these factors to create a context in which the research is valuable. The research has been conducted by a single researcher in limited time period. Due to limited time and resources, some scoping decisions in the research process had to be made. The choices that were made during this research and it's limiting factors will be reflected in this section.

- Due to the time constraints of the research, and the amount of experiments that had to be conducted. The experiments of this research have only been run with 100.000 function evaluations. Some RBFs showed signs of not fully converging and would benefit from more function evaluations. While this would probably not alter the outcome of the research, it would probably display the found local optima more clearly.
- The amount of random seeds that were chosen was limited to 10 for this thesis. This has been done deliberately, to reduce the run time that was necessary to complete all the experiments. However, the Mann-Whitney test required at least 20 samples to be able to compare hypervolume samples of the activation functions against each other. Therefore this test could not be performed.
- The research has only been conducted with one MOEA, ϵ-NSGAII. The activation functions that were tested in this research will behave differently with other MOEAs (Maier et al., 2014), such as other well performing algorithms like Borg or ϵ-MOEA (Salazar et al., 2016). However, testing multiple MOEAs was considered out of scope for this research.

- Some activation functions had to be modified to be able to use them in conjunction with the EMODPS model. This had to be done because of the current normalization requirement of the model. While the adapted function look visually exactly the same, it remains unknown if they would perform exactly the same as the unadapted activation function.
- The model is written in Python mostly because of the popularity of the language. The language has been growing steadily and is widely used among academics and therefore has wide a support of libraries. One big disadvantage however, is the speed of Python. It took several days for the model to run optimize all seven functions across 10 seeds for 100.000 function evaluations on a high performance server. The Python model is inherently slower than other languages such as C, if kept in pure Python. This can partly be resolved with libraries such as numba, cython or other libraries that can speed up python code. But this will also sacrifice readability of the code.

8.4. Future Research

A number of new research questions were encountered during this thesis. These topics for future research are highlighted in a list below.

- As mentioned in the discussion, literature suggests that different optimization algorithms or even different parameter values of optimization algorithm can influence the fitness landscape, and thus the behavior of the activation function. It therefore is worth investigating how drastic the effects of different optimization algorithms are on activation functions. Diving deeper into the the evolutionary dynamics of the MOEAs in conjunction with different activation functions. Exploring how the shape of the fitness landscape evolves during the MOEA runtime.
- Currently, only isotropic positive-definite activation functions were used. This was done for good reason, since the impact of different activation functions on EMODPS models was still unknown. However, this is likely to remain trial and error until the characteristics of activation functions which are important for EMODPS are better understood. Therefore, further research into the preferred characteristics of activation functions for EMODPS models would be beneficial to be able to select or even create a better activation function given a case or MOEA. Future research in this direction can also help create guidelines for non-expert users and even better understanding for expert users. It can further discover the relative merits of each activation function and in which situation it would be best to use them.
- Investigate the effects of varying activation functions on other case studies. The question is if activation functions will still perform comparably with other cases which have different input or release behavior. Currently, the chosen activation functions were only tested with the Susquehanna case. As Maier et al. (2014) mentioned, the fitness landscape can be influenced by merely using a different parameters of the model, applying the same experiment on a different model can therefore yield different results. Other case studies will have different water flows, different release requirements and different weather patterns, which will influence the input and release values of the model. The difference in performance of the activation function will probably depend on the amount of noise of these input variables of the model.
- It was noteworthy that the shape of the inverse multiquadric with the maximum radius and the shape of the original RBF with the mean radius looked very much alike (Figure 7.1f). It was expected that the optimization algorithm would shift toward an inverse multiquadric RBF with a larger radius to match the shape if the original RBF if this would be beneficial. Interestingly this did not happen. It would therefore be interesting to explore if limiting the decision variables to a certain range, to force a bandwidth onto the optimization algorithm would yield better results. This could be tested for RBFs such as the inverse multiquadric or the inverse quadratic.

References

Aggarwal, C. C. (2018). Neural networks and deep learning. *Springer*, *10*, 978–3.

ASCE. (2017). 2017 infrastructure report card. In *American society of civil engineers.*

Askari, M., & Adibi, H. (2015). Meshless method for the numerical solution of the fokker–planck equation. *Ain Shams Engineering Journal*, *6*(4), 1211–1216.

Bertsekas, D., & Birge, J. (1976). *Dynamic programming and stochastic control.* Academic Press, New York.

Castelletti, A., Antenucci, J., Limosani, D., Quach Thi, X., & Soncini-Sessa, R. (2011). Interactive response surface approaches using computationally intensive models for multiobjective planning of lake water quality remediation. *Water Resources Research*, *47*(9).

Deb, K., Mohan, M., & Mishra, S. (2003). Towards a quick computation of well-spread pareto-optimal solutions. In *International conference on evolutionary multi-criterion optimization* (pp. 222–236).

Deb, K., Pratap, A., Agarwal, S., & Meyarivan, T. (2002). A fast and elitist multiobjective genetic algorithm: Nsga-ii. *IEEE transactions on evolutionary computation*, *6*(2), 182–197.

De Bruijn, H., & Ten Heuvelhof, E. (1999). Scientific expertise in complex decision-making processes. *Science and public policy*, *26*(3), 179–184.

De Bruijn, H., & Ten Heuvelhof, E. (2008). *Management in networks: On multi-actor decision making (1st ed.).* Routledge.

Doering, K., Quinn, J., Reed, P. M., & Steinschneider, S. (2021). Diagnosing the time-varying value of forecasts in multiobjective reservoir control. *Journal of Water Resources Planning and Management*, *147*(7), 04021031.

Duvenaud, D. (2014). *Automatic model construction with gaussian processes* (Unpublished doctoral dissertation). University of Cambridge.

Fasshauer, G. E. (2007). *Meshfree approximation methods with matlab* (Vol. 6). World Scientific.

Fung, F., Lopez, A., & New, M. (2011). Water availability in+ 2 c and+ 4 c worlds. *Philosophical transactions of the Royal Society A: mathematical, physical and engineering sciences*, *369*(1934), 99–116.

Gerring, J. (2006). *Case study research: Principles and practices.* Cambridge university press.

Giuliani, M., Castelletti, A., Pianosi, F., Mason, E., & Reed, P. M. (2016). Curses, tradeoffs, and scalable management: Advancing evolutionary multiobjective direct policy search to improve water reservoir operations. *Journal of Water Resources Planning and Management*, *142*(2), 04015050.

Giuliani, M., Herman, J. D., Castelletti, A., & Reed, P. (2014). Many-objective reservoir policy identification and refinement to reduce policy inertia and myopia in water management. *Water resources research*, *50*(4), 3355–3377.

Giuliani, M., Li, Y., Cominola, A., Denaro, S., Mason, E., & Castelletti, A. (2016). A matlab toolbox for designing multi-objective optimal operations of water reservoir systems. *Environmental Modelling & Software*, *85*, 293–298.

Golbabai, A., Mammadov, M., & Seifollahi, S. (2009). Solving a system of nonlinear integral equations by an rbf network. *Computers & Mathematics with Applications*, *57*(10), 1651–1658.

Guerreiro, A. P., Fonseca, C. M., & Paquete, L. (2020). The hypervolume indicator: Problems and algorithms. *arXiv preprint arXiv:2005.00515*.

Gupta, R. S., Hamilton, A. L., Reed, P. M., & Characklis, G. W. (2020). Can modern multi-objective evolutionary algorithms discover high-dimensional financial risk portfolio tradeoffs for snow-dominated water-energy systems? *Advances in Water Resources*, *145*, 103718.

Hadka, D., & Reed, P. (2012). Diagnostic assessment of search controls and failure modes in many-objective evolutionary optimization. *Evolutionary computation*, *20*(3), 423–452.

Hadka, D., & Reed, P. (2013). Borg: An auto-adaptive many-objective evolutionary computing framework. *Evolutionary computation*, *21*(2), 231–259.

Hammarberg, K., Kirkman, M., & de Lacey, S. (2016). Qualitative research methods: when to use them and how to judge them. *Human reproduction*, *31*(3), 498–501.

Hardy, R. L. (1990). Theory and applications of the multiquadric-biharmonic method 20 years of discovery 1968–1988. *Computers & Mathematics with Applications*, *19*(8-9), 163–208.

Hartman, E. J., Keeler, J. D., & Kowalski, J. M. (1990). Layered neural networks with gaussian hidden units as universal approximations. *Neural computation*, *2*(2), 210–215.

Hashimoto, T., Stedinger, J. R., & Loucks, D. P. (1982). Reliability, resiliency, and vulnerability criteria for water resource system performance evaluation. *Water resources research*, *18*(1), 14–20.

Haykin, S. (2010). *Neural networks and learning machines, 3/e.* Pearson Education India.

Kollat, J. B., & Reed, P. M. (2005). The value of online adaptive search: a performance comparison of nsgaii, ε-nsgaii and εmoea. In *International conference on evolutionary multi-criterion optimization* (pp. 386–398).

Koutsoyiannis, D., & Economou, A. (2003). Evaluation of the parameterization-simulation-optimization approach for the control of reservoir systems. *Water Resources Research*, *39*(6).

Kwakkel, J. H. (2017). The exploratory modeling workbench: An open source toolkit for exploratory modeling, scenario discovery, and (multi-objective) robust decision making. *Environmental Modelling & Software*, *96*, 239–250.

Kwakkel, J. H. (2019). A generalized many-objective optimization approach for scenario discovery. *Futures & Foresight Science*, *1*(2), e8.

Kwakkel, J. H., & Haasnoot, M. (2019). Supporting dmdu: A taxonomy of approaches and tools. In *Decision making under deep uncertainty* (pp. 355–374). Springer, Cham.

Lau, L. (2021, Jun). *The abcs of moeas.* Retrieved 03-10-21, from `https://waterprogramming.wordpress.com/2021/06/21/the-abcs-of-moeas/`

Lundstedt, T., Seifert, E., Abramo, L., Thelin, B., Nyström, Å., Pettersen, J., & Bergman, R. (1998). Experimental design and optimization. *Chemometrics and intelligent laboratory systems*, *42*(1-2), 3–40.

Maier, H. R., Kapelan, Z., Kasprzyk, J., Kollat, J., Matott, L. S., Cunha, M. C., ... others (2014). Evolutionary algorithms and other metaheuristics in water resources: Current status, research challenges and future directions. *Environmental Modelling & Software*, *62*, 271–299.

Momtahen, S., & Dariane, A. (2007). Direct search approaches using genetic algorithms for optimization of water reservoir operating policies. *Journal of water resources planning and management*, *133*(3), 202–209.

Orr, M. J. (1996). *Introduction to radial basis function networks.* Technical Report, center for cognitive science, University of Edinburgh ....

Park, J., & Sandberg, I. W. (1991). Universal approximation using radial-basis-function networks. *Neural computation*, *3*(2), 246–257.

Pritchard, H. D. (2019). Asia's shrinking glaciers protect large populations from drought stress. *Nature*, *569*(7758), 649–654.

Reed, P. M., Hadka, D., Herman, J. D., Kasprzyk, J. R., & Kollat, J. B. (2013). Evolutionary multiobjective optimization in water resources: The past, present, and future. *Advances in water resources*, *51*, 438–456.

Rosenstein, M. T., & Barto, A. G. (2001). Robot weightlifting by direct policy search. In *International joint conference on artificial intelligence* (Vol. 17, pp. 839–846).

Salazar, J. Z., Reed, P. M., Herman, J. D., Giuliani, M., & Castelletti, A. (2016). A diagnostic assessment of evolutionary algorithms for multi-objective surface water reservoir control. *Advances in water resources*, *92*, 172–185.

Sarle, W. S. (1994). Neural networks and statistical models. *Proceedings of the Nineteenth Annual SAS Users Group International Conference*, 1538-1550.

Schaback, R. (2007). A practical guide to radial basis functions. *Electronic Resource*, *11*, 1–12.

Schmidhuber, J. (2000). Sequential decision making based on direct search. In *Sequence learning* (pp. 213–240). Springer.

Smith, T., Husbands, P., & O'Shea, M. (2002). Fitness landscapes and evolvability. *Evolutionary computation*, *10*(1), 1–34.

Svensén, M., & Bishop, C. M. (2007). *Pattern recognition and machine learning.* Springer Berlin/Heidelberg, Germany.

Thomas, J. J. (2005). *Illuminating the path:[the research and development agenda for visual analytics].* IEEE Computer Society.

UNEP. (2020). *Emissions gap report 2020.* UN Environment Programme DTU Partnership.

United Nations. (2015). *Paris agreement.* United Nations.

Williams, C. K., & Rasmussen, C. E. (2006). *Gaussian processes for machine learning* (Vol. 2) (No. 3). MIT press Cambridge, MA.

Yalew, S., Kwakkel, J., & Doorn, N. (2021). Distributive justice and sustainability goals in transboundary rivers: Case of the nile basin. *Frontiers in Environmental Science*, *8*, 281.

Zhang, G. (2018, Nov). *What is the kernel trick? why is it important?* Retrieved 01-09-21, from `https://medium.com/@zxr.nju/what-is-the-kernel-trick-why-is-it-important-98a98db0961d`

Zhang, H., Chen, Y., Guo, C., & Fu, Z. (2014). Application of radial basis function method for solving nonlinear integral equations. *Journal of Applied Mathematics*, *2014*.

Zitzler, E., Thiele, L., Laumanns, M., Fonseca, C. M., & Da Fonseca, V. G. (2003). Performance assessment of multiobjective optimizers: An analysis and review. *IEEE Transactions on evolutionary computation*, *7*(2), 117–132.

A

Appendix A

This appendix has a section for every release plot that has been generated to help verify the model. This visually shows the releases of water in cubic feet per second (cfs) as produced by individual solutions over time with the demand on the y-axis and the amount of days on the x-axis. Each figure also displays the maximum water released as the demand for the objectives atomic power plant, Baltimore and Chester. The release plot of the Original RBF is also included in this appendix, eventhough it was also featured in the main text. This has been done so to be able to more easily compare the individual plots in this appendix, and gain a better understanding of what the rbfs are doing. Some RBFs have visibly worse performance than other RBFs, this is for instance very noticeable in the release plot of the exponential RBFs. This RBF really struggles to meet demand for the three objectives in Figure A.5a,b,c. And to a lesser extent, but still noticeable by for the Matern32 and Matern52 RBF in Figure A.6a,b,c and Figure A.7a,b,c.

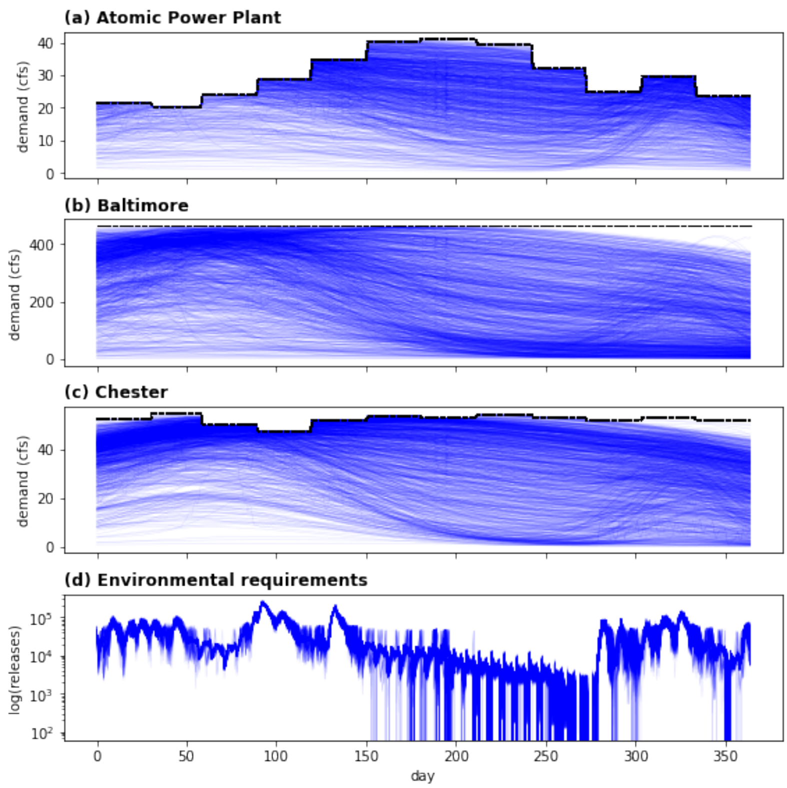

Figure A.1: Releases Original RBF

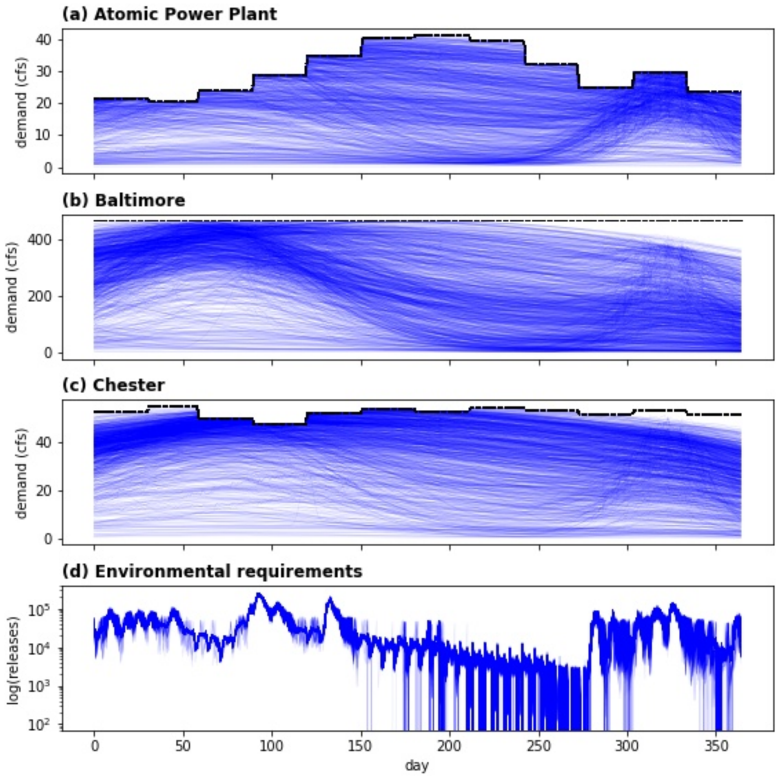

Figure A.2: Releases Squared Exponential RBF

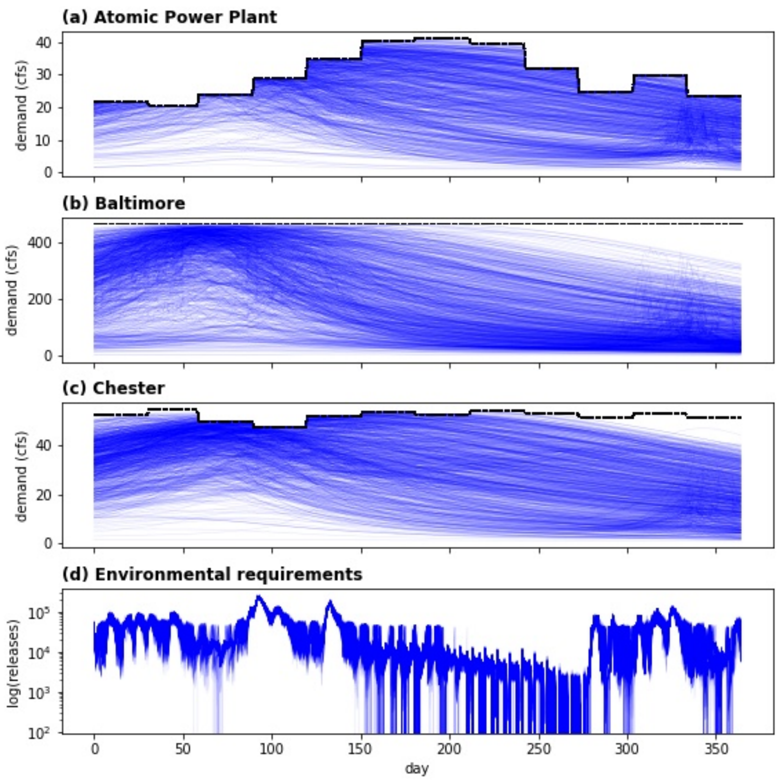

Figure A.3: Releases Inverse Quadratic RBF

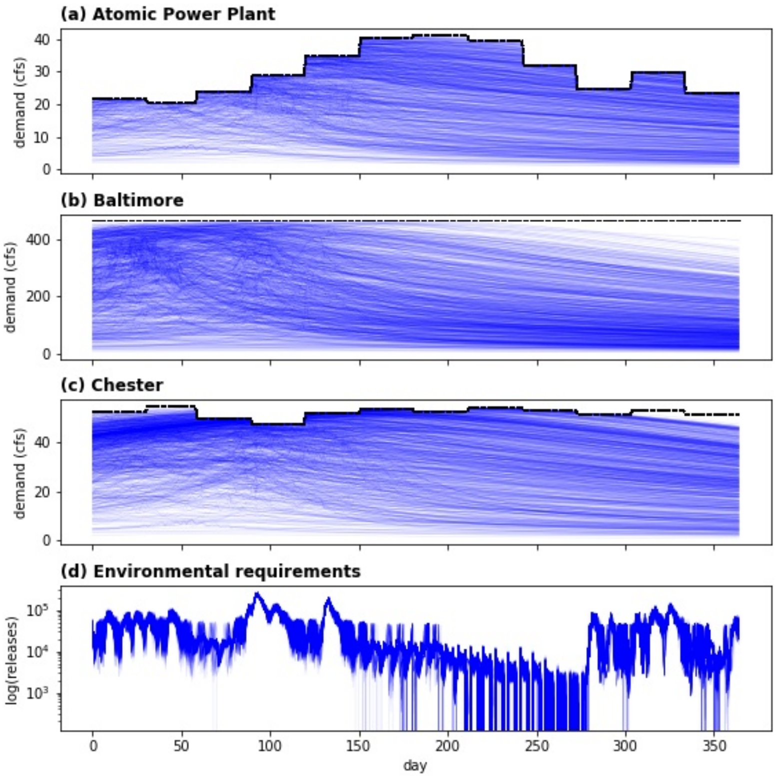

Figure A.4: Releases Multiquadric RBF

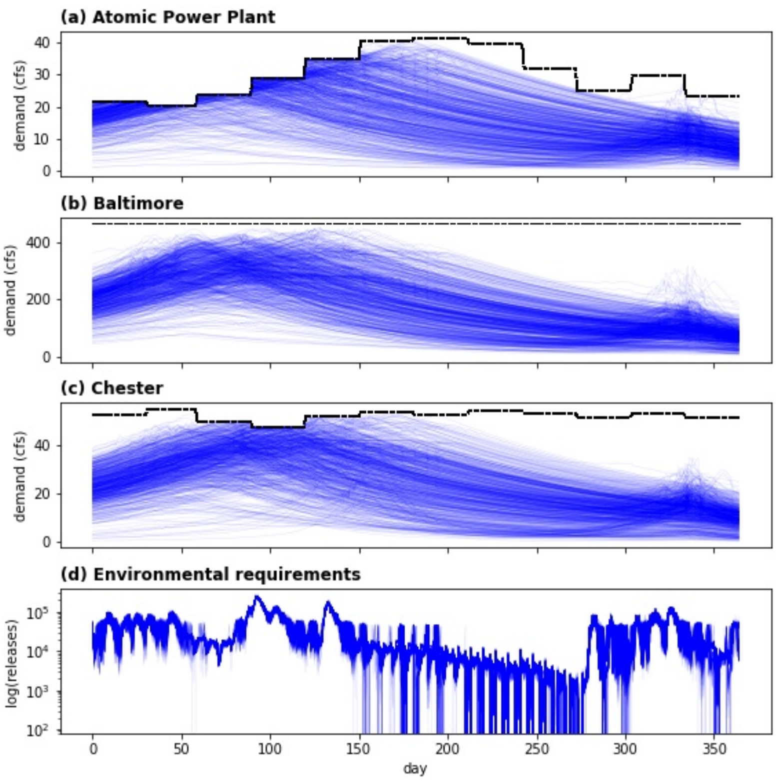

Figure A.5: Releases Exponential RBF

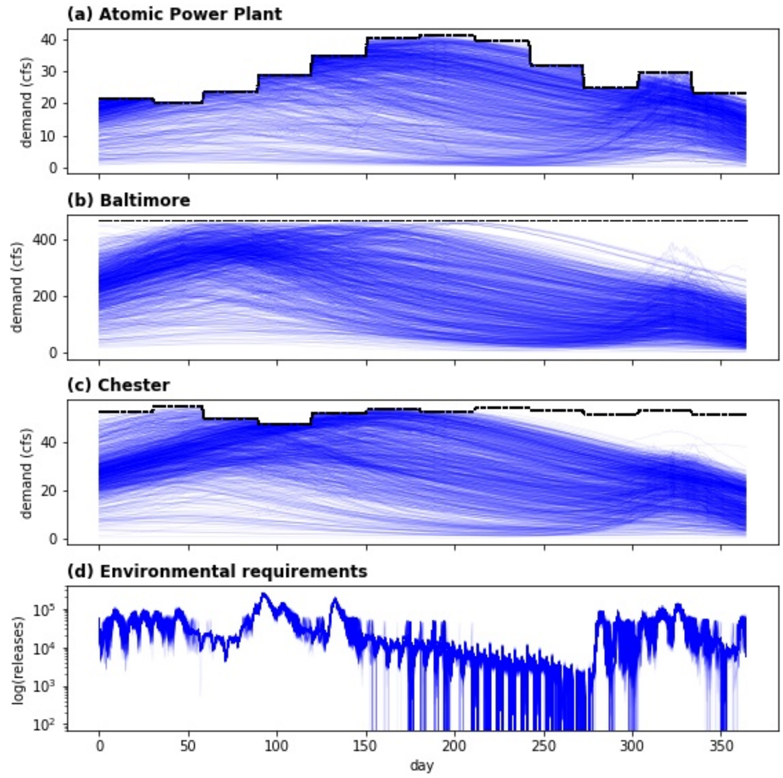

Figure A.6: Releases Matern32 RBF

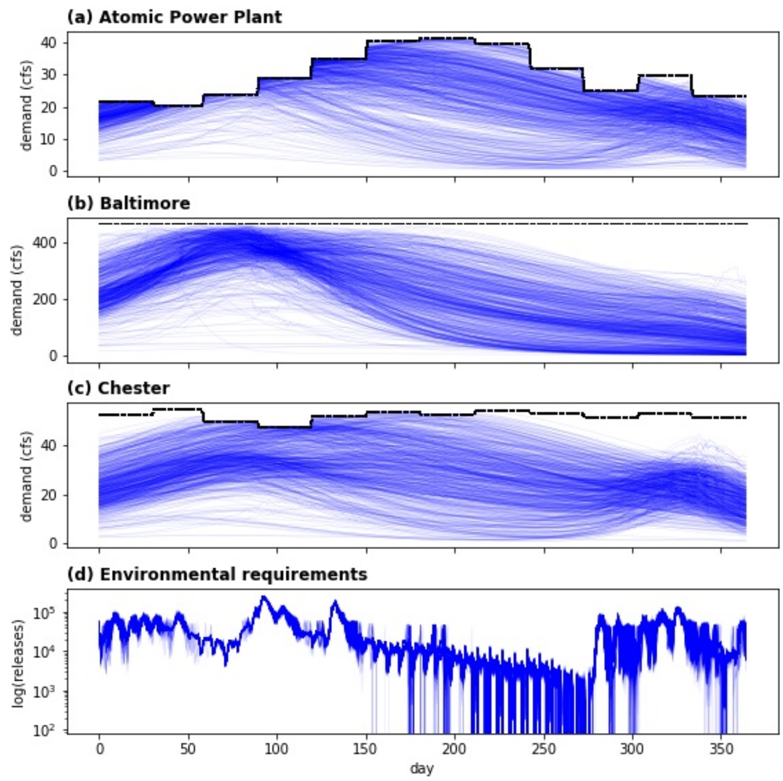

Figure A.7: Releases Matern52 RBF

B

Appendix B

A feature scoring analysis is performed in this appendix to check the impact of the different decision variables used. Feature scoring is a family of machine learning techniques for identifying the relative importance of various features for a certain outcome or class of outcomes (Kwakkel, 2017). The feature scoring analysis has been performed considering all used decision variables and all model outcomes of interest, with the extra trees algorithm. The analysis is performed for each activation functions to be able to see differences. The results are presented as heat maps to be able to quickly inspect the highest scoring parameters. It was expected that the radii (r1 - r8) would score higher compared to the centers (c1 - c8) and the weights (w1 - w16). The radius variables seem to affect some objectives notably more than others, especially hydropower and environment seem to score higher relative to the other objectives. It can also be noted that not all radius variables score high, some are even scoring really low, as can be seen in Figure B.1, where r2 scores 0,01 on hydropower. When comparing the heat maps of all activation functions, a trend emerges that shows that the radii do influence the objectives the most, and the radii can therefore be considered to be the most important decision variables. The only exception is the Matern32 kernel (Figure B.6, where the radius variables do not score high. While the radii are scoring the highest overall across most functions relative to all other variables, the score is only influencing the objectives slightly more than the other decision variables. The outcomes are therefore not as clear cut as initially expected.

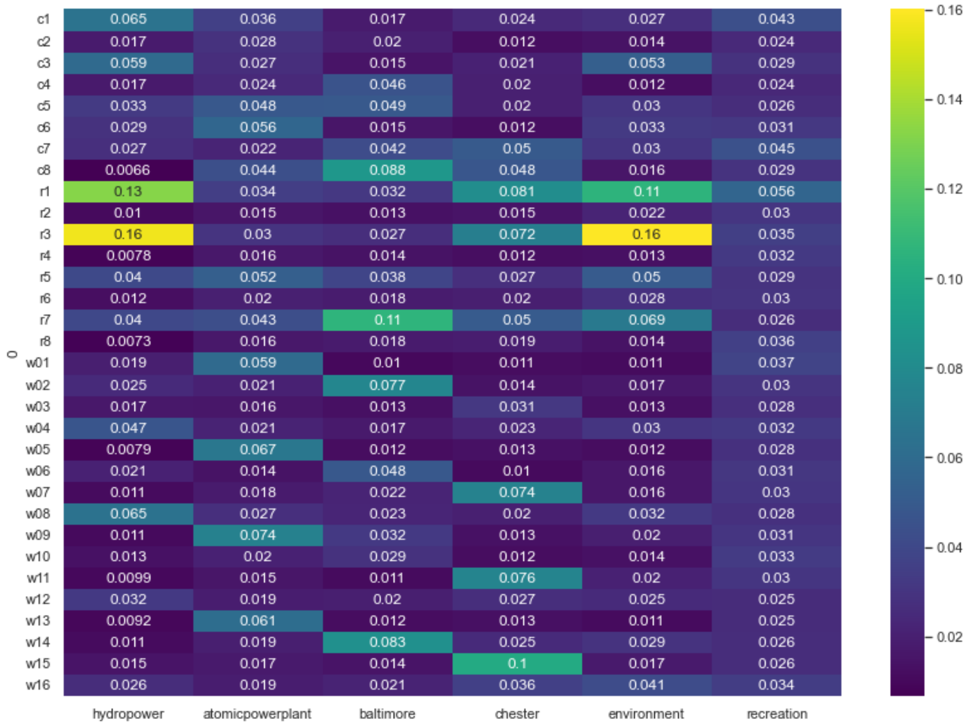

Figure B.1: Original RBF feature scoring analysis

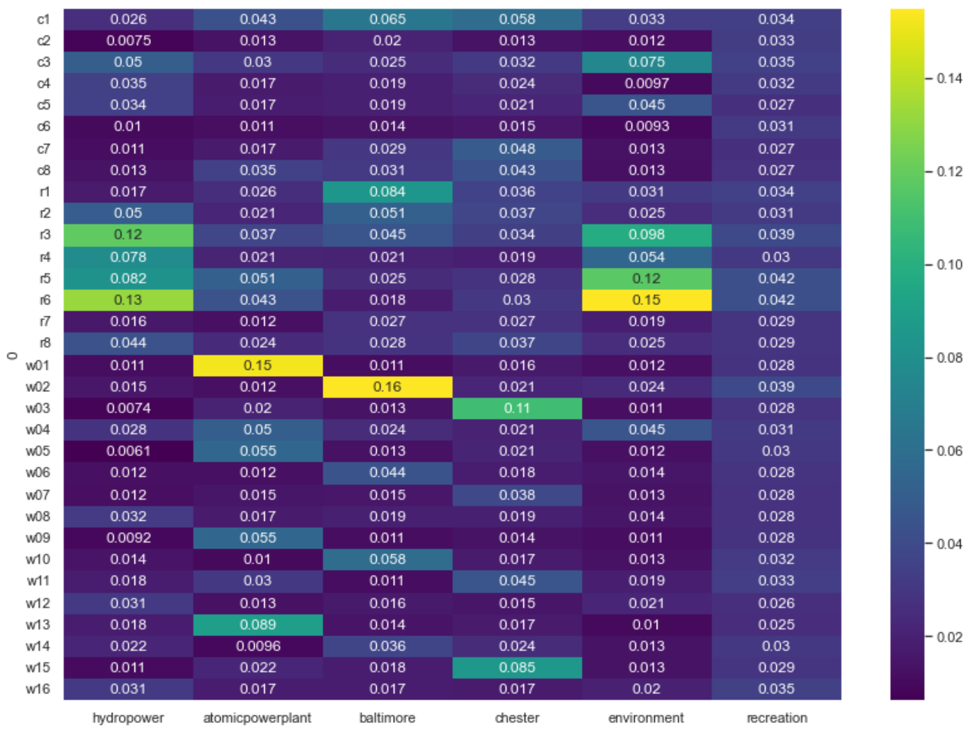

Figure B.2: Squared Exponential RBF feature scoring analysis

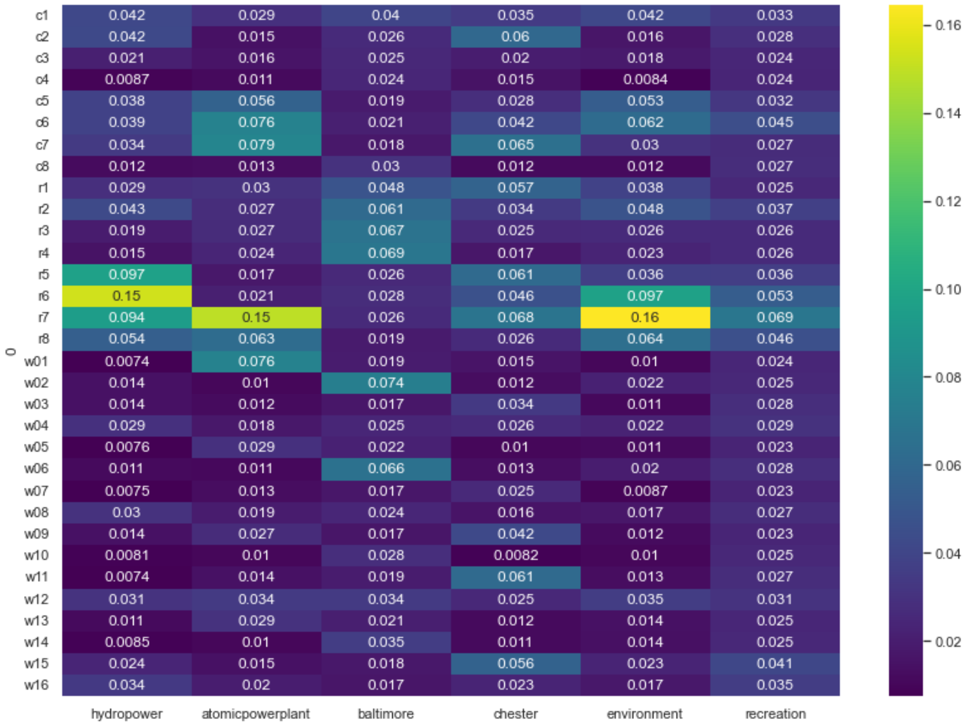

Figure B.3: Inverse Quadratic RBF feature scoring analysis

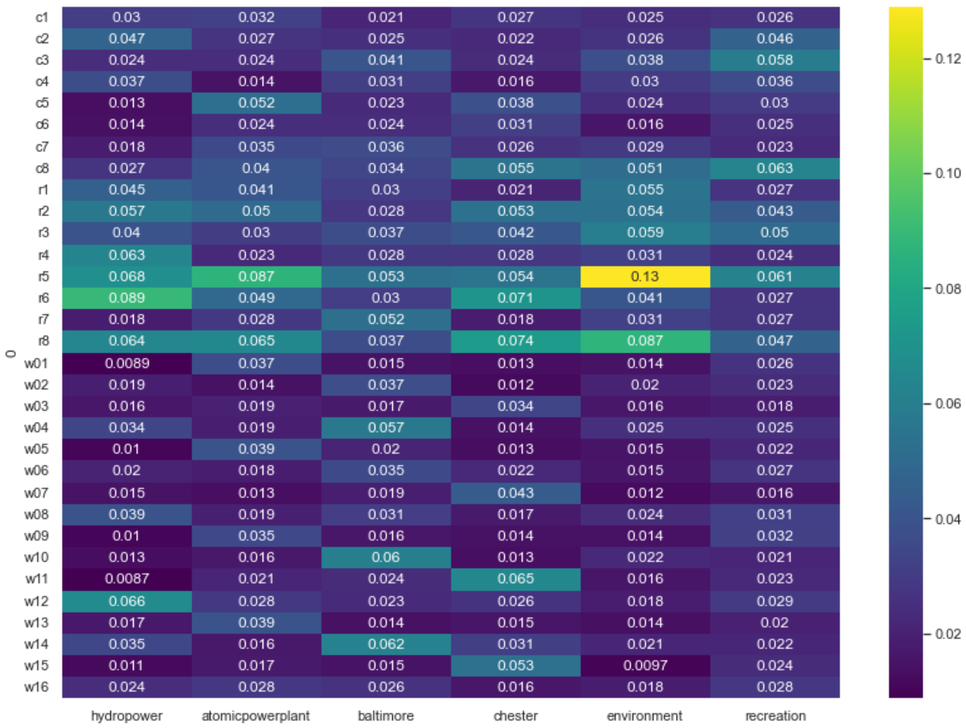

Figure B.4: Inverse multiquadric RBF feature scoring analysis

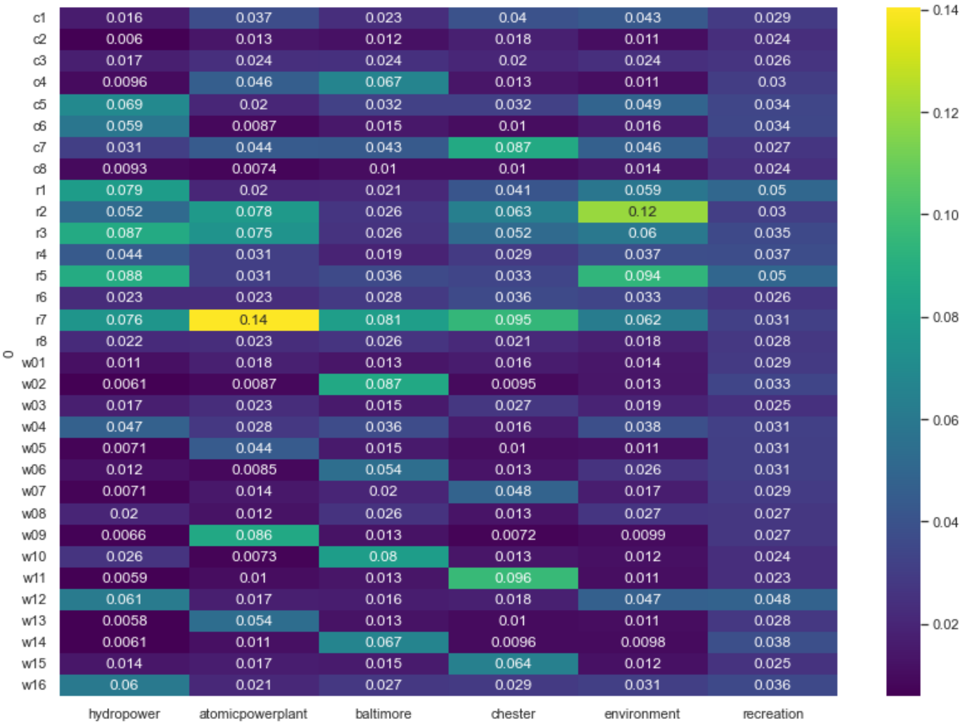

Figure B.5: Exponential RBF feature scoring analysis

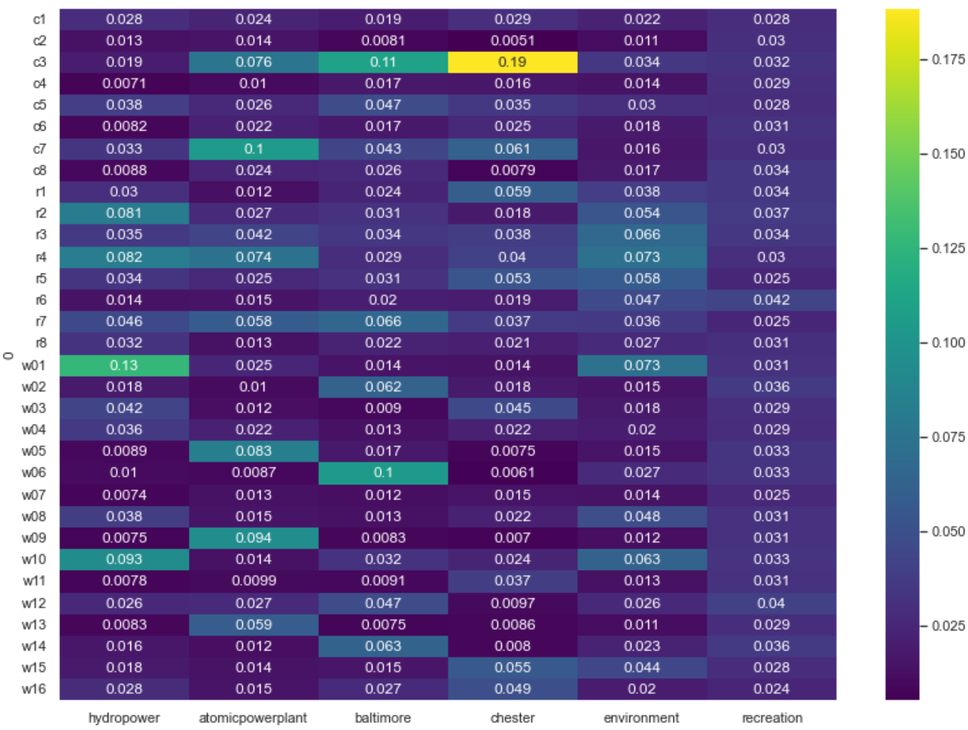

Figure B.6: Matern32 kernel feature scoring analysis

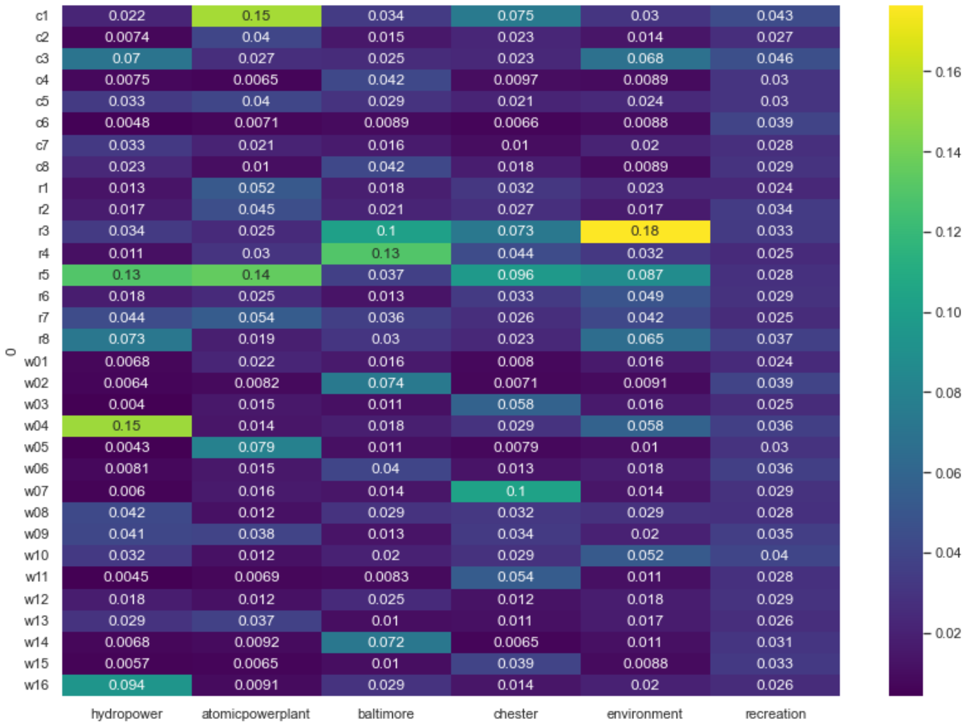

Figure B.7: Matern52 kernel feature scoring analysis

C

Appendix C

This appendix is the analysis

C.1. Metrics Squared Exponential RBF

In this section the visual analytics (parallel coordinates and boxplot) will be analysed as well as the performance metrics.

C.1.1. Parallel Coordinates

The trade-off space of the reference set of the Original RBF can be seen in Figure C.1. Each line represents a potential policy choice (a solution set of 6 objectives) that was found by the model, with lines closer to the top of the y-axis scoring more favorable. The objectives are hydropower ($/MWh), water supply reliability to the atomic power plant, Baltimore and Chester, the daily average shortage index for the environmental shortage and the storage reliability of the water level for recreation. The environmental shortage objective is to be minimized but has been inverted in these figures to make them easier to interpret. This particular parallel coordinates plot is scaled between the maximum and minimum value found for this RBF. The maximum extreme solutions for each objective are represented by a colored line, to be able to better visualize trade-offs. All other solutions are greyed out to illustrate the full objective space.

It can be noted that two solutions have been found that score high on the objectives: hydropower revenue, atomic power plant demand, Baltimore demand, Chester demand and recreation. While scoring relatively low on the environmental shortage index. These two policies were found by selecting the maximum solution for the objectives atomic power plant and Baltimore. The only objective where this policy is scoring low, is on the environmental shortage index. When inspecting the maximum solution of the environmental objective almost the exact opposite is true, scoring high on both environment and recreation while scoring low on all other objectives. This indicates a trade-off is between the environmental shortage index and the other objectives.

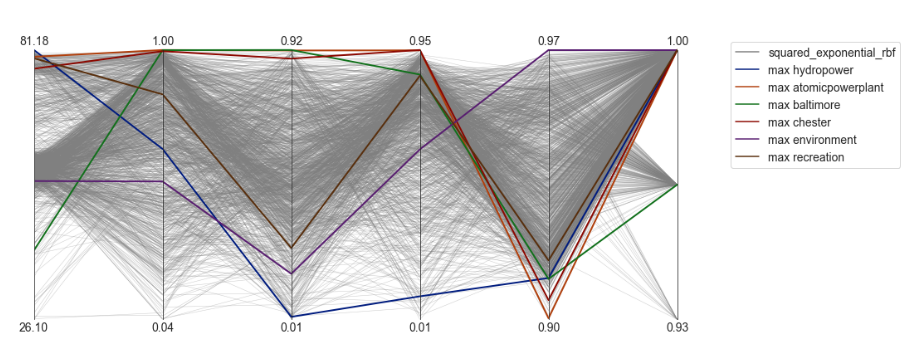

Figure C.1: Parallel Coordinates plot Squared Exponential RBF of reference set

C.1.2. Boxplot

The purpose of Figure C.2 is to better understand the distribution of the decision space of the pareto set. The hydropower objective has been normalized in this figure to be able to compare it more easily to the other objectives. The Atomic power plant, Chester and Baltimore are all demand reliability objectives. When comparing these objectives it can be noted that the water supply reliability for Baltimore, and to a lesser extent, Chester, are unable to achieve a reliability of 100% for the majority of policies. These objective are therefore harder to meet. The environmental shortage index scores between 90 and 97% reliability for this RBF. When looking at the spread of the objectives, it can be noted that the squared exponential RBF has found a large trade-off space containing a wide range of solution sets. This is especially visible for the objectives atomic power plant, baltimore and chester, where solutions were found ranging from close to 0% reliability to almost 100% reliability.

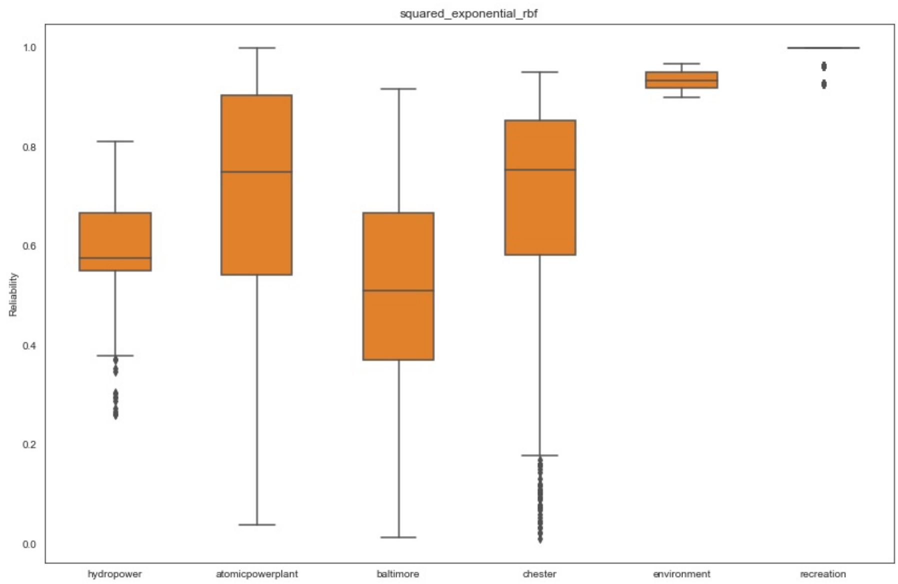

Figure C.2: Boxplot Squared Exponential RBF per generation across 10 seeds

C.1.3. Generational distance

Figure C.3 shows the generational distance per generation across 10 different seeds. All seeds start with a generational distance value of approximately 0,20 at the beginning of the optimization. This then drops rapidly to very low values at the end of the run. Figure C.3 illustrates that all 10 seeds of the model were able to fairly quickly attain one or more points near the reference set. Resulting in a low generational distance score for all seeds. This means that all seeds have a at least one point on it's approximation set close to the reference set.

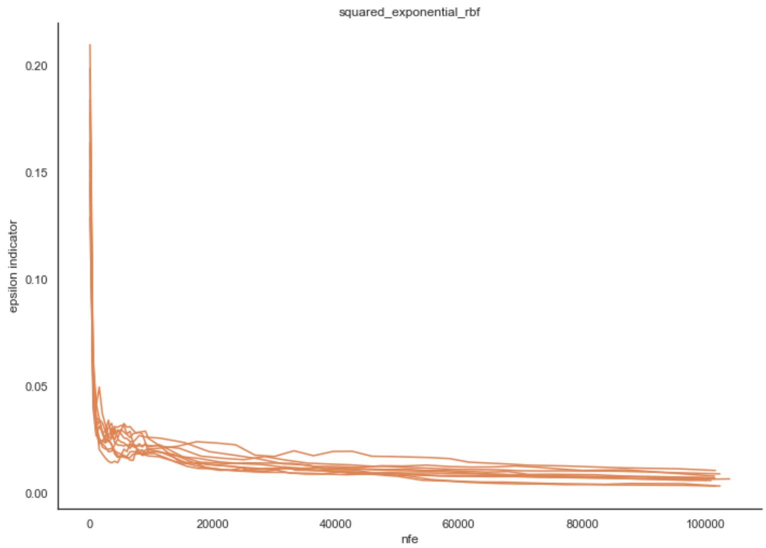

Figure C.3: Generational Distance Squared Exponential RBF per generation across 10 seeds

C.1.4. Epsilon Indicator

If any gaps are found the value of the additive epsilon indicator will increase. This metric is therefore to be minimized. Figure C.4 illustrates the epsilon indicator plotted across the amount of function evaluations for the original RBF across 10 seeds. All seeds start at the beginning of the optimization run with a value between 0.7 and 1. The additive epsilon indicator slowly improves until the optimization stops at 100.000 function evaluations. It can be noted that the epsilon indicator is fluctuating between high and low values, sometimes pretty drastically. This can be explained by new found solution sets that dominate previously found Pareto sets, but are less diverse. The lack of diversity creates gaps in the Pareto front which causes a larger additive epsilon value. The spread is fairly contained for the squared exponential RBF, with values ranging from 0.55 to 0.3 at the end of the optimization run.

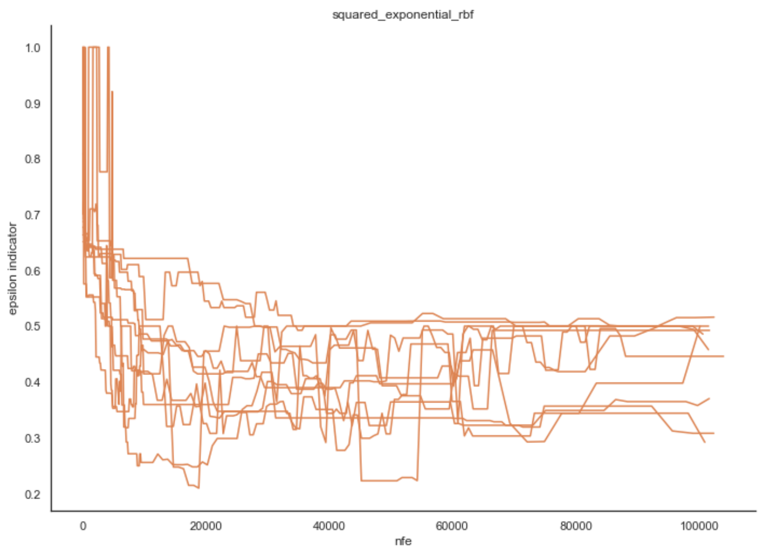

Figure C.4: Epsilon Indicator Squared Exponential RBF per generation across 10 seeds

C.1.5. Hypervolume

Hypervolume is the volume of objective space dominated by a given set of solutions. By computing the archive's hypervolume for each iteration, progress can be tracked (Kwakkel, 2019). The hypervolume indicator (Zitzler et al., 2003) takes into account both proximity and diversity. The Squared Exponential RBF kernel is still progressing in hypervolume since there is still a trend upwards noticeable for most of the seeds. This indicates that the hypervolume is not fully converged yet. This is also clear when looking at the epsilon progress in figure C.6, which shows no sign of flattening. The seeds of the squared exponential also show a fairly big spread, ranging from 0.5 to 0.3. Therefore there are some seeds that were contributing more to the reference set than others. Zooming in on the progression of seeds. This plot shows two seed where the line stabilizes and then picks up again around 25.000 and 50.000 nfe respectively, this could be explained as a second evolutionary drive. However, an alternative explanation could be that those seeds were temporarily stuck in the local optimum, and were able to recover after some time.

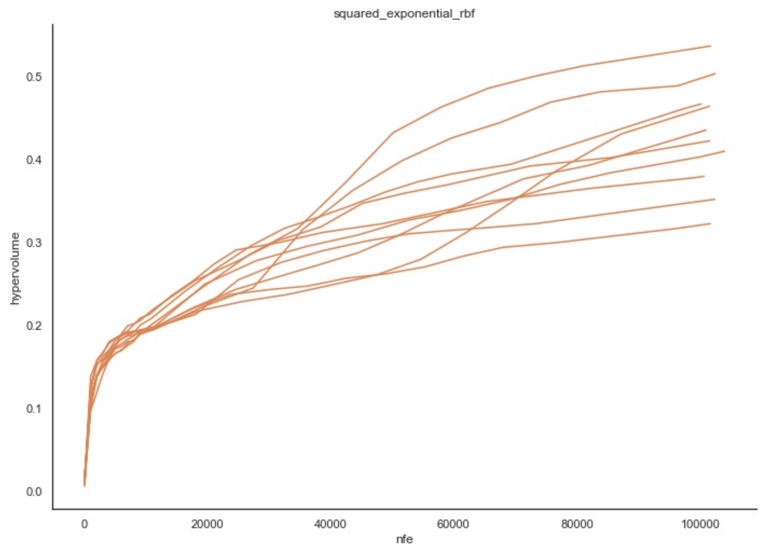

Figure C.5: Hypervolume Squared Exponential RBF per generation across 10 seeds

C.1.6. Epsilon progress

The squared exponential still has a lot of epsilon progress for all seeds. This suggests that the activation function is not converged yet and will gain more hypervolume given more nfe.

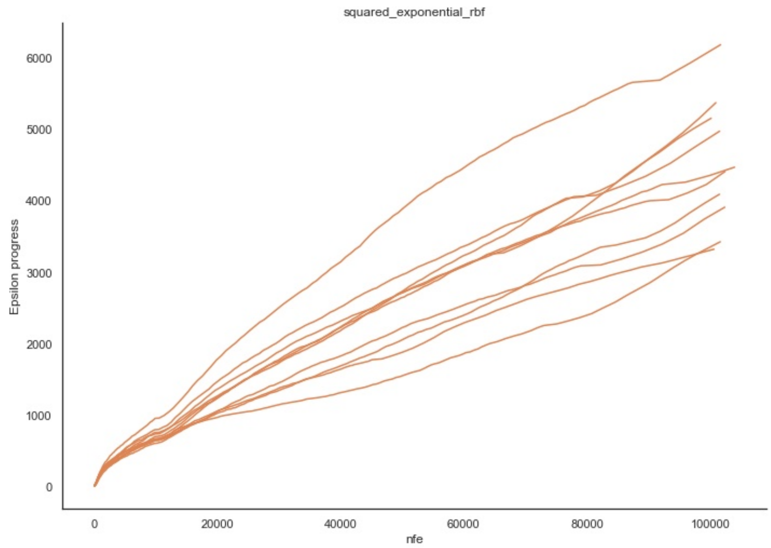

Figure C.6: Epsilon Progress Squared Exponential RBF per generation across 10 seeds

C.1.7. Archive size

Figure C.7 shows the archive size progress for the original RBF, it slowly increases per generation for all seeds. The largest archive size of 1200 is twice as big as the smallest archive is of 600. Less non-dominated solutions in the archive isn't necessarily bad, since quality of the Pareto sets is also important.

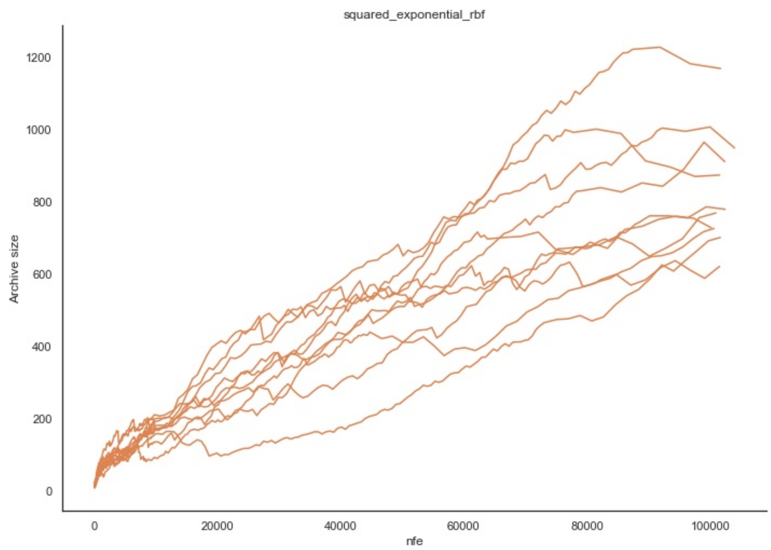

Figure C.7: Archive size Squared Exponential RBF per generation across 10 seeds

C.2. Metrics Inverse Quadratic RBF

C.2.1. Parallel Coordinates

The trade-off space of the reference set of the Original RBF can be seen in Figure C.8. Each line represents a potential policy choice (a solution set of 6 objectives) that was found by the model, with lines closer to the top of the y-axis scoring more favorable. The objectives are hydropower ($/MWh), water supply reliability to the atomic power plant, Baltimore and Chester, the daily average shortage index for the environmental shortage and the storage reliability of the water level for recreation. The environmental shortage objective is to be minimized but has been inverted in these figures to make them easier to interpret. This particular parallel coordinates plot is scaled between the maximum and minimum value found for this RBF. The maximum extreme solutions for each objective are represented by a colored line, to be able to better visualize trade-offs. All other solutions are greyed out to illustrate the full objective space.

It can be noted that one policy has been found that scores high on the objectives: hydropower revenue, atomic power plant demand, Baltimore demand, Chester demand and recreation. While scoring relatively low on the environmental shortage index. This policy were found by selecting the maximum solution for the objectives atomic power plant and Baltimore. The only objective where this policy is scoring low, is on the environmental shortage index. When inspecting the maximum solution of the environmental objective almost the exact opposite is true, scoring high on both environment and recreation while scoring low on all other objectives. This indicates a trade-off is between the environmental shortage index and the other objectives. In previous analysis of the original and squared exponential rbf the maximum policy for atomic power plant also scored high for Baltimore. That is no longer the case in this plot.

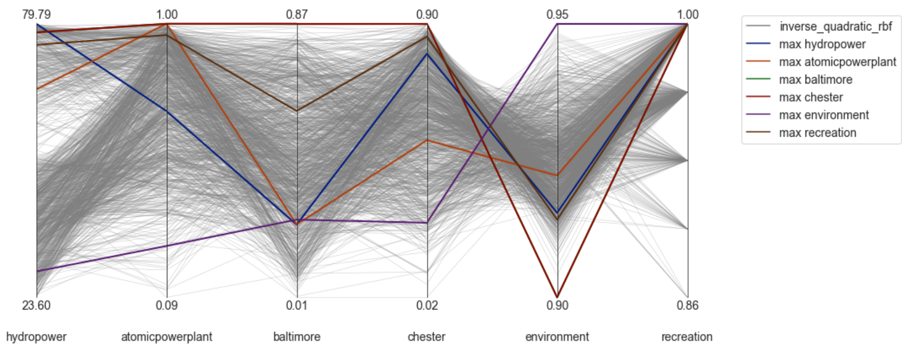

Figure C.8: Parallel Coordinates plot Inverse Quadratic RBF

C.2.2. Boxplot

The purpose of Figure C.9 is to better understand the distribution of the decision space of the pareto set. The hydropower objective has been normalized in this figure to be able to compare it more easily to the other objectives. The Atomic power plant, Chester and Baltimore are all demand reliability objectives. When comparing these objectives it can be noted that the water supply reliability for Baltimore, and to a lesser extent, Chester, are unable to achieve a reliability of 100% for the majority of policies. These objective are therefore harder to meet. The environmental shortage index scores between 90 and 97% reliability for this RBF, however, this is a bit misleading since this objective has to process a lot more water flow compared to the other objectives, this means that a deficit of 5% in reliability is still a lot of missing water which would be able to cause a shortage. When looking at the spread of the objectives, it can be noted that the Inverse Quadratic RBF has found a reasonably large objective space containing a wide range of solution sets. This is especially visible for the atomic power plant objective, where solutions were found ranging from close to 0% reliability to almost 100% reliability. And for Baltimore and chester, which ranged from 0 to 92% and 95% respectively.

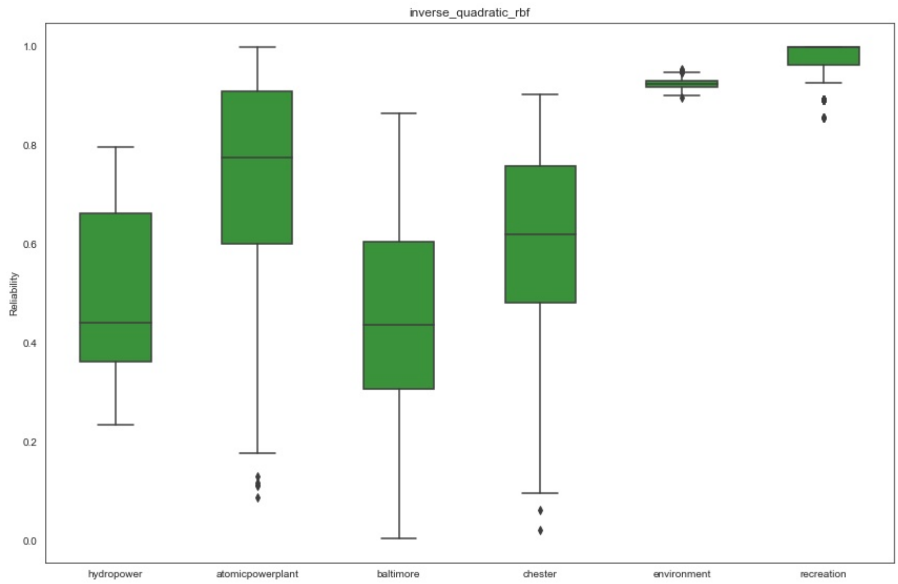

Figure C.9: Boxplot Inverse Quadratic RBF

C.2.3. Generational Distance

Figure C.10 shows the generational distance per generation across 10 different seeds. All seeds start with a generational distance value of approximately 0,20 at the beginning of the optimization. This then drops rapidly to very low values at the end of the run. Figure C.10 illustrates that all 10 seeds of the model were able to fairly quickly attain one or more points near the reference set. Resulting in a low generational distance score for all seeds. This means that all seeds have a at least one point on it's approximation set close to the reference set.

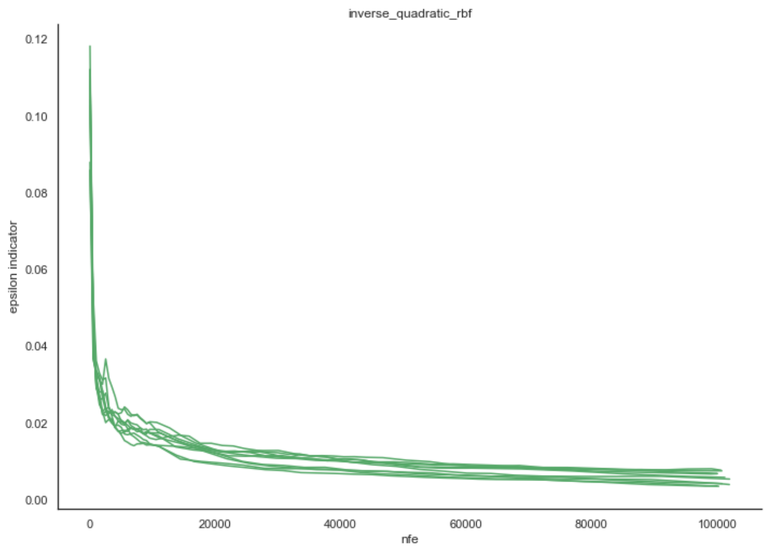

Figure C.10: Generational Distance Inverse Quadratic RBF per generation across 10 seeds

C.2.4. Epsilon Indicator

If any gaps are found the value of the additive epsilon indicator will increase. Low values are therefore desirable for this metric. Figure C.11 illustrates the epsilon indicator plotted across the amount of function evaluations for the original RBF across 10 seeds. All seeds start at the beginning of the optimization run with a value between 0.6 and 1. The additive epsilon indicator slowly improves until the optimization stops at 100.000 function evaluations. It can be noted that the epsilon indicator is also fluctuating between high and low values, sometimes pretty drastically, for example around the 27.000 nfe point at the top section of the graph, where a seed is alternating between an epsilon indicator value of 0.75 and 0.5. This can be explained by new found solution sets that dominate previously found Pareto sets, but are less diverse. The lack of diversity creates gaps in the Pareto front which causes a larger additive epsilon value. It must be said that there also more stable seeds in this plot, especially the ones on the lower side of the graph seem to fluctuate less. The seeds that started out low are staying there, only one seed jumped to the lower half of the graph around 60.000 nfe.

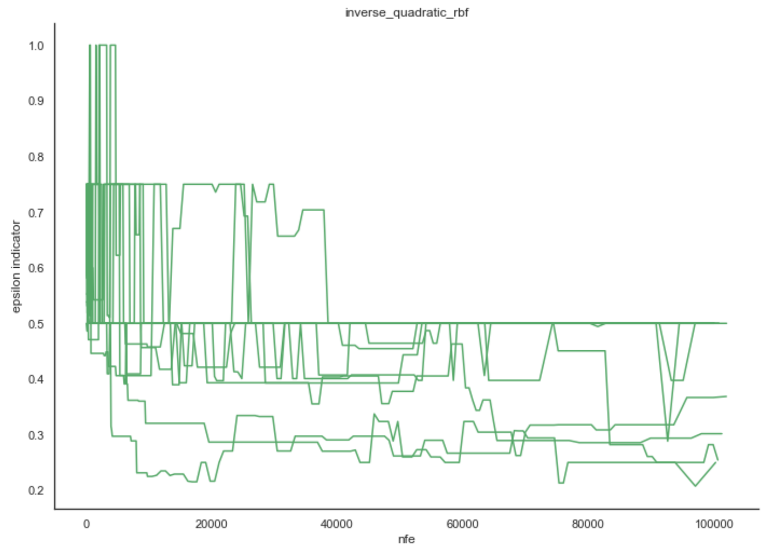

Figure C.11: Epsilon Indicator Inverse Quadratic RBF per generation across 10 seeds

C.2.5. Hypervolume

Hypervolume is the volume of objective space dominated by a given set of solutions. By computing the archive's hypervolume for each iteration, progress can be tracked (Kwakkel, 2019). The hypervolume indicator (Zitzler et al., 2003) takes into account both proximity and diversity. The hypervolume progress of the inverse quadratic RBF has a very low amount of spread. But it does make good progress especially in the first 20.000 nfe. After that, the hypervolume progress seems to converge. Due to the lack of spread, it might be that the inverse quadratic RBF is less sentitive to the random starting points of seeds. Around 80.000 nfe two groups are emerging. This could be explained by looking at the episilon indicator graph in Figure C.18. The same two group are also present in that graph, indicating that one group has larger gaps, and thus less diversity compared to the reference set. This group is has likely less hypervolume than the other group.

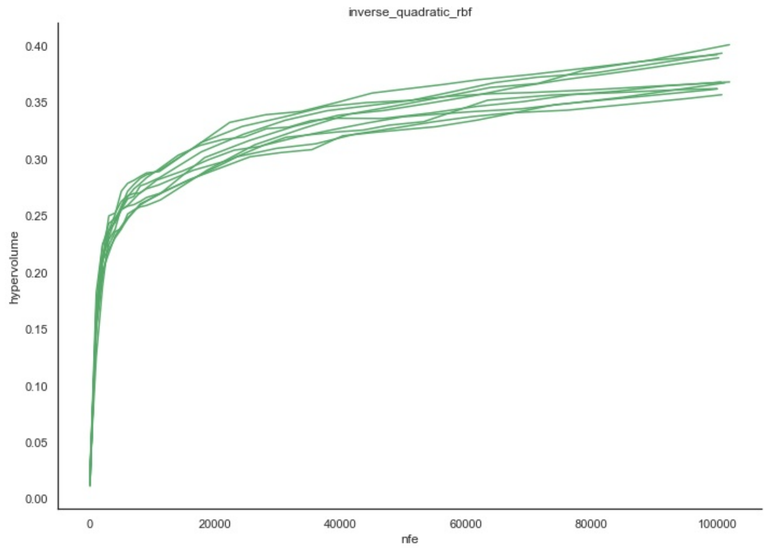

Figure C.12: Hypervolume Inverse Quadratic RBF per generation across 10 seeds

C.2.6. Epsilon Progress

The inverse quadratic still has a lot of epsilon progress for all seeds. This suggests that the activation function is not converged yet and will gain more hypervolume given more nfe. 2 seeds especially were still gaining a lot of progress, even though this not shown in the hypervolume figure.

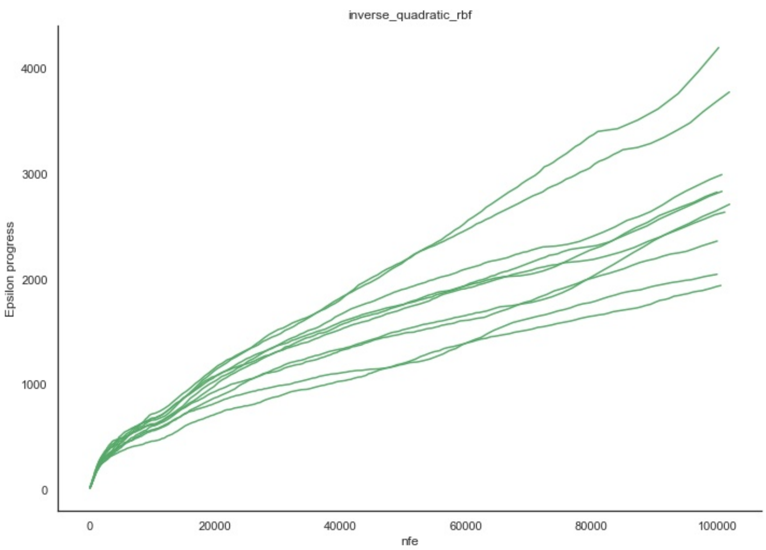

Figure C.13: Epsilon progress Inverse Quadratic RBF per generation across 10 seeds

C.2.7. Archive size

Figure C.21 shows the archive size progress for the original RBF, it slowly increases per generation for all seeds. There is one seed which has a large archive compared to the others. This largest archive size of 900 is almost four times as big as the smallest archive is of 250. Less non-dominated solutions in the archive isn't necessarily bad, since quality of the Pareto sets is also important.

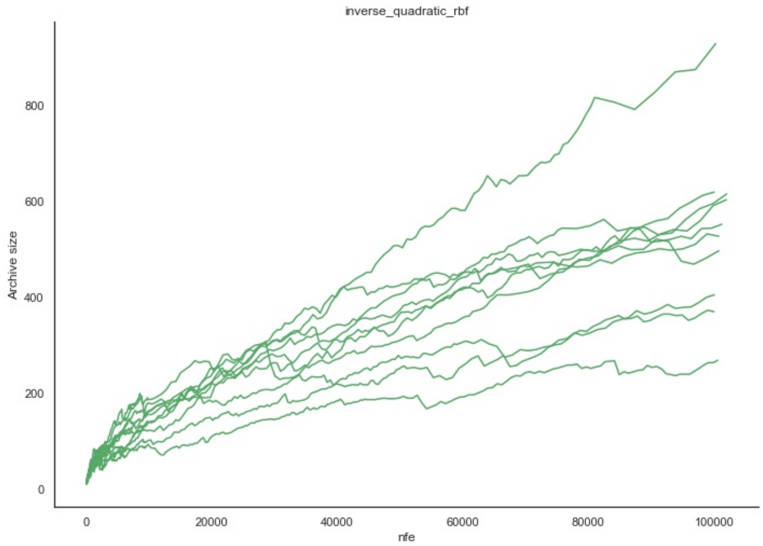

Figure C.14: Archive size Inverse Quadratic RBF per generation across 10 seeds

C.3. Metrics Inverse Multiquadric RBF

C.3.1. Parallel Coordinates

The trade-off space of the reference set of the Original RBF can be seen in Figure C.15. Each line represents a potential policy choice (a solution set of 6 objectives) that was found by the model, with lines closer to the top of the y-axis scoring more favorable. The objectives are hydropower ($/MWh), water supply reliability to the atomic power plant, Baltimore and Chester, the daily average shortage index for the environmental shortage and the storage reliability of the water level for recreation. The environmental shortage objective is to be minimized but has been inverted in these figures to make them easier to interpret. This particular parallel coordinates plot is scaled between the maximum and minimum value found for this RBF. The maximum extreme solutions for each objective are represented by a colored line, to be able to better visualize trade-offs. All other solutions are greyed out to illustrate the full objective space.

It can be noted that three policies have been found that score high on the objectives: hydropower revenue, atomic power plant demand, Baltimore demand, Chester demand and recreation. While scoring relatively low on the environmental shortage index. These two policies were found by selecting the maximum solution for the objectives atomic power plant and Baltimore. The only objective where this policy is scoring low, is on the environmental shortage index. When inspecting the maximum solution of the environmental objective almost the exact opposite is true, scoring high on both environment and recreation while scoring low on all other objectives. This indicates a trade-off is between the environmental shortage index and the other objectives.

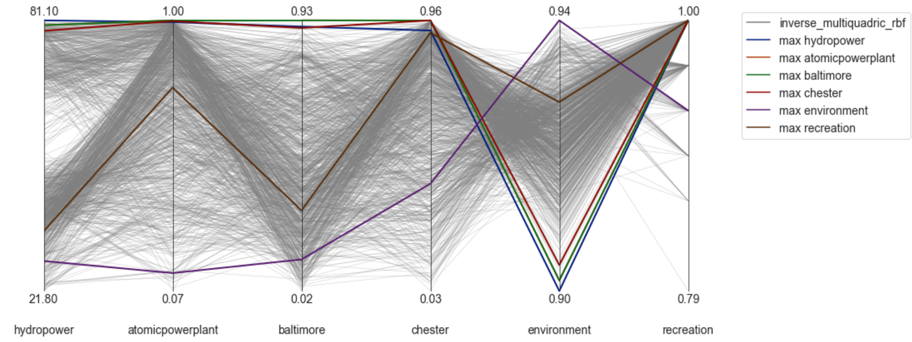

Figure C.15: Parallel Coordinates plot Inverse Multiquadric RBF

C.3.2. Boxplot

The purpose of Figure C.16 is to better understand the distribution of the decision space of the Pareto set. The hydropower objective has been normalized in this figure to be able to compare it more easily to the other objectives. The Atomic power plant, Chester and Baltimore are all demand reliability objectives. When comparing these objectives it can be noted that the water supply reliability for Baltimore, and to a lesser extent, Chester, are unable to achieve a reliability of 100% for the majority of policies. These objective are therefore harder to meet. The environmental shortage index scores between 90 and 94% reliability for this RBF, however, this objective has to process a lot more water flow compared to the other objectives, this means that a deficit of 5% in reliability is still a lot of missing water which would be able to cause a shortage. When looking at the spread of the objectives, it can be noted that the Inverse multiquadric RBF has found a reasonably large objective space containing a wide range of solution sets. This is especially visible for the atomic power plant objective, where solutions were found ranging from close to 0% reliability to almost 100% reliability. And for Baltimore and Chester, which ranged from 0 to 93% and 96% respectively.

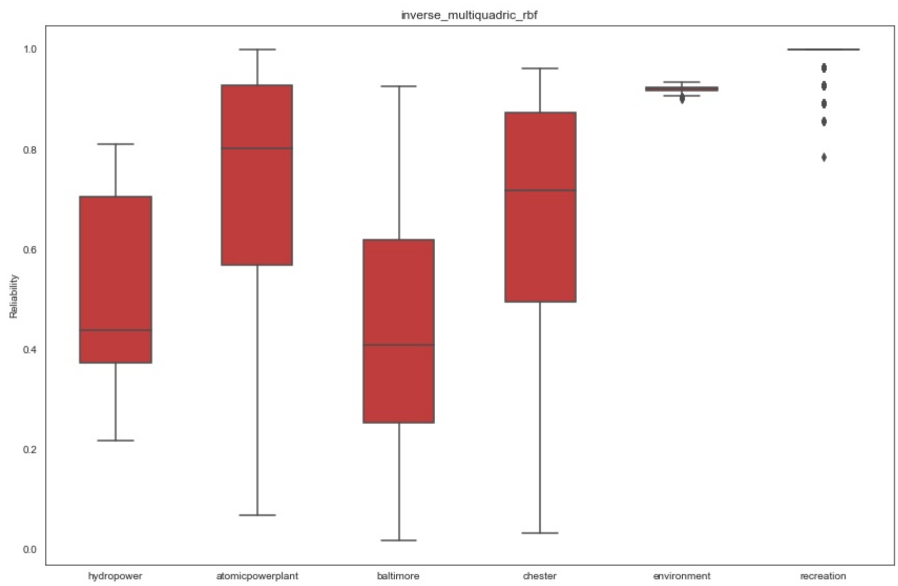

Figure C.16: Boxplot Inverse Multiquadric

C.3.3. Generational Distance

Figure C.17 shows the generational distance per generation across 10 different seeds. All seeds start with a generational distance value of approximately 0,20 at the beginning of the optimization. This then drops rapidly to very low values at the end of the run. Figure C.17 illustrates that all 10 seeds of the model were able to fairly quickly attain one or more points near the reference set. Resulting in a low generational distance score for all seeds. This means that all seeds have a at least one point on it's approximation set close to the reference set.

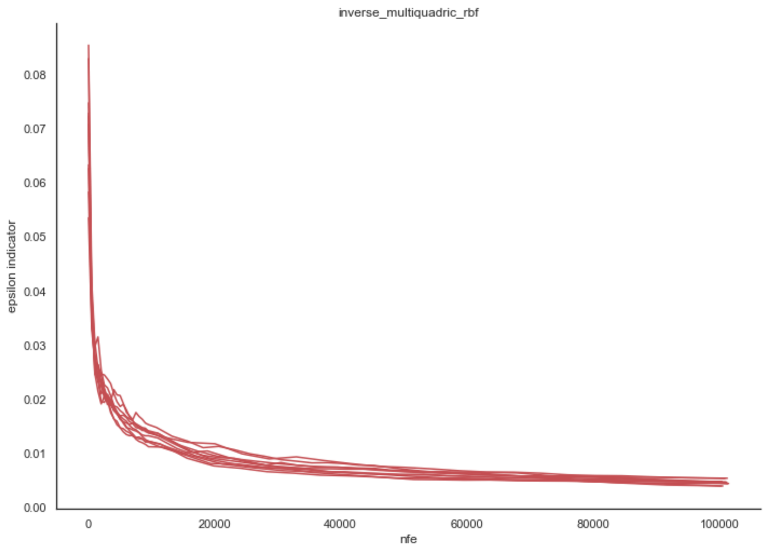

Figure C.17: Generational Distance Inverse Multiquadric RBF per generation across 10 seeds

C.3.4. Epsilon Indicator

If any gaps are found the value of the additive epsilon indicator will increase. Low values are therefore desirable for this metric. Figure C.18 illustrates the epsilon indicator plotted across the amount of function evaluations for the original RBF across 10 seeds. All seeds start at the beginning of the optimization run with a value between 0.8 and 1. The additive epsilon indicator slowly improves until the optimization stops at 100.000 function evaluations. It can be noted that the epsilon indicator is fluctuating a lot between high and low values, but most seeds seem to gravitate to lower epsilon indicator values. In the end there is only one seed that remains around a epsilon indicator of 0.7. All the other seeds have gradually dropped to the lower half of the graph.

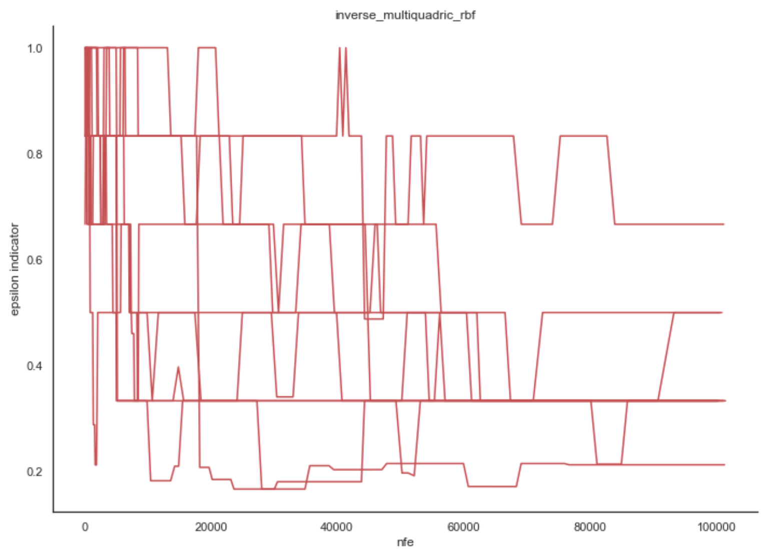

Figure C.18: Epsilon IndicatorInverse Multiquadric RBF per generation across 10 seeds

C.3.5. Hypervolume

Hypervolume is the volume of objective space dominated by a given set of solutions. By computing the archive's hypervolume for each iteration, progress can be tracked (Kwakkel, 2019). The hypervolume indicator (Zitzler et al., 2003) takes into account both proximity and diversity. The hypervolume progress of the inverse multiquadric RBF (Figure C.19) has a very low amount of spread. But it does make good progress especially in the first 20.000 nfe, just like the inverse quadratic. After that, the hypervolume progress seems to converge. Due to the lack of spread, it might be that the inverse multiquadric RBF is less sensitive to the random starting points of seeds. No groups are emerging for this activation function, but a single seed has slightly less hypervolume than the rest. When comparing it with the epsilon indicator in Figure C.18, this seed is most likely the same as the one with the high epsilon indicator score.

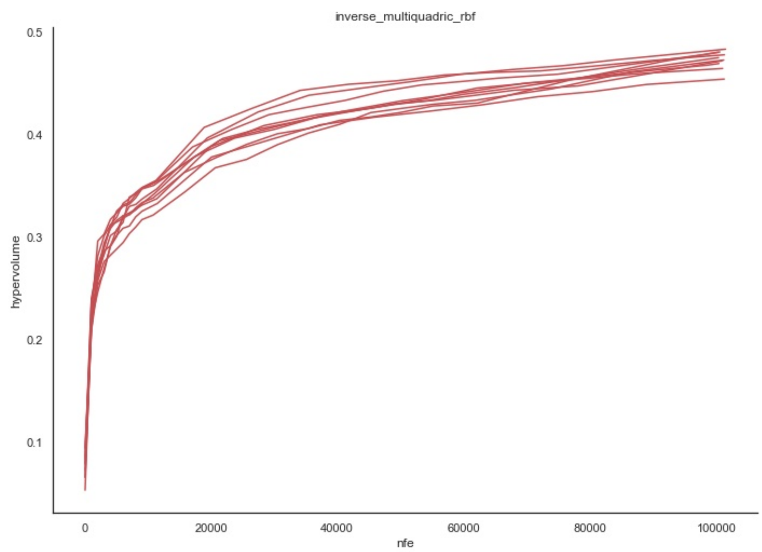

Figure C.19: Hypervolume Inverse Multiquadric RBF per generation across 10 seeds

C.3.6. Epsilon progress

The epsilon progress of the inverse multiquadric is still increasing even though the hypervolume of the inverse multiquadric has almost converged. However, it is a very light trend upwards so it might be converging soon. Just like the hypervolume, it has a small spread.

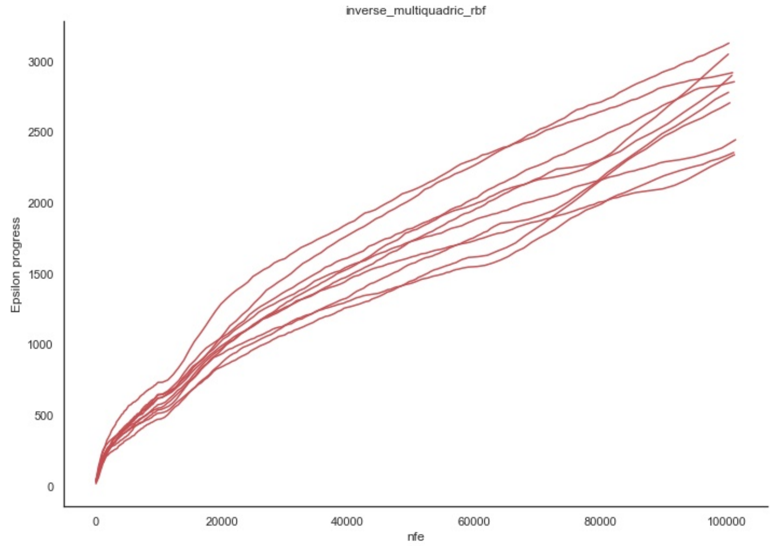

Figure C.20: Epsilon progress Inverse Multiquadric RBF per generation across 10 seeds

C.3.7. Archive size

The archive size of the inverse multiquadric is steadily increasing per generation, with a very small spread. The largest achive is twice as big as the smallest.

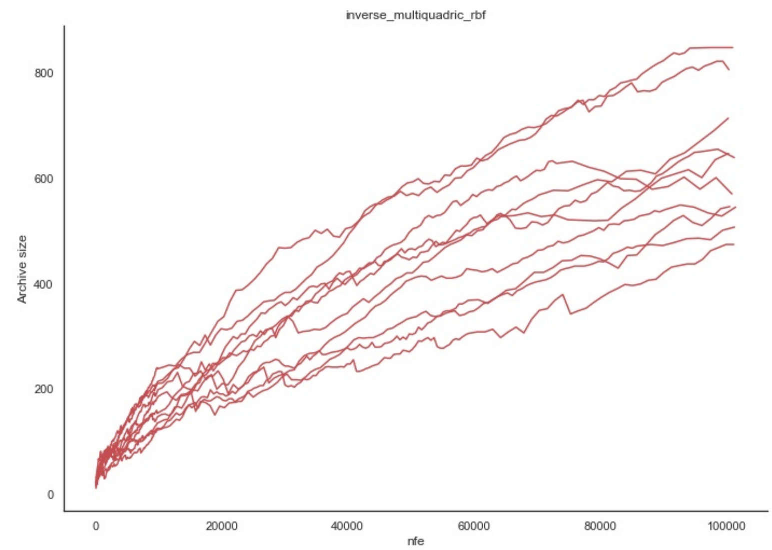

Figure C.21: Archive size Inverse Multiquadric RBF per generation across 10 seeds

C.4. Metrics Exponential RBF

C.4.1. Parallel Coordinates

The trade-off space of the reference set of the Original RBF can be seen in Figure C.22. Each line represents a potential policy choice (a solution set of 6 objectives) that was found by the model, with lines closer to the top of the y-axis scoring more favorable. The objectives are hydropower ($/MWh), water supply reliability to the atomic power plant, Baltimore and Chester, the daily average shortage index for the environmental shortage and the storage reliability of the water level for recreation. The environmental shortage objective is to be minimized but has been inverted in these figures to make them easier to interpret. This particular parallel coordinates plot is scaled between the maximum and minimum value found for this RBF. The maximum extreme solutions for each objective are represented by a colored line, to be able to better visualize trade-offs. All other solutions are greyed out to illustrate the full objective space.

The colored lines illustrate that a few policies have been found that score relatively high on the objectives: hydropower revenue, atomic power plant demand, Baltimore demand, Chester demand and recreation. The policy that maximizes hydropower looks to be most promising. While scoring low on the environmental shortage index. These policies were found by selecting the maximum solution for the objectives atomic power plant and Baltimore. The only objective where these policies are scoring low, is on the environmental shortage index. When inspecting the maximum solution of the environmental objective almost the exact opposite is true, scoring high on both environment and recreation while scoring low on all other objectives. Even though this objective space is a lot narrower than parallel coordinate plots from other activation functions. There is still a trade-off visible between the environmental shortage index and the other objectives.

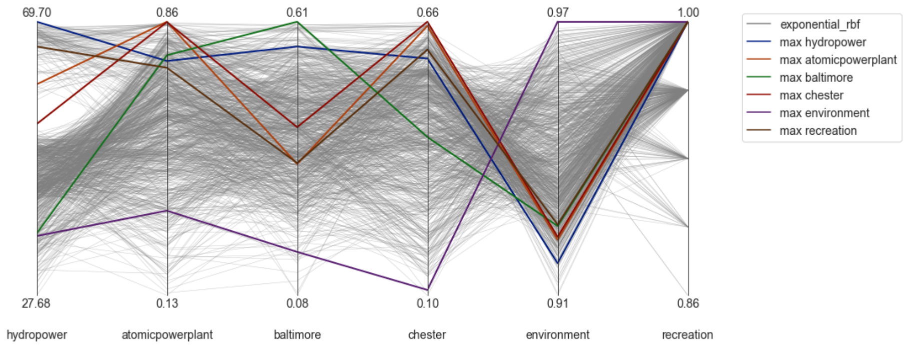

Figure C.22: Parallel Coordinates plot Exponential RBF

C.4.2. Boxplot

The purpose of Figure C.23 is to better understand the distribution of the decision space of the Pareto set. The hydropower objective has been normalized in this figure to be able to compare it more easily to the other objectives. The Atomic power plant, Chester and Baltimore are all demand reliability objectives. When comparing these objectives it can be noted that the water supply reliability for all of these objectives are unable to achieve a reliability of 100% for all policies. The environmental shortage index scores between 91% and 97% reliability for this RBF. When looking at the spread of the objectives, it can be noted that the Exponential RBF has found a narrow objective space containing a small range of solution sets. This is especially visible for the objectives Baltimore and Chester, where solutions were found ranging from close to 0% reliability to almost 61% and 66% reliability respectively. Hydropower also scores low, 75% of the solutions are between the 30 and 60 M$/year.

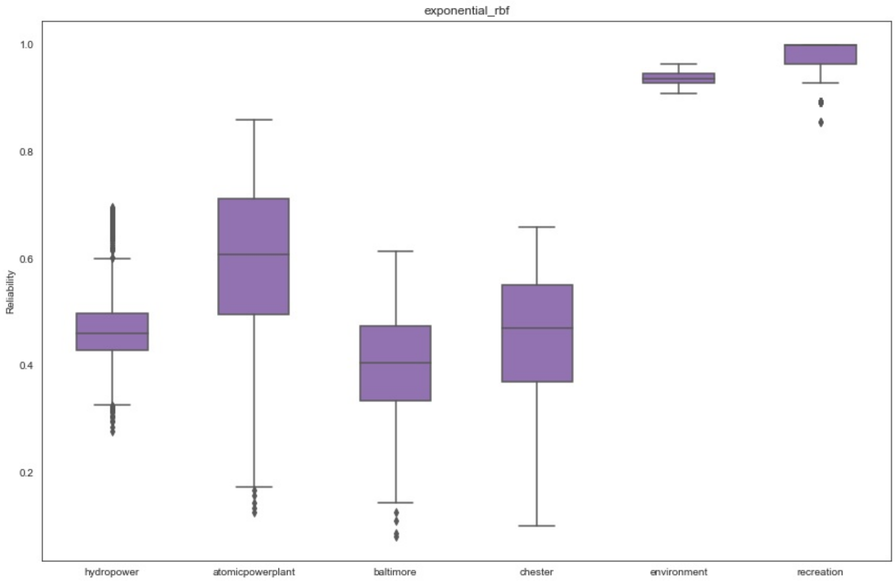

Figure C.23: Boxplot Exponential RBF

C.4.3. Generational Distance

Figure C.24 shows the generational distance per generation across 10 different seeds. All seeds start with a generational distance value of approximately 0,20 at the beginning of the optimization. This then drops rapidly to very low values at the end of the run. Figure C.24 illustrates that all 10 seeds of the model were able to fairly quickly attain one or more points near the reference set. Resulting in a low generational distance score for all seeds. This means that all seeds have a at least one point on it's approximation set close to the reference set.

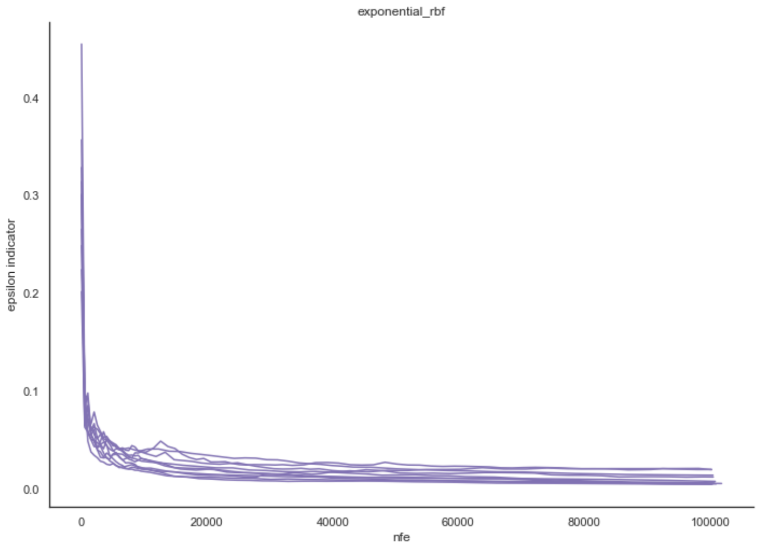

Figure C.24: Generational Distance Exponential RBF per generation across 10 seeds

C.4.4. Epsilon Indicator

If any gaps are found the value of the additive epsilon indicator will increase. Low values are therefore desirable for this metric. Figure C.25 illustrates the epsilon indicator plotted across the amount of function evaluations for the original RBF across 10 seeds. All seeds start at the beginning of the optimization run with a value between 0.8 and 1. The additive epsilon indicator slowly improves until the optimization stops at 100.000 function evaluations. It can be noted that the epsilon indicator split between two groups. The three Pareto sets in the top half of the graph with gaps in them do not seem to improve enough to drop down to the level of the other seeds. The lower half of the graph also seems to be fairly stable. This behavior might be explained by a local optimum that was found by the three seeds in the top half of the graph. This would indicate that the Exponential RBF is more sensitive for local optima.

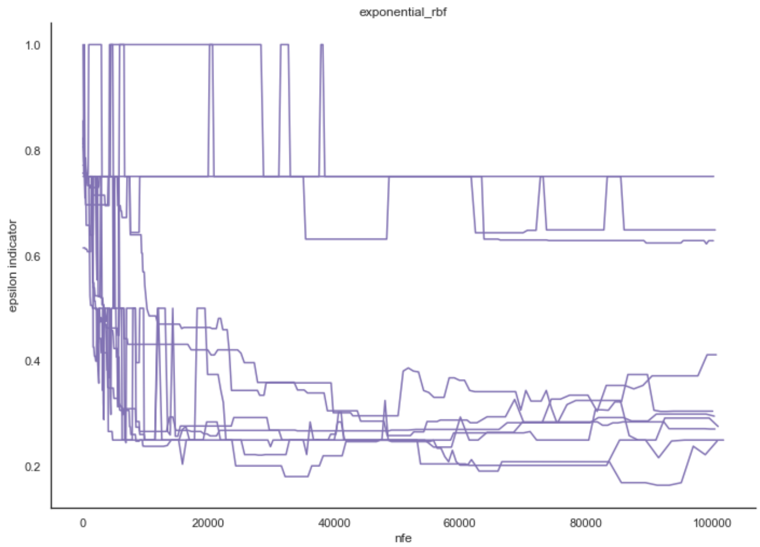

Figure C.25: Epsilon Indicator Exponential RBF per generation across 10 seeds

C.4.5. Hypervolume

Hypervolume is the volume of objective space dominated by a given set of solutions. By computing the archive's hypervolume for each iteration, progress can be tracked (Kwakkel, 2019). The hypervolume indicator (Zitzler et al., 2003) takes into account both proximity and diversity. The hypervolume progress of the exponential RBF (Figure C.26) is almost fully converged for just four seeds, in the lower half of the graph, even though it is lacking in hypervolume. Even the epsilon progress in (Figure C.25) indicates convergence for three seeds. The other seeds are still progressing, and some even have a trend upwards. This indicates that there are two groups, which can also be seen in the epsilon indicator (figure C.25). The seeds that 'converged' with low hypervolume have also a very high epsilon indicator.

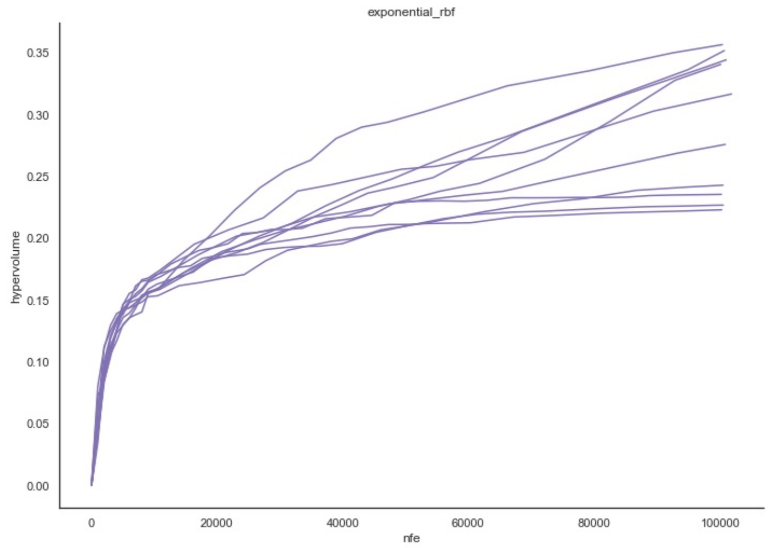

Figure C.26: Hypervolume Exponential RBF per generation across 10 seeds

C.4.6. Epsilon progress

As mentioned at the hypervolume section, there are three seeds that have converged and stopped progressing. The other seeds are still on a strong trend upwards. This confirms to the analysis in the hypervolume section.

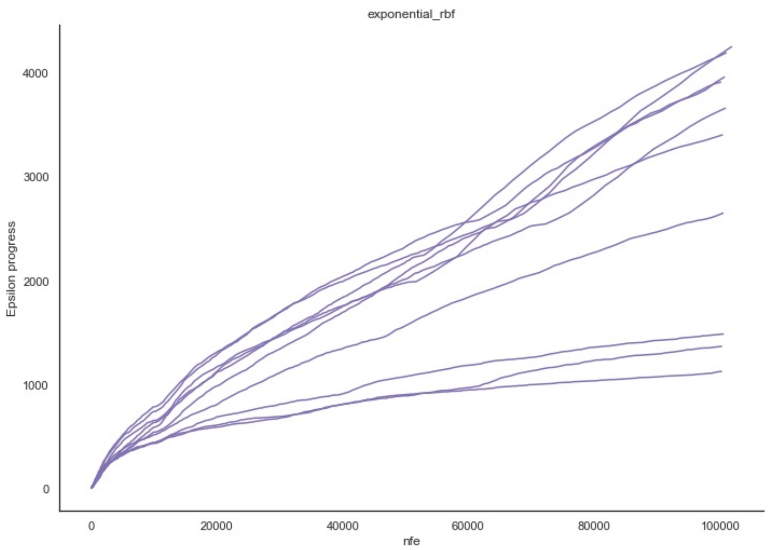

Figure C.27: Epsilon progress Exponential RBF per generation across 10 seeds

C.4.7. Archive size

In the archive size progress of the exponential RBF there are also three seeds present with a low archive. There are probably not a lot of non-dominating solutions in that archive because it has not progressed much. It converged very fast, explaining the archives without much solutions. The other 7 seeds are steadily increasing.

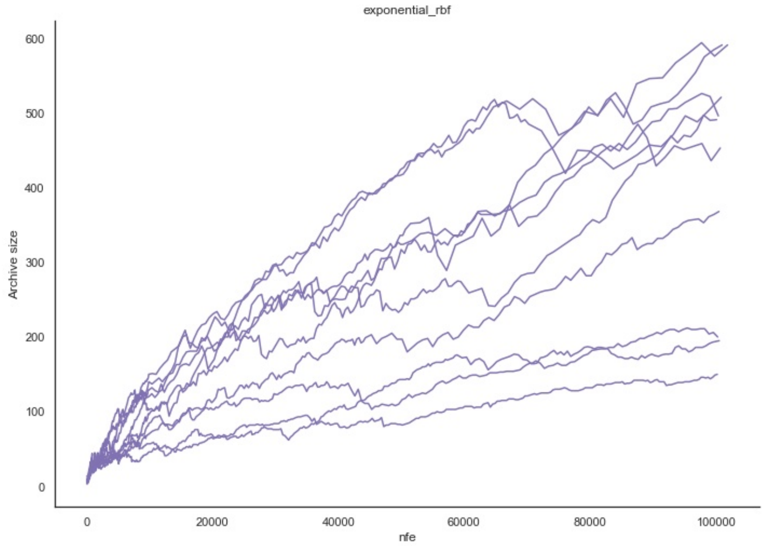

Figure C.28: Archive size Exponential RBF per generation across 10 seeds

C.5. Metrics Matern32 kernel

C.5.1. Parallel Coordinates

The trade-off space of the reference set of the Original RBF can be seen in Figure C.29. Each line represents a potential policy choice (a solution set of 6 objectives) that was found by the model, with lines closer to the top of the y-axis scoring more favorable. The objectives are hydropower ($/MWh), water supply reliability to the atomic power plant, Baltimore and Chester, the daily average shortage index for the environmental shortage and the storage reliability of the water level for recreation. The environmental shortage objective is to be minimized but has been inverted in these figures to make them easier to interpret. This particular parallel coordinates plot is scaled between the maximum and minimum value found for this RBF. The maximum extreme solutions for each objective are represented by a colored line, to be able to better visualize trade-offs. All other solutions are greyed out to illustrate the full objective space.

Two solutions have been found that score relatively high on the objectives: hydropower revenue, atomic power plant demand, Baltimore demand, Chester demand and recreation. While scoring relatively low on the environmental shortage index. These two policies were found by selecting the maximum solution for the objectives atomic power plant and Baltimore. The only objective where this policy is scoring low, is on the environmental shortage index. When inspecting the maximum solution of the environmental objective almost the exact opposite is true, scoring high on both environment and recreation while scoring low on all other objectives. This indicates a trade-off is between the environmental shortage index and the other objectives.

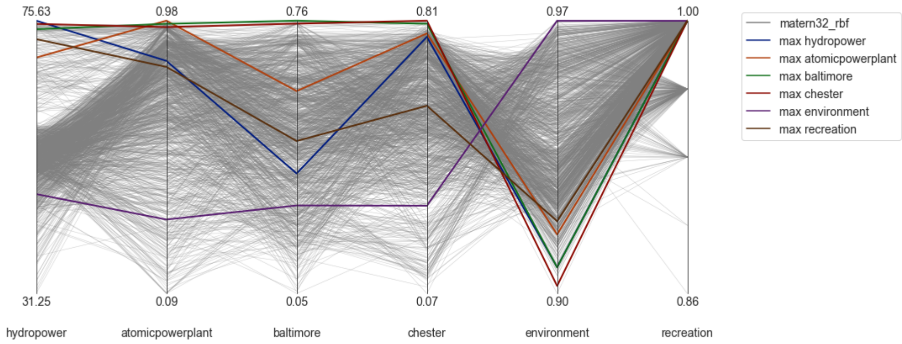

Figure C.29: Parallel Coordinates plot Matern32 kernel

C.5.2. Boxplot

The purpose of Figure C.30 is to better understand the distribution of the decision space of the Pareto set. The hydropower objective has been normalized in this figure to be able to compare it more easily to the other objectives. The Atomic power plant, Chester and Baltimore are all demand reliability objectives. When comparing these objectives it can be noted that the water supply reliability for all of these objectives are unable to achieve a reliability close to 100% for all policies. The environmental shortage index scores between 91% and 97% reliability for this RBF. When looking at the spread of the objectives, it can be noted that the Matern32 kernel has found a narrow objective space containing a small range of solution sets. This is especially visible for the objectives Baltimore and Chester, where solutions were found ranging from close to 0% reliability to almost 61% and 66% reliability respectively. Hydropower also scores low, where a big part of the solutions lie between the 30 and 60 $/MWh.

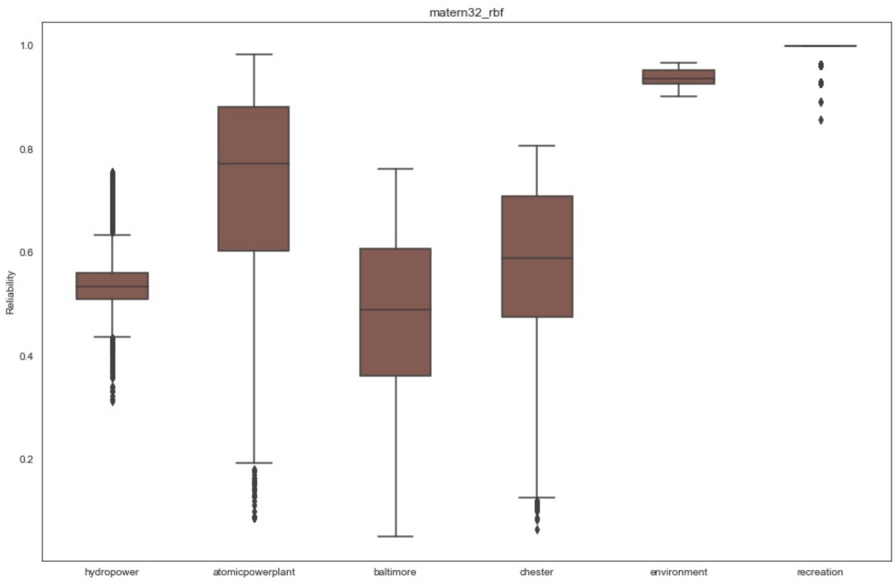

Figure C.30: Boxplot Matern32 kernel

C.5.3. Generational Distance

Figure C.31 shows the generational distance per generation across 10 different seeds. All seeds start with a generational distance value of approximately 0,20 at the beginning of the optimization. This then drops rapidly to very low values at the end of the run. Figure C.31 illustrates that all 10 seeds of the model were able to fairly quickly attain one or more points near the reference set. Resulting in a low generational distance score for all seeds. This means that all seeds have a at least one point on it's approximation set close to the reference set.

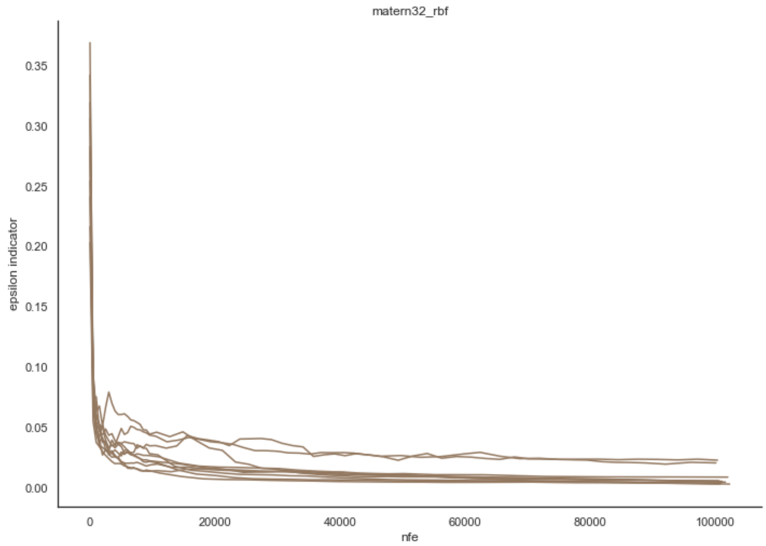

Figure C.31: Generational Distance Matern32 kernel per generation across 10 seeds

C.5.4. Epsilon Indicator

If any gaps are found the value of the additive epsilon indicator will increase. Low values are therefore desirable for this metric. Figure C.32 illustrates the epsilon indicator plotted across the amount of function evaluations for the original RBF across 10 seeds. All seeds start at the beginning of the optimization run with a value between 0.6 and 1. The additive epsilon indicator improves fairly quickly for all seeds until around 20.000 nfe, then it remains constant until the optimization stops at 100.000 function evaluations. It can be noted that the epsilon indicator is fluctuating between high and low values. This can be explained by new found solution sets that dominate previously found Pareto sets, but are less diverse. The lack of diversity creates gaps in the Pareto front which causes a larger additive epsilon value. The Matern32 kernel scores fairly wel for the epsilon indicator, this could be explained by the narrow reference set that was found by this activation function. Since the reference set was narrow, the reference would be less diverse, making it easier to score well for as a single seed compared to the reference set.

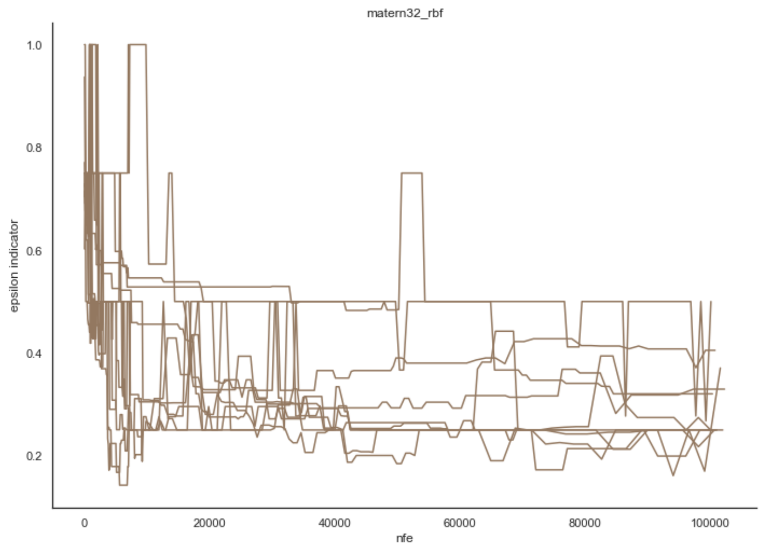

Figure C.32: Epsilon Indicator Matern32 kernel per generation across 10 seeds

C.5.5. Hypervolume

Hypervolume is the volume of objective space dominated by a given set of solutions. By computing the archive's hypervolume for each iteration, progress can be tracked (Kwakkel, 2019). The hypervolume indicator (Zitzler et al., 2003) takes into account both proximity and diversity. Three of the seeds of the matern32 kernel are converging, while the others are still progressing. This is also clear when looking at the epsilon progress in figure C.27, which shows no sign of flattening for most of the seeds, however, two seeds seemed to have converged, while the others are still progressing. The seeds of the matern32 kernel also show a fairly big spread, ranging from 0.5 to 0.25. But this is mostly due to the two seeds that have converged. These might be stuck in a local optimum.

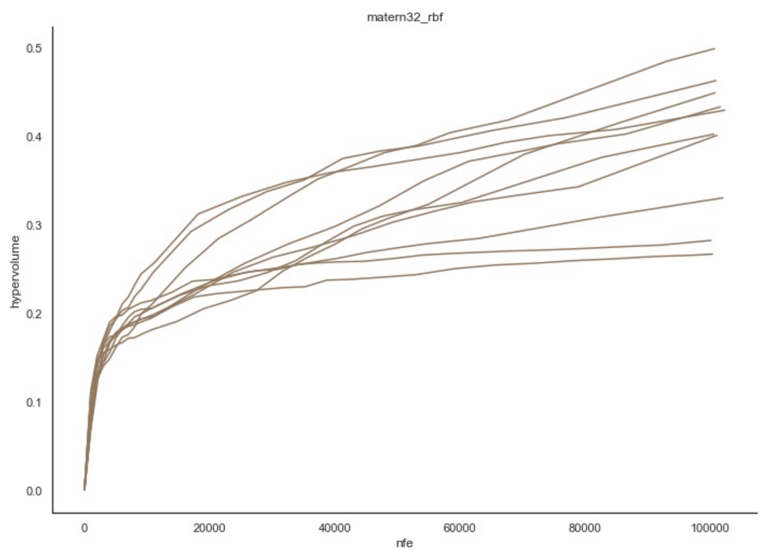

Figure C.33: Hypervolume Matern32 kernel per generation across 10 seeds

C.5.6. Epsilon progress

As mentioned at the hypervolume section, there are two seeds that have converged and stopped progressing. The other seeds are still on a strong trend upwards. This confirms to the analysis in the hypervolume section.

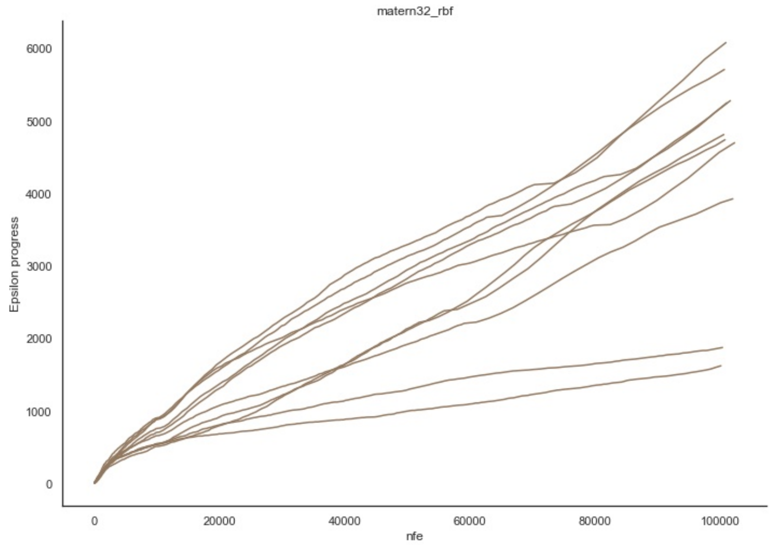

Figure C.34: Epsilon progress Matern32 kernel per generation across 10 seeds

C.5.7. Archive size

The archive size is slowly increasing with each generation, except for the two seeds that have converged and also show no sign of increasing epsilon progress and hypervolume.

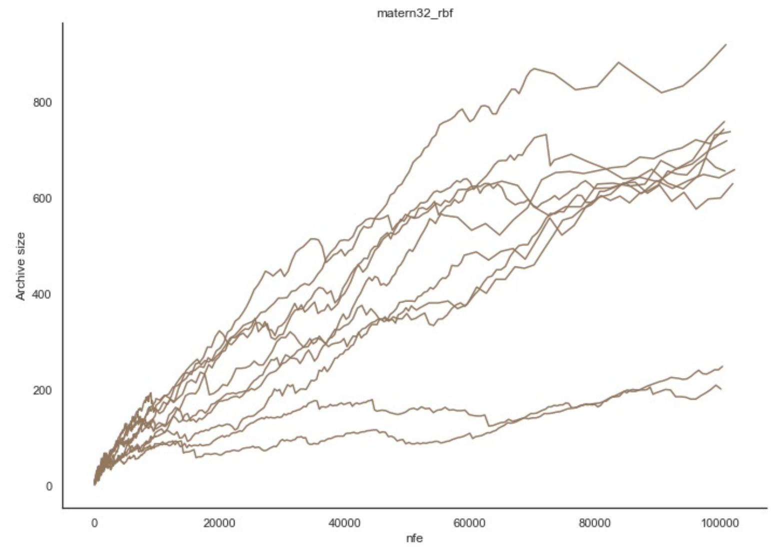

Figure C.35: Archive size Matern32 kernel per generation across 10 seeds

C.6. Metrics Matern52 kernel

The trade-off space of the reference set of the Original RBF can be seen in Figure C.36. Each line represents a potential policy choice (a solution set of 6 objectives) that was found by the model, with lines closer to the top of the y-axis scoring more favorable. The objectives are hydropower ($/MWh), water supply reliability to the atomic power plant, Baltimore and Chester, the daily average shortage index for the environmental shortage and the storage reliability of the water level for recreation. The environmental shortage objective is to be minimized but has been inverted in these figures to make them easier to interpret. This particular parallel coordinates plot is scaled between the maximum and minimum value found for this RBF. The maximum extreme solutions for each objective are represented by a colored line, to be able to better visualize trade-offs. All other solutions are greyed out to illustrate the full objective space.

One solutions has been found that scores high on the objectives: hydropower revenue, atomic power plant demand, Baltimore demand, Chester demand and recreation. While scoring relatively low on the environmental shortage index. This policies was found by selecting the maximum solution for Chester. The maximum policy from the atomic powerplant and of hydropower also come close but they score fairly low on the Baltimore objective. The only objective where the Chester policy is scoring low, is on the environmental shortage index. When inspecting the maximum solution of the environmental objective almost the exact opposite is true, scoring high on both environment and recreation while scoring low on all other objectives. This indicates a trade-off is between the environmental shortage index and the other objectives.

C.6.1. Parallel Coordinates

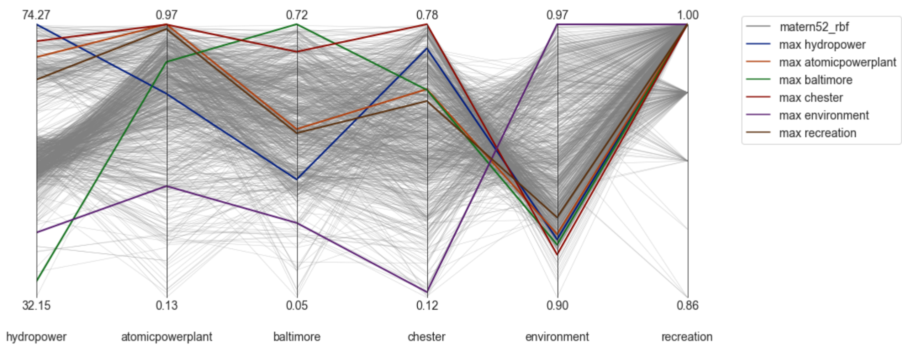

Figure C.36: Parallel Coordinates plot Matern52 kernel

The purpose of Figure C.37 is to better understand the distribution of the decision space of the Pareto set. The hydropower objective has been normalized in this figure to be able to compare it more easily to the other objectives. The Atomic power plant, Chester and Baltimore are all demand reliability objectives. When comparing these objectives it can be noted that the water supply reliability for all of these objectives are unable to achieve a reliability of 100% for all policies. The environmental shortage index scores between 90% and 97% reliability for this RBF. When looking at the spread of the objectives, it can be noted that the Matern52 kernel has found a relatively narrow objective space containing a small range of solution sets. This is especially visible for the objectives Baltimore and Chester, where solutions were found ranging from close to 0% reliability to almost 72% and 78% reliability respectively.

C.6.2. Boxplot

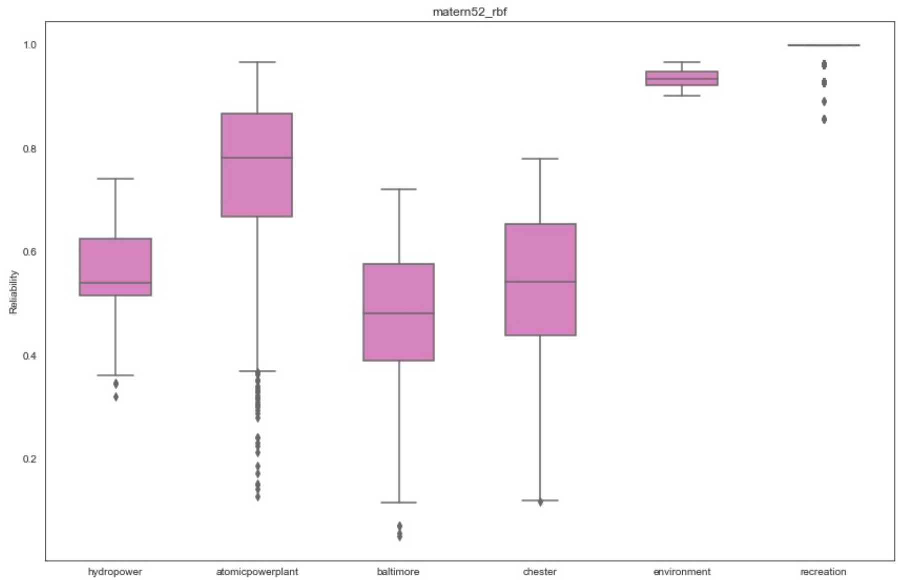

Figure C.37: Boxplot Matern52 kernel

C.6.3. Generational Distance

Figure C.38 shows the generational distance per generation across 10 different seeds. Some seeds have a higher starting value than others, oen starts at a very high value (0.7) for instance, others from 0.45. This then drops rapidly to very low values at the end of the run. Figure C.38 illustrates that all 10 seeds of the model were able to fairly quickly attain one or more points near the reference set. Resulting in a low generational distance score for all seeds. This means that all seeds have a at least one point on it's approximation set close to the reference set.

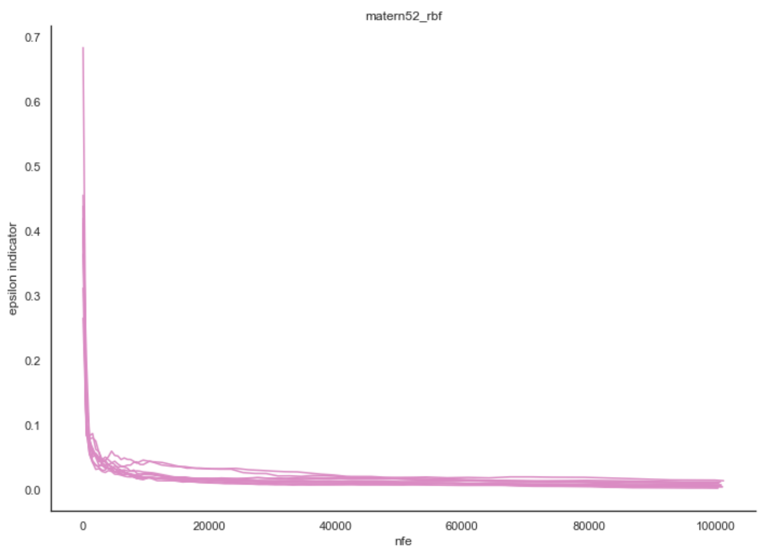

Figure C.38: Generational Distance Matern52 kernel per generation across 10 seeds

C.6.4. Epsilon Indicator

If any gaps are found the value of the additive epsilon indicator will increase. Low values are therefore desirable for this metric. Figure C.39 illustrates the epsilon indicator plotted across the amount of function evaluations for the original RBF across 10 seeds. All seeds start at the beginning of the optimization run with a value between 0.6 and 1. The additive epsilon indicator slowly improves for most seeds, until the optimization stops at 100.000 function evaluations. The one exception remains in the top half of the graph. This could again be explained by a local optimum in the fitness landscape.

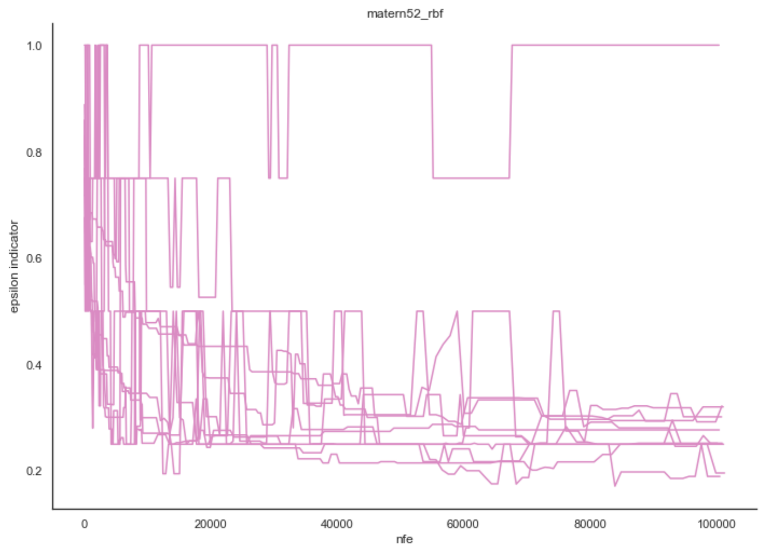

Figure C.39: Epsilon Indicator Matern52 kernel per generation across 10 seeds

C.6.5. Hypervolume

Hypervolume is the volume of objective space dominated by a given set of solutions. By computing the archive's hypervolume for each iteration, progress can be tracked (Kwakkel, 2019). The hypervolume indicator (Zitzler et al., 2003) takes into account both proximity and diversity. The matern53 kernel (Figure C.40 has one seeds that is converging, while others are still having hypervolume progression. This is most likely the solution with the extremely high epsilon indicator (figure C.39) and flat epsilon progress (figure C.41). Furthermore the matern52 hypervolume progression is pretty spread out.

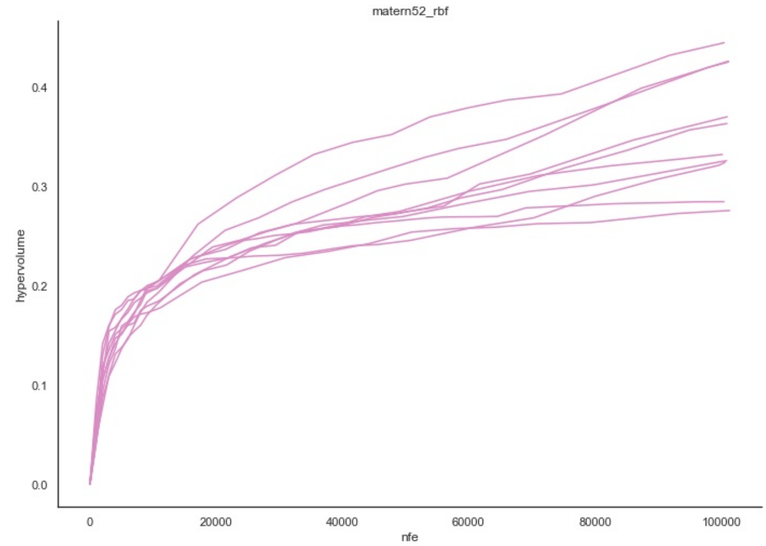

Figure C.40: Hypervolume Matern52 kernel per generation across 10 seeds

C.6.6. Epsilon progress

As stated in the hypervolume section, there is one seed that has converged. The others are still progressing with little spread.

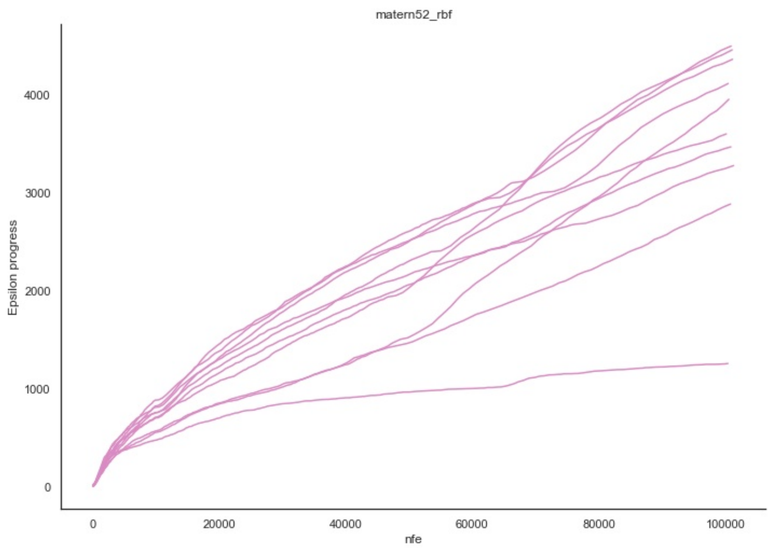

Figure C.41: Epsilon progress Matern52 kernel per generation across 10 seeds

C.6.7. Archive size

Similar to the hypervolume and epsilon indicator section for the matern52, there is one seed that has a low archive because it has converged. The others still have a trend to progress further.

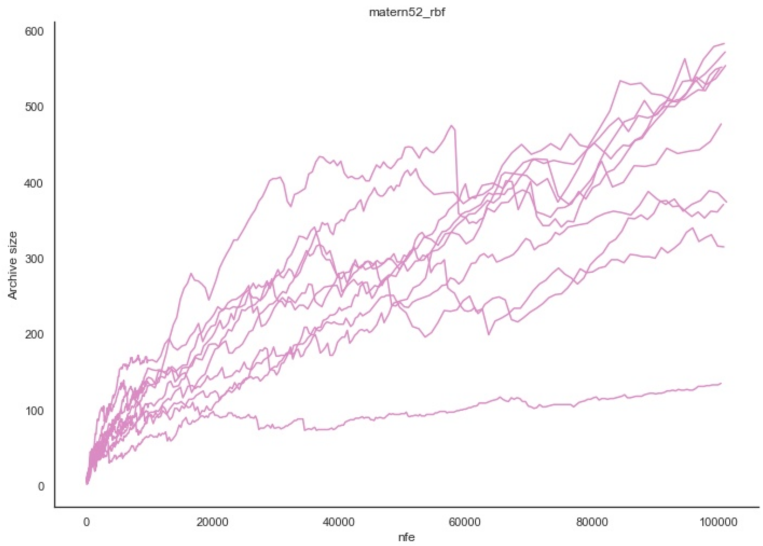

Figure C.42: Archive size Matern52 kernel per generation across 10 seeds

D

Appendix D

In this appendix, a Kruskal-Wallis is performed on the maximum attained hypervolume for all seeds for all activation functions. Next, the Kruskall-Wallis and Mann-Whitney tests are performed on all outcomes found for each objective for each activation function. These statistical tests are used to check if the tested samples are a statistically similar or not.

The Kruskal-Wallis test checks whether there is a difference between several independent groups for not normally distributed data. The Kruskal-Wallis test requires a minimum sample size of 5. Because the samples does not have to be normally distributed, the Kruskal-Wallis test ranks each value and measures the difference in the ranked totals.

Kruskal-Wallis:
$\alpha = 0.05$
The null hypothesis H0 = There is no difference between groups (if < 3.84146)
The alternative hypothesis H1 = There is a difference between groups (if > 3.84146)
Degrees of freedom = 1 (2 samples tested against each other) $\chi^2 = 3.84146$

The Mann-Whitney U-Test checks if sample A is the same as the distribution underlying sample B. The Mann-Whitney U-Test requires a minimum sample size of 20. For this test the samples also do not have to be normally distributed. The Mann-Whitney U-Test ranks each value and measures the difference in the ranked totals.

Mann-Whitney:
$\alpha = 0.05$
The null hypothesis H0 = There is no difference between the ranks of the two groups (if <-1.96 or >1.96)
The alternative hypothesis H1 = There is a difference between the ranks of the two groups (if
Z = 1.96 (if samples bigger than 20)

D.1. Hypervolume

The Kruskal-Wallis test can be used to check if the hypervolume scores of each activation functions are considered statistically the same or not. The Mann-Whitney test cannot be used to check the hypervolume, since only 10 different seeds were used for each activation function, and the required sample size is 20.

	original	squared exponential	inverse quadratic	inverse multiquadric	exponential	matern32	matern52
original	0.0	1.85	13.17	0.02	14.29	4.48	10.57
squared exponential	1.85	0.0	3.86	3.86	11.57	0.97	4.17
inverse quadratic	13.17	3.86	0.0	14.29	14.29	2.06	0.69
inverse multiquadric	0.02	3.86	14.29	0.0	14.29	8.69	14.29
exponential	14.29	11.57	14.29	14.29	0.0	7.0	4.48
matern32	4.48	0.97	2.06	8.69	7.0	0.0	1.65
matern52	10.57	4.17	0.69	14.29	4.48	1.65	0.0

Table D.1: Kruskal-Wallis test, hypervolume

For each score below a χ^2 of 3.84146 the null hypothesis is accepted (The 0 scores are disregarded since they compare the same sample.). The null hypothesis is accepted for a six of combinations, which would mean that there is no difference between these groups. However, the p-value also needs to be below 0.05 before this measurement is considered statistically significant. This is not the case for any of the values where H0 was accepted. As can be seen in the table D.2 below.

	original	squared exponential	inverse quadratic	inverse multiquadric	exponential	matern32	matern52
original	1.0	0.17	0.0	0.88	0.0	0.03	0.0
squared exponential	0.17	1.0	0.05	0.05	0.0	0.33	0.04
inverse quadratic	0.0	0.05	1.0	0.0	0.0	0.15	0.41
inverse multiquadric	0.88	0.05	0.0	1.0	0.0	0.0	0.0
exponential	0.0	0.0	0.0	0.0	1.0	0.01	0.03
matern32	0.03	0.33	0.15	0.0	0.01	1.0	0.2
matern52	0.0	0.04	0.41	0.0	0.03	0.2	1.0

Table D.2: Kruskal-Wallis test, hypervolume, P value

D.2. Hydropower

In the Kruskal-Wallis test, For each score below a χ^2 of 3.84146 the null hypothesis is accepted (The 0 scores are disregarded since they compare the same sample.). The null hypothesis is accepted for a 2 pair of combinations, which would mean that there is no difference between these groups. However, both groups that accepted H0 are not statistically significant, with a p value higher than 0.05.

	original	squared exponential	inverse quadratic	inverse multiquadric	exponential	matern32	matern52
original	0.0	0.8	402.93	192.35	790.68	376.61	137.22
squared exponential	0.8	0.0	439.35	211.46	915.63	553.74	245.67
inverse quadratic	402.93	439.35	0.0	5.95	12.77	240.18	245.01
inverse multiquadric	192.35	211.46	5.95	0.0	0.83	86.13	93.12
exponential	790.68	915.63	12.77	0.83	0.0	564.97	635.85
matern32	376.61	553.74	240.18	86.13	564.97	0.0	22.45
matern52	137.22	245.67	245.01	93.12	635.85	22.45	0.0

Table D.3: Kruskal-Wallis test, hydropower

	original	squared exponential	inverse quadratic	inverse multiquadric	exponential	matern32	matern52
original	1.0	0.37	0.0	0.0	0.0	0.0	0.0
squared exponential	0.37	1.0	0.0	0.0	0.0	0.0	0.0
inverse quadratic	0.0	0.0	1.0	0.01	0.0	0.0	0.0
inverse multiquadric	0.0	0.0	0.01	1.0	0.36	0.0	0.0
exponential	0.0	0.0	0.0	0.36	1.0	0.0	0.0
matern32	0.0	0.0	0.0	0.0	0.0	1.0	0.0
matern52	0.0	0.0	0.0	0.0	0.0	0.0	1.0

Table D.4: Kruskal-Wallis test, hydropower, P value

For the Mann-Whitney U test, the Z value needs to be between -1.96 and 1.96 to be able accept the null hypothesis. If it is greater than 1.96 or lower than -1.96, there is a difference between the ranks of the two groups. All values are far exceeding 1.96, so the null hypothesis can be rejected for all pairs.

	original	squared exponential	inverse quadratic	inverse multiquadric	exponential	matern32	matern52
original	1146098.0	1007360.0	1381423.0	1149758.0	1198040.0	1395145.0	836346.0
squared exponential	1047138.0	920724.5	1265240.0	1048806.0	1116918.0	1341540.0	811117.0
inverse quadratic	535301.0	452722.0	801378.0	690426.0	545703.0	529321.0	325569.0
inverse multiquadric	601940.0	521243.0	774336.0	669324.5	534664.0	586255.0	371258.0
exponential	234204.0	166804.0	651933.0	559858.0	447458.0	252682.0	126979.0
matern32	563971.0	414418.0	1108883.0	910903.0	971442.0	837218.0	487662.0
matern52	461152.0	351832.0	759393.0	620291.0	683743.0	621296.0	367224.5

Table D.5: Mann-Whitney test, hydropower

D.3. Atomic power plant

For each score below a χ^2 of 3.84146 the null hypothesis is accepted (The 0 scores are disregarded since they compare the same sample.). The null hypothesis is accepted for a 6 pair of combinations, which would mean that there is no difference between these groups. However, all groups that accepted H0 do not have a p value below 0.05, which means that the similarity between the groups is not statistically significant.

	original	squared exponential	inverse quadratic	inverse multiquadric	exponential	matern32	matern52
original	0.0	75.36	39.31	21.29	646.66	97.58	60.57
squared exponential	75.36	0.0	8.28	9.19	198.45	0.01	2.88
inverse quadratic	39.31	8.28	0.0	0.26	340.6	9.44	1.12
inverse multiquadric	21.29	9.19	0.26	0.0	260.49	13.45	3.83
exponential	646.66	198.45	340.6	260.49	0.0	296.25	378.46
matern32	97.58	0.01	9.44	13.45	296.25	0.0	2.13
matern52	60.57	2.88	1.12	3.83	378.46	2.13	0.0

Table D.6: Kruskal-Wallis test, atomic power plant

	original	squared exponential	inverse quadratic	inverse multiquadric	exponential	matern32	matern52
original	1.0	0.0	0.0	0.0	0.0	0.0	0.0
squared exponential	0.0	1.0	0.0	0.0	0.0	0.91	0.09
inverse quadratic	0.0	0.0	1.0	0.61	0.0	0.0	0.29
inverse multiquadric	0.0	0.0	0.61	1.0	0.0	0.0	0.05
exponential	0.0	0.0	0.0	0.0	1.0	0.0	0.0
matern32	0.0	0.91	0.0	0.0	0.0	1.0	0.14
matern52	0.0	0.09	0.29	0.05	0.0	0.14	1.0

Table D.7: Kruskal-Wallis test, P value, atomic power plant

For the Mann-Whitney U test, the Z value needs to be between -1.96 and 1.96 to be able accept the null hypothesis. If it is greater than 1.96 or lower than -1.96, there is a difference between the ranks of the two groups. All values are far exceeding 1.96, so the null hypothesis can be rejected for all pairs.

	original	squared exponential	inverse quadratic	inverse multiquadric	exponential	matern32	matern52
original	1146098.0	1219750.0	1090500.0	966971.0	1151946.0	1191100.0	773385.0
squared exponential	834748.0	920724.5	803197.0	730027.0	863022.0	880128.0	556626.0
inverse quadratic	826224.0	914765.0	801378.0	723611.0	873093.0	876541.0	557166.0
inverse multiquadric	784727.0	840022.0	741151.0	669324.5	770844.0	812724.0	521013.0
exponential	280298.0	420700.0	324543.0	323678.0	447458.0	351825.0	190590.0
matern32	768016.0	875830.0	761663.0	684434.0	872299.0	837218.0	533889.0
matern52	524113.0	606323.0	527796.0	470536.0	620132.0	575069.0	367224.5

Table D.8: Mann-Whitney test, atomic power plant

D.4. Baltimore

For each score below a χ^2 of 3.84146 the null hypothesis is accepted (The 0 scores are disregarded since they compare the same sample.). The null hypothesis is accepted for a 4 pair of combinations, which would mean that there is no difference between these groups. However, all groups that accepted H0 do not have a p value below 0.05, which means that the similarity between the groups is not statistically significant.

	original	squared exponential	inverse quadratic	inverse multiquadric	exponential	matern32	matern52
original	0.0	1.38	75.07	89.87	189.18	29.46	24.34
squared exponential	1.38	0.0	65.58	83.11	219.45	17.86	15.85
inverse quadratic	75.07	65.58	0.0	3.75	28.79	20.17	20.35
inverse multiquadric	89.87	83.11	3.75	0.0	2.86	37.52	39.36
exponential	189.18	219.45	28.79	2.86	0.0	168.97	189.77
matern32	29.46	17.86	20.17	37.52	168.97	0.0	0.3
matern52	24.34	15.85	20.35	39.36	189.77	0.3	0.0

Table D.9: Kruskal-Wallis test, Baltimore

	original	squared exponential	inverse quadratic	inverse multiquadric	exponential	matern32	matern52
original	1.0	0.24	0.0	0.0	0.0	0.0	0.0
squared exponential	0.24	1.0	0.0	0.0	0.0	0.0	0.0
inverse quadratic	0.0	0.0	1.0	0.05	0.0	0.0	0.0
inverse multiquadric	0.0	0.0	0.05	1.0	0.09	0.0	0.0
exponential	0.0	0.0	0.0	0.09	1.0	0.0	0.0
matern32	0.0	0.0	0.0	0.0	0.0	1.0	0.58
matern52	0.0	0.0	0.0	0.0	0.0	0.58	1.0

Table D.10: Kruskal-Wallis test, P value, Baltimore

For the Mann-Whitney U test, the Z value needs to be between -1.96 and 1.96 to be able accept the null hypothesis. If it is greater than 1.96 or lower than -1.96, there is a difference between the ranks of the two groups. All values are far exceeding 1.96, so the null hypothesis can be rejected for all pairs.

	original	squared exponential	inverse quadratic	inverse multiquadric	exponential	matern32	matern52
original	1146098.0	1053288.0	1140972.0	1063075.0	951847.0	1095785.0	727761.0
squared exponential	1001210.0	920724.5	1015943.0	950392.0	874430.0	961233.0	639808.0
inverse quadratic	775752.0	702019.0	801378.0	765695.0	678562.0	735125.0	479960.0
inverse multiquadric	688623.0	619657.0	699067.0	669324.5	570690.0	641449.0	414819.0
exponential	480397.0	409292.0	519074.0	523832.0	447458.0	415525.0	253280.0
matern32	863331.0	794725.0	903079.0	855709.0	808599.0	837218.0	562232.0
matern52	569737.0	523141.0	605002.0	576730.0	557442.0	546726.0	367224.5

Table D.11: Mann-Whitney test, Baltimore

D.5. Chester

For the Kruskal-Wallis test each score which has score below χ^2 3.84146, the null hypothesis is accepted (The 0 scores are disregarded since they compare the same sample.). The null hypothesis is accepted for 3 pair of combinations, which would mean that there is no difference between these groups. However, all groups that accepted H0 do not have a p value below 0.05, which means that the similarity between the groups is not statistically significant.

	original	squared exponential	inverse quadratic	inverse multiquadric	exponential	matern32	matern52
original	0.0	0.16	159.03	1.6	702.39	320.28	368.4
squared exponential	0.16	0.0	170.09	1.37	759.49	364.52	423.23
inverse quadratic	159.03	170.09	0.0	80.13	413.79	29.93	96.33
inverse multiquadric	1.6	1.37	80.13	0.0	480.57	173.17	224.02
exponential	702.39	759.49	413.79	480.57	0.0	340.63	150.27
matern32	320.28	364.52	29.93	173.17	340.63	0.0	40.08
matern52	368.4	423.23	96.33	224.02	150.27	40.08	0.0

Table D.12: Kruskal-Wallis test, Chester

	original	squared exponential	inverse quadratic	inverse multiquadric	exponential	matern32	matern52
original	1.0	0.69	0.0	0.21	0.0	0.0	0.0
squared exponential	0.69	1.0	0.0	0.24	0.0	0.0	0.0
inverse quadratic	0.0	0.0	1.0	0.0	0.0	0.0	0.0
inverse multiquadric	0.21	0.24	0.0	1.0	0.0	0.0	0.0
exponential	0.0	0.0	0.0	0.0	1.0	0.0	0.0
matern32	0.0	0.0	0.0	0.0	0.0	1.0	0.0
matern52	0.0	0.0	0.0	0.0	0.0	0.0	1.0

Table D.13: Kruskal-Wallis test, P value, Chester

For the Mann-Whitney U test, the Z value needs to be between -1.96 and 1.96 to be able accept the null hypothesis. If it is greater than 1.96 or lower than -1.96, there is a difference between the ranks of the two groups. All values are far exceeding 1.96, so the null hypothesis can be rejected for all pairs.

	original	squared exponential	inverse quadratic	inverse multiquadric	exponential	matern32	matern52
original	1146098.0	1036064.0	1224148.0	900867.0	1170338.0	1362807.0	956131.0
squared exponential	1018434.0	920724.5	1111756.0	806233.0	1074522.0	1254090.0	882888.0
inverse quadratic	692576.0	606206.0	801378.0	578403.0	901128.0	921402.0	678491.0
inverse multiquadric	850831.0	763816.0	886359.0	669324.5	850945.0	978745.0	688902.0
exponential	261906.0	209200.0	296508.0	243577.0	447458.0	333010.0	270027.0
matern32	596309.0	501868.0	716802.0	518413.0	891114.0	837218.0	643753.0
matern52	341367.0	280061.0	406471.0	302647.0	540695.0	465205.0	367224.5

Table D.14: Mann-Whitney test, Chester

D.6. Environment

For the Kruskal-Wallis test each score which has score below χ^2 3.84146, the null hypothesis is accepted (The 0 scores are disregarded since they compare the same sample.). The null hypothesis is accepted for 3 pair of combinations, which would mean that there is no difference between these groups. However, all groups that accepted H0 do not have a p value below 0.05, which means that the similarity between the groups is not statistically significant.

	original	squared exponential	inverse quadratic	inverse multiquadric	exponential	matern32	matern52
original	0.0	0.0	166.03	388.5	20.46	39.5	4.61
squared exponential	0.0	0.0	182.48	397.43	13.74	32.25	3.13
inverse quadratic	166.03	182.48	0.0	172.74	497.74	491.03	246.16
inverse multiquadric	388.5	397.43	172.74	0.0	947.6	910.86	545.15
exponential	20.46	13.74	497.74	947.6	0.0	2.52	7.98
matern32	39.5	32.25	491.03	910.86	2.52	0.0	16.06
matern52	4.61	3.13	246.16	545.15	7.98	16.06	0.0

Table D.15: Kruskal-Wallis test, environment

	original	squared exponential	inverse quadratic	inverse multiquadric	exponential	matern32	matern52
original	1.0	0.97	0.0	0.0	0.0	0.0	0.03
squared exponential	0.97	1.0	0.0	0.0	0.0	0.0	0.08
inverse quadratic	0.0	0.0	1.0	0.0	0.0	0.0	0.0
inverse multiquadric	0.0	0.0	0.0	1.0	0.0	0.0	0.0
exponential	0.0	0.0	0.0	0.0	1.0	0.11	0.0
matern32	0.0	0.0	0.0	0.0	0.11	1.0	0.0
matern52	0.03	0.08	0.0	0.0	0.0	0.0	1.0

Table D.16: Kruskal-Wallis test, P value, environment

For the Mann-Whitney U test, the Z value needs to be between -1.96 and 1.96 to be able accept the null hypothesis. If it is greater than 1.96 or lower than -1.96, there is a difference between the ranks of the two groups. All values are far exceeding 1.96, so the null hypothesis can be rejected for all pairs.

	original	squared exponential	inverse quadratic	inverse multiquadric	exponential	matern32	matern52
original	1146098.0	1026490.0	686789.0	486576.0	793653.0	1114141.0	683137.0
squared exponential	1028008.0	920724.5	597161.0	423393.0	700065.0	989847.0	607375.0
inverse quadratic	1229935.0	1120801.0	801378.0	506304.0	930378.0	1233437.0	759904.0
inverse multiquadric	1265122.0	1146656.0	958458.0	669324.5	973701.0	1276452.0	797050.0
exponential	638591.0	583657.0	267258.0	120821.0	447458.0	636056.0	374166.0
matern32	844975.0	766111.0	404767.0	220706.0	588068.0	837218.0	497962.0
matern52	614361.0	555574.0	325058.0	194499.0	436556.0	610996.0	367224.5

Table D.17: Mann-Whitney test, environment

D.7. Recreation

For the Kruskal-Wallis test each score which has score below χ^2 3.84146, the null hypothesis is accepted (The 0 scores are disregarded since they compare the same sample.). The null hypothesis is accepted for 5 pair of combinations, which would mean that there is no difference between these groups. However, all groups that accepted H0 do not have a p value below 0.05, which means that the similarity between the groups is not statistically significant.

	original	squared exponential	inverse quadratic	inverse multiquadric	exponential	matern32	matern52
original	0.0	2.41	205.16	0.25	118.36	13.05	8.5
squared exponential	2.41	0.0	159.51	3.54	86.69	4.24	2.35
inverse quadratic	205.16	159.51	0.0	169.15	6.73	108.98	88.51
inverse multiquadric	0.25	3.54	169.15	0.0	102.44	13.58	9.51
exponential	118.36	86.69	6.73	102.44	0.0	52.65	45.29
matern32	13.05	4.24	108.98	13.58	52.65	0.0	0.09
matern52	8.5	2.35	88.51	9.51	45.29	0.09	0.0

Table D.18: Kruskal-Wallis test, recreation

	original	squared exponential	inverse quadratic	inverse multiquadric	exponential	matern32	matern52
original	1.0	0.12	0.0	0.62	0.0	0.0	0.0
squared exponential	0.12	1.0	0.0	0.06	0.0	0.04	0.13
inverse quadratic	0.0	0.0	1.0	0.0	0.01	0.0	0.0
inverse multiquadric	0.62	0.06	0.0	1.0	0.0	0.0	0.0
exponential	0.0	0.0	0.01	0.0	1.0	0.0	0.0
matern32	0.0	0.04	0.0	0.0	0.0	1.0	0.77
matern52	0.0	0.13	0.0	0.0	0.0	0.77	1.0

Table D.19: Kruskal-Wallis test, P value, recreation

For the Mann-Whitney U test, the Z value needs to be between -1.96 and 1.96 to be able accept the null hypothesis. If it is greater than 1.96 or lower than -1.96, there is a difference between the ranks of the two groups. All values are far exceeding 1.96, so the null hypothesis can be rejected for all pairs.

	original	squared exponential	inverse quadratic	inverse multiquadric	exponential	matern32	matern52
original	1146098.0	1050358.5	1195092.0	869461.0	855692.0	1032961.5	680522.5
squared exponential	1004139.5	920724.5	1054901.0	762311.0	754060.0	906691.5	597221.5
inverse quadratic	721632.0	663061.0	801378.0	554739.5	565517.0	660003.0	434563.0
inverse multiquadric	882237.0	807738.0	910022.5	669324.5	653112.5	792856.0	522593.0
exponential	576552.0	529662.0	632119.0	441409.5	447458.0	525830.0	346214.0
matern32	926154.5	849266.5	978201.0	704302.0	698294.0	837218.0	551467.5
matern52	616975.5	565727.5	650399.0	468956.0	464508.0	557490.5	367224.5

Table D.20: Mann-Whitney test, recreation